Flow Modelling in Low Permeability Unconventional Reservoirs

Nicolas Farah

THÈSE DE DOCTORAT DE
L'UNIVERSITÉ PIERRE ET MARIE CURIE

École Doctorale Géosciences, Ressources Naturelles et Environnement (Paris)

Présenté par :

Nicolas FARAH

Pour obtenir le grade de :

DOCTEUR DE L'UNIVERSITÉ DE PIERRE ET MARIE CURIE

Sujet de la thèse :

Flow Modelling in Low Permeability Unconventional Reservoirs

soutenue le 6 Décembre 2016 :

devant le jury composé de :

Pr. Virginie	Marry	UPMC	Paris,	France	Président
Pr. Jean-Raynald	De Dreuzy	Rennes 1	Rennes,	France	Rapporteur
Pr. Xialong	Yin	CSM	Colorado,	États-Unis	Rapporteur
Pr. Yu-Shu	Wu	CSM	Colorado,	États-Unis	Examinateur
Dr. Didier-Yu	Ding	IFPEn	Rueil Malmaison	France	Directeur de Thèse

EXECUTIVE SUMMARY

Unconventional shale-gas reservoirs hold a significant amount of the world's hydrocarbon reserves. The exploitation of unconventional reservoirs in the United States has increased enormously in the last decades. These reservoirs present specific characteristics such as tight reservoir rock with nano-Darcy permeability. Moreover, they are generally naturally fractured with a complex fracture network. Compared to conventional reservoirs, production from unconventional shale-gas reservoirs with a very low permeability rock requires multi-stage hydraulic fracturing with a horizontal well. Once the hydraulic stimulation is done, a complex fracture networks, including hydraulic/natural/micro-fractures, is created connecting a huge reservoir volume leading to enhance gas recovery.

Meanwhile, flow modelling from unconventional fractured reservoirs remains a big challenge for the petroleum industry, where numerous research programs have been focusing on this topic. One of the key problems from unconventional reservoir simulation is the simulation of matrix/fracture interaction due to the low matrix permeability, a complex fracture network and non-linear pressure distribution into the matrix. In the literature, many approaches based on single-porosity or dual-continuum models are presented for flow modelling from unconventional reservoirs. However, neither a single-porosity model nor a dual-porosity model is suitable for such problem. It must be mentioned that a single-porosity approach where fractures are explicitly discretized requires a large computational CPU time due to the large number of grid cells needed in order to describe the reservoir. On the other hand, dual-continuum models (dual-porosity/permeability) are not accurate due to the large grid cells and extremely low matrix permeability. Also, during the transient period in shale-gas reservoirs, a non-linear variation of the pressure in the matrix media emphasizes the duration of the transient period leading to a very

long transient period for both single-phase flow and multiphase flow simulations which could not be handled by standards dual-continuum models.

Lately, to model a realistic reservoir fracture network, a new type of models called discrete fracture models (DFMs) has received a great attention. These kinds of models, which discretize explicitly complex fracture networks such as; hydraulic, stimulated and non-stimulated natural fractures; involve many unknowns and often non tractable numerical system to solve. This work proposes a methodology to address this challenge, taking into account reservoir key parameters such as fracture locations, orientations, anisotropy and reservoir low permeability in a unique model as simple as possible. To overcome the challenges presented from a single-porosity, dual-continuum models and DFM proposed in literature, we present a hybrid approach based on the concept of the classic MINC (Multiple Interacting Continua) method. Note that, the MINC method is a generalization of the dual-porosity (DP) concept, where the matrix media is subdivided into nested volumes. In other words, the DP is a particular case of the MINC method where the matrix refinement (matrix subdivision) is equal to 1. Our approach consists in a hierarchical method where different existing fractures in our reservoirs are classified. Based on a conductivity criterion, high conductive fractures are explicitly discretized due to their important role in production while, other fractures (natural fractures, induced and stimulated/un-stimulated fractures) are homogenized to form a homogenized fracture media. Also, our model subdivides the matrix media using the MINC method to simulate properly the flow exchange between matrix and all sorts of fractures (including both high and low conductive fractures). So, this hybrid technique discretizes explicitly high conductive fractures, homogenized low conductive fractures and associates the MINC method which is required to improve the flow exchange between the matrix and fracture media. This hybrid approach could be incorporated in existing reservoir simulators.

In summary, due to the hydraulic fracturing stimulation, a very complex fracture network will be created increasing the heterogeneity and the complexity of the reservoir and make flow modelling for such reservoirs quite challenging. The presence of multi-scale heterogeneities, including stimulated fractures (hydraulically induced or open), natural fractures of various sizes embedded in unconventional low permeability reservoirs, increases the complexity of the reservoir simulation. This work proposes a methodology to address this challenge, taking into account reservoir key parameters such as fractures locations, orientation, anisotropy and reservoir low permeability in a unique model as simple as possible.

In Chapter 1 - Shale-Gas Reservoirs, an introduction on shale-gas reservoirs and fluid properties in unconventional shale reservoirs additionally to different physics phenomena from such reservoirs are presented. Also, the hydraulic fracturing stimulation method and the impact of the fracturing fluid induced formation damage are discussed. Finally, the research objectives from this work are fixed.

In Chapter 2 - Reservoirs Simulation Models, different simulations models found in the literature from explicit discretized model, dual-porosity/permeability models, the MINC method and discrete fracture model (DFM) are presented. Besides, the general equations governing the flow in naturally fractured reservoirs are described.

In Chapter 3 - Hybrid Approach Based on the Classic MINC Method, the ability of the classic MINC method for unconventional reservoir flow simulation is tested on a simple case. Moreover, a typical regular fractures distribution (Warren and Root type) for different fractures spacing's, with the presence of a stimulated reservoir volume (SRV) and a non-SRV zone, is studied. In this chapter, the efficiency of the MINC method for both single-phase and two-phase flow is discussed. Finally, the impact of fracturing fluid invasion on gas production is presented.

In Chapter 4 - Extension of the Hybrid Approach to the Discrete Fracture Model, a generalization of the hybrid approach to handle Discrete Fracture Networks (DFNs) taking into account an irregular fractures distribution is presented. Our extended model is called "Discrete Fracture Model based on a MINC proximity function". First, a description of our methodology is presented, and the connections between different media are described. Then, the validation of our approach on simple cases and on a large fracture network is presented.

In Chapter 5 - Application of the Discrete Fracture Model to a Field Scale Problem, the robustness of our DFM based on a MINC proximity function is tested through a synthetic problem. An application on a shale-gas reservoir example and tight-oil reservoir example are presented. Although the first objective of our study was to model shale-gas reservoirs, however this proposed approach looks also suitable for the simulation of multiphase flow from different reservoirs types (all types of low permeability reservoirs), including tight-oil reservoirs.

In Chapter 6 - Discussions and Prospects, a discussion concerning some future works which could be implemented in order to improve the actual Discrete Fracture Model are presented. In particular, the presence of different block size into a grid cell and the problem of

the flow exchange between adjacent matrix grid cells are discussed. Finally, this work is concluded in Chapter 7 - Conclusions.

ACKNOWLEDGEMENTS

I am sincerely grateful to my supervisor, Dr. Didier-Yu Ding, for his invaluable advices and excellent supervision throughout my PhD study. I would also like to express my gratitude to Pr. Yu-Shu Wu, for his excellent guidance and continuous support and encouragement during this research. I am privileged to have had an opportunity to work with them. I would also like to thank other members of my dissertation committee, Pr. Jean-Raynald De Dreuzy, Pr. Xiaoling Yin and Pr. Virginie Marry, for their time and effort to serve on my committee and review my dissertation.

I greatly acknowledge the members of the GéoThermoHydroMécanique Department at the IFP Énergies nouvelles at Rueil-Malmaison for the financial support of this research. I would also like to acknowledge the head of the Department of GéoThermoHydroMécanique, Mr. Frédéric Roggero.

I would like to express my gratitude to all friends who helped and supported me throughout my PhD study. I am especially grateful to Dr. Bernard Bourbiaux for his indispensable help and guidance during this research. I would also express my gratitude to Matthieu Delorme for his technical advices during this research. I am also very thankful to Fadi Nader, Dan Bossie Codréanu and Jean-Claude Lecomte for the valuable discussion we had together.

I am also very thankful to Thomas Pouchou, Thibaut Somma, Paul Bertrand, Chahir Jerbi, Arthur Thenon, Omar Gassara, and many other friends that I have not mentioned their names.

I would like to express my deepest gratitude to my parents and my beloved Vanessa for their endless love, support, and encouragements throughout my graduate study at IFPEn at Rueil-Malmaison. My achievements would not have been possible without their help and inspiration. Finally, I would like to thank my brother and my sister, who have supported me in every possible way.

TABLE OF CONTENTS

LIST OF FIGURES

LIST OF TABLES

NOMENCLATURE

Abbreviation

DK-LS-LGR	Dual-Permeability - Logarithmically Spaced - Local Grid Refinement
DP (2ϕ-1K)	Dual-Porosity Single-Permeability Model
DP (2ϕ-2K)	Dual-Porosity Dual-Permeability Model
DFMs	Discrete Fracture Models
EDFM	Embedded Discrete Fracture Model
EUR	Estimated Ultimate Recovery
FBHP	Fluid Bottom Hole Pressure
GIP	Gas In Place
HF	Hydraulic Fractures
HFM	Hierarchical Fracture Model
MINC	Multiple INteracting Continua
NNC	Non-Neighboring Connection
NFx	Stimulated Fractures Parallel to the Well Direction

NFy	Stimulated Fractures Perpendicular to the Well Direction
SRV	Stimulated Reservoir Volume
TOC	Total Organic Content
USDFM	Unstructured Discrete Fracture Model

Symbols

A_{ij}	Interface area between two grid cells (cells) i and j
A_{mf}	Interface area between a matrix and a fracture cells
a	Matrix block dimension
b	Matrix block dimension
b_k	Klinkenberg factor
c	Component
<d>	Average distance
d	Distance from a cell center to its interface with a neighboring cell
$F_{p,ij}$	Flow component of fluid p across an interface between grid cells (or cells) i and j
g	gravity
k	Absolute permeability
k_g	Gas phase absolute permeability
k_{ini}	Initial reservoir permeability
k_{rp}	Relative permeability to phase p

k_{rg}	Gas relative permeability
k_{rw}	Water relative permeability
k_{∞}	Absolute gas permeability at large gas pressure
m_g	Adsorption or desorption term per unit volume of formation
p	Number of random points
P	Pressure
P_C	Capillary pressure
P_f	Pressure inside the fracture
P_L	Langmuir pressure
P_{nw}	Non-wetting fluid pressure
P_w	Wetting fluid pressure
q	Source/sink term
Q_p^{mf}	Matrix-fracture interaction for phase p
S	Fluid saturation
Sw_{ini}	Initial water saturation
Sw_{ir}	Irreducible water saturation
t	Time
T_{ij}	Transmissibility between grid cells (cells) i and j
$\vec{u}_p$	Darcy's volumetric velocity of phase p

V_E	Volume of adsorbed gas in standard condition per unit mass of solid
v_β	Volumetric velocity vector of fluid β
v_{sg}	Gas sorption term (mole)
V_i	Volume of grid cell i
V_L	Langmuir volume
V_s	Volume of adsorbed gas in standard condition par unit mass of solid
Z	Depth (vertical direction)

Greek Symbols

Δt	Time step
ϕ	Effective porosity of formation
Φ	Flow potential
$\lambda_{p,ij}$	Mobility of phase p between grid cells i and j
μ	Viscosity
σ	Shape-factor
σ_h	Horizontal stress perpendicular to the fracture
ρ_r	Solid rock density
ρ_g	Gas density
ρ_g	Mole density

ρ_{sc}	Gas mole density at standard condition
Γ_{ij}	Interface between two grid cells i and j

Subscript

f	Denotes fracture
g	Denotes gas
i	Grid cell i
j	Grid cell j
m	Denotes matrix
n	Time level
p	Index of fluid phase
w	Denotes water

Chapter 1 - SHALE-GAS RESERVOIRS

Shale-gas reservoirs hold a significant amount of world hydrocarbon reserves. Compared to conventional reservoirs, shale-gas reservoirs present an extreme low-permeability, a higher heterogeneity and a complex of fracture network. Usually, in order to enhance gas recovery from such low permeability reservoirs, a hydraulic stimulation is needed.

Thus, this part will introduce the different characteristics of shale formation and discuss the various phenomena existing in shale reservoirs. As a fracturing operation is required in such reservoirs, leading to a multi-scale fracture network in order to enhance gas production from shale formations, the process of a hydraulic stimulation is also briefly described. Besides, the problem of fluid invasion into the matrix formation is discussed, as a huge amount of water is injected into the reservoir formation during hydraulic fracturing and the fracturing fluid invasion induced formation damage may greatly reduce the fluid flow (gas) relative permeability leading to a decreasing in gas production. Finally, the research objectives are defined in this chapter.

1.1 Introduction

Unconventional gas resources from shale-gas reservoirs have received a great attention in the past decade and become the focus of the petroleum industry for the development of energy resources worldwide (see, Figure 1.1). With the increased demand for hydrocarbons, the unconventional resources represented by tight gas, shale-gas and tight oil are becoming more and more crucial. Facing such low permeability from these reservoirs, the development of a stimulation technology is needed in order to evacuate trapped hydrocarbons, gas or oil.

Usually, unconventional low permeability reservoirs are dependent upon artificial stimulation like hydraulic fracturing technology to obtain an economical production rate. Usually, permeability in conventional formation ranges generally from 10 mD to 1000 mD, where for example it could be less than 0.1 mD in tight gas reservoirs. Considering ultra-tight gas reservoirs like shale-gas may have in-situ permeability down to 0.0001 mD or 0.00001 mD.

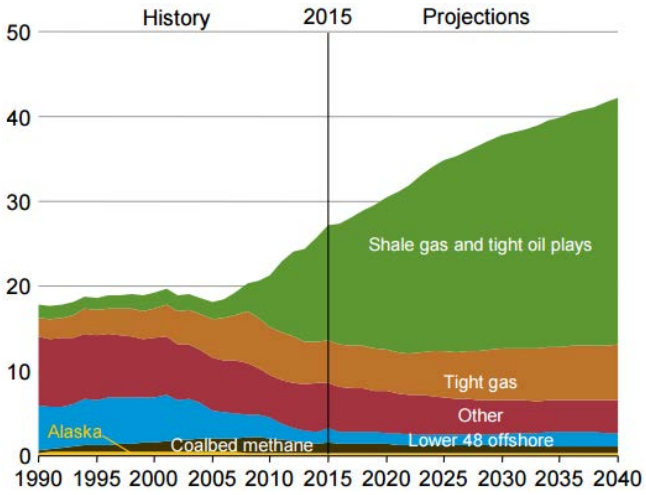

Figure 1.1: Annual US Natural Gas Production and Projected Production by Gas Type, 1990-2040; after EIA (2016).

Moreover, concerning unconventional shale-gas reservoirs, hydraulic fracturing is a technique that makes it possible to extract trapped gas from tight rocks. Many features distinguish shale-gas reservoirs from classic reservoirs such as, (1) shale-gas with high total organic content (TOC); (2) gas can exist in two forms, adsorbed on the matrix surface and free

gas; (3) very low matrix permeability; (4) nano-pore physics for fluid flow. Additionally, in such low permeability reservoirs the fractures are presented as high conductive pathways. Moreover, the presence of fractures at various scales (hydraulic fractures, natural and induced fractures, micro-fractures, etc.), coupled with small fracture volumes, make numerical simulation of fluid flow very challenging.

Thus, the flow behavior in unconventional reservoirs from shale-gas/tight-oil can be characterized by single-phase flow (gas/oil) and/or multi-phase flow in extremely low-permeability, highly heterogeneous porous/fractured, and stress-sensitive rock. In fact, referring to shale-gas reservoirs the conventional gas recovery mechanism is the depletion recovery assisted by hydraulic fracturing stimulation. In extreme cases, due to fracturing fluid invasion associated with the hydraulic stimulation, gas relative permeability can be reduced to zero as water saturation increases. Furthermore, simulation from unconventional reservoirs presents several challenges, where these challenges are not limited to the large contrast between hydraulic fracture and tight rock matrix permeabilities. One of the most important challenges from unconventional reservoir simulations is often the presence of complex fracture network geometry.

Handling flow through fractured media is critical in shale-gas reservoir simulations. In fact, gas production from such low-permeability formations relies on fractures, from hydraulic fractures/network to various scaled natural fractures, to provide pathways for gas flow into producing wells. In order to model natural fractured reservoirs, many approaches have been proposed. The key issue for simulating flow in fractured rock is how to handle fracture-matrix interaction, in terms of mass or energy exchange, under different conditions. In the literature (see for example, Warren and Root (1963); Kazemi (1969); Wu *et al.* (2004 and 2013); Rubin (2010); James Li *et al.* (2011); Bicheng Yan *et al.* (2013)), various approaches from analytical solutions to commercial simulators are presented on how to model gas flow in shale-gas reservoirs.

Moreover, most approaches used dual-continuum model or an explicit discretized model to handle fracture-matrix interaction. On one hand, the dual-continuum models represented by dual-porosity and/or dual-permeability concept are not adequate for modelling these complex networks of natural and hydraulic fractures in extremely low permeability reservoirs. Furthermore, due to the very low permeability in shale-gas reservoirs, the transient period is long and the simulation of the matrix-fracture interaction with a large matrix cell is very challenging.

On the other hand, it is not beneficent to modelling these reservoirs with an explicit discretized model using a grid refinement around the fractures due to the large number of grid cells and the complex fractures network. Therefore, a simplified approach to model fluid flow from unconventional shale-gas and tight-oil reservoirs is needed. This approach should consist in coupling the explicit discretized model, concerning only the large-scale high conductive hydraulic fractures, with a dual-continuum model that accounts for flow in the naturally fractured networks.

Beside the challenges presented by shale-gas formations, these reservoirs introduce also many physical phenomena such as adsorption/desorption, geomechanics effect, Klinkenberg effect, etc., which are neglected in a conventional reservoir. Contrary to conventional reservoirs, gas flow in ultra-low permeability coupled with several processes, including rock deformation, nano-pore physics. In the literature, many works (see for example, Cipolla *et al.* (2008, 2009a); Cipolla and Lolon (2010); Ding *et al.* (2014)) studied the impact of various phenomena on gas production from shale-gas reservoirs. Essentially, the flow exchange between matrix and fractures known also by inter-porosity flow could be easily impacted by one of these phenomena. As a result, the gas recovery behavior from shale-gas reservoirs will be dependent on considering or not each mechanism, where these phenomena should be coupled with fluid flow in the simulation model. Therefore, quantifying flow in unconventional gas reservoirs has been a significant challenge during the last decades.

Furthermore, the use of a horizontal drilling with hydraulic fracturing has increased the ability to produce natural gas from low permeability formations, particularly shale formations. However, after hydraulic operation a major concern consists in water blocking effect in tight formation due to the high capillary pressure and the presence of water sensitive clays. In fact, the essential objective from hydraulic fracturing is to have an economical production by increasing the effective drainage area of the reservoir, where a very complex fractures network should be created to connect a huge reservoir area to the wellbore effectively. During hydraulic fracturing, an enormous amount of water is injected into the matrix formation, where only a part of the injected water (30-60%) can be reproduced during a flow-back and a long production period. Unfortunately, instead of enhancing gas production, the presence of high water saturation in the invaded zone near the fracture face may reduce greatly the gas relative permeability and impedes gas production. Clearly, pumping fluid into shale formation may impact on gas recovery.

1.2 Hydraulic Stimulation Method

The earliest attempts of artificially hydraulic stimulations in the US go back to the 1860s, and involved lowering explosive charges down the boreholes of oil wells. In oil and gas industry hydraulic fracturing operation began early in the 1930 with Dow chemical Company. In fact, they discovered that downhole proppant pressures could be applied into fracking the formation rock. The process of injecting liquid at high pressure into subterranean rocks leads formation to crack and deform. The first hydraulic fracturing treatment was applied in Kansas in 1947 on a gas reservoir in the Hugoton field. In 1949 the first commercial applications of the technique had been carried out for oil exploration in Texas and Oklahoma by Halliburton. In the 1990s, hydraulic fracking was tested in the Barnett Shale area in Texas. By 2014, more than 2.5 million hydraulic fracturing operations had been performed on oil and gas wells worldwide, more than one million of them are done in the US.

The technique of a horizontal well was unusual until the 1980s. The first horizontal well was drilled in the Barnett Shale in north Texas in 1991 and the technique was then applied more effectively in 1997 by George Mitchell (father of fracking).

The hydraulic fracturing started with vertical wells. Once the drilling is done and the rig and derrick are removed, the hydraulic treatment could take place. It consists in pumping water mixed with proppants (mostly sand) and chemicals under high pressure. This fracking fluid can be injected at various pressures and reach up to 100 MPa (1000 bar) with flow rates of up to 265 liters/second. Note that hydraulic treatment could take several hours depending on fractures shape, stage number and the total proppant volume to be placed. Nowadays, horizontal drillings associated with multi-stage hydraulic fracturing (up to 30 – 40 stages) are commonly used for shale-gas productions.

Additionally, fracturing fluid consists of about 98-99.5 per cent of water and proppant, where the rest (0.5–2 per cent by volume) is composed of chemicals, that enhance the fluid's properties. In our days, hydraulic treatments are used by petroleum industry on oil and gas reservoirs in order to increase the formation permeability and enhance oil/gas recovery from unconventional reservoirs. Clearly, fracking operation will lead to open existing fissures, so extracting oil or gas will be much easier.

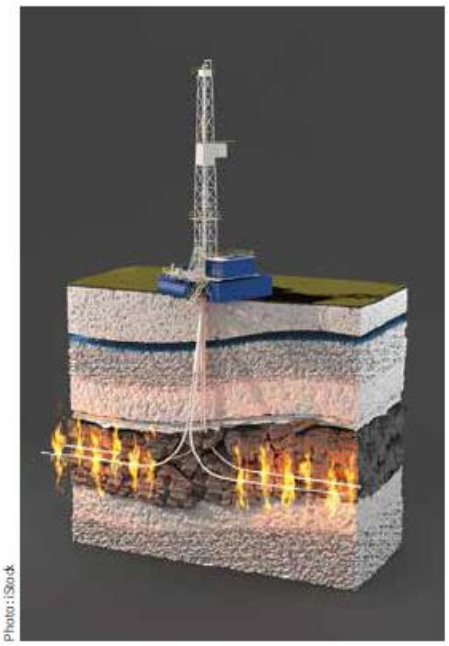

Figure 1.2: Stimulation technique using a horizontal well.

This exploitation technique is used essentially for shale-gas reservoirs and it is illustrated in Figure 1.2. Most shale-gas reservoirs are fractured and have low matrix permeability, where matrix media contains the most gas volume and global flow in the reservoir is assumed to occur through the fracture network. Hydraulic fracturing stimulates also natural fractures. Some natural fractures are opened and the conductivity in these fractures is greatly increased. If injected proppant reaches into the reactivated natural fractures, gas production will be greatly enhanced.

1.3 Rock and Fluid Properties

According to a huge amount of hydrocarbon in place, shale-gas (GIP) and tight-oil (OIP) reservoirs are today's interest of petroleum companies. Table 1.1 and Table 1.2 present the top 10 countries with the most recoverable shale oil and shale-gas resources respectively. In order to improve gas production, huge investments have been spent since 1970's on shale-gas research programs in the United States of America, in a way to understand the geological, geochemical and hydro-dynamical nature of organic shale formations.

Table 1.1: Top 10 countries with technically recoverable shale-oil resources; after EIA (2015).

Rank	Country	Shale Oil (Billion Barrels)
1	Russia	75
2	U.S.	58
3	China	32
4	Argentina	27
5	Libya	26
6	Australia	18
7	Venezuela	13
8	Mexico	13
9	Pakistan	9
10	Canada	9
	World Total	345

Table 1.2: Top 10 countries with technically recoverable shale-gas resources; after EIA (2015).

Rank	Country	Shale-Gas (Tcf)
1	China	1115
2	Argentina	802
3	Algeria	707
4	U.S.	665
5	Canada	573
6	Mexico	545
7	Australia	437
8	South Africa	390
9	Russia	285
10	Brazil	245
	World Total	7299

Gas in shale formations could be characterized into different forms: (1) free gas in natural fractures and inter-granular porosity, (2) gas sorbed into kerogen or on clay particles surfaces. Each shale-gas reservoir has particular characteristics, where fracability and productibility are the most important ones. The fracability defines the capability of the reservoir rock to be fractured and the productibility is dedicated to the capacity of the reservoir to produce a significant volume of gas. Note that, the main components in shale-gas composition are hydrocarbons (CH4 mainly from 15-99%), carbon dioxide CO2 (30% in Romania, 17% in Poland, 12% in Canada), nitrogen (1-76%), hydrogen sulfide (some percent) and noble gases: Ar, He up to 1%. In order to evaluate the production capability of the reservoir, it is important to take into account several physics related to unconventional gas reservoirs such as, adsorption/desorption and geomechanics effects, etc.

Gas desorption may be a major additional gas production and an important factor for ultimate gas recovery. Neglecting this phenomenon might results in an underestimation of reservoir potential, especially in a shale formation with a high TOC. Many papers in the literature have studied the effect of gas desorption on the gas production. Jarvie (2004) demonstrated that both adsorbed and free gas stored in the shale matrix increased with TOC content. Passey *et al.* (2010); Javadpour *et al.* (2007); Cipolla and Lolon (2010); Mirzaei and Cipolla (2012), Wei Yu and kamy Sepehrnoori (2013), discussed the contribution of gas desorption to gas flow in shale plays.

Also, Javadpour (2009) proposed that beside free gas storage in shale, gas could be adsorbed on the surface of kerogen and dissolved within it. Gas desorption has proved to be essential to understanding the production capacity of shale-gas reservoirs. Also, the volume of adsorbed gas can be significantly important in shale-gas production, where the percentage of adsorbed gas can varies from 15% up to 60% of initial GIP. The GIP can exist in two forms, as an adsorbed on the shale surface or as a free gas in the matrix pore. The gas desorption may contribute additional gas production in shale-gas reservoirs. Cipolla *et al.* (2010) investigated the Barnett and Marcellus shale reservoirs and concluded that gas desorption may constitute about 5-15% of the total gas production during 30 year. Thompson *et al.* (2011) observed that gas desorption contributes to 17% increase in the estimated ultimate recovery (EUR), from the Marcellus shale during 30 year of production.

Mengal and Wattenbarger (2011) compared shale-gas reservoirs with conventional reservoirs in order to quantify gas desorption phenomena. Studies confirmed that shale formation can hold significant quantities of adsorbed gas on the surface of the organics in shale formation. Moreover, gas desorption can contribute approximately in 30% increase in original GIP. Note that, the impact of desorption phenomenon is more significant at later time of production depending on reservoir permeability, flowing bottom hole pressure (FBHP) and fracture spacing. As the reservoir pressure decreases during production, gas is liberated from solid to free gas phase, where such process is known as gas desorption. Figure 1.3 shows the gas content versus pressure for the free gas and adsorbed gas used for the Barnett Shale. Both free gas and adsorbed gas together form the total gas content. Figure 1.4 illustrates the Langmuir isotherm curve of the Barnett Shale. In unconventional reservoirs, Langmuir's isotherm is used to model the amount of adsorbed gas. The gas content V_E in scf/ton is calculated below:

$$V_E = V_L\left(\frac{P}{P + P_L}\right) \tag{1.1}$$

where, V_L is the Langmuir's volume in scf/ton, P is the reservoir gas pressure; and P_L is Langmuir's pressure, the pressure at which 50% of the gas is desorbed. It is clear that higher Langmuir pressure releases more adsorbed gas and results in higher gas production.

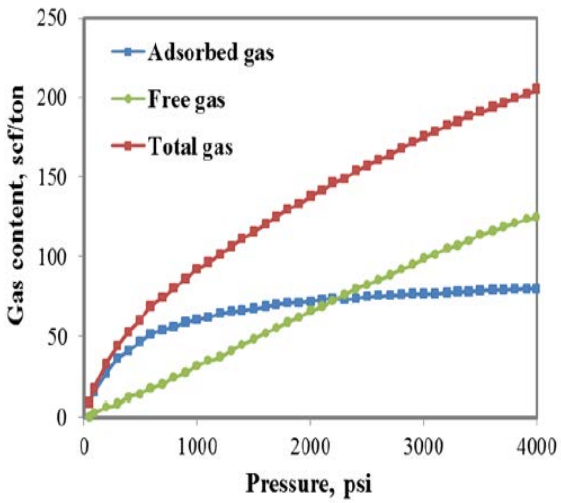

Figure 1.3: An example of Barnett shale-gas content; after Wei Yu and Kamy Sepehrnoori (2013).

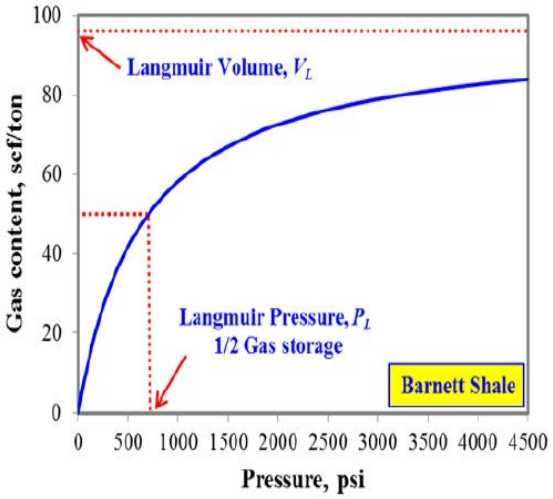

Figure 1.4: Langmuir isotherm curve for Barnett Shale; after Wei Yu and Kamy Sepehrnoori (2013).

Langmuir's characteristic volume and pressure, V_L and P_L, depend on the organic richness or TOC. Passey *et al.* (2010), reported that the TOC volume within shale reservoirs can occupy till 40% of the reservoir rock in some cases, such as Woodford shale. In other words, reservoirs with higher TOC contain more adsorbed gas. Langmuir isotherm curves for five different shale formations containing lean and/or rich shale are represented in Figure 1.5.

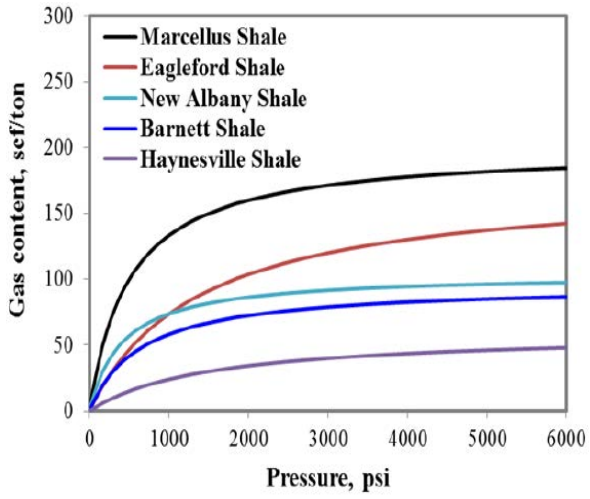

Figure 1.5: Langmuir isotherm curves for five different shale formations; after Wei Yu and Kamy Sepehrnoori (2013).

Furthermore, geomechanics plays a critical role in gas production and development from unconventional resources. Gas production from shale-gas reservoirs depends enormously on

different parameters, especially on hydraulic fractures, induced secondary fractures and micro-fractures. During gas production from shale-gas reservoirs, pressure field drops significantly leading to a large change in effective stress, which could result in rock deformation.

Increasing in the closure stress due to gas production may impact matrix and fracture permeabilities. Fredd *et al.* (2001) investigates the effects of fracture properties on conductivity, where a series of laboratory conductivity experiments were performed with fractured cores from the east Texas Cotton Valley sandstone formation. Bustin *et al.* (2008) report the effect of stress (confining pressure) in Barnett, Muskwa, Ohio, and Woodford shales. Furthermore, a higher reduction of permeability was founded with confining pressure in shales than that in consolidated sandstone or carbonate. Wang *et al.* (2009) shows that permeability in the Marcellus Shale is pressure-dependent and decreases with an increase in confining of pore pressure (or total stress). Cipolla *et al.* (2008, 2009a) investigated fracture conductivity depending on closure stress and young modulus. From previous works in the literature concerning geomechanics effects assumed that, when the reservoir is depleted, both fracture and matrix permeabilities (conductivies) may be reduced due to rock deformation which could impede the gas production. The geomechanics effect has a significantly higher impact on unconventional shale-gas reservoirs than conventional reservoirs, due to the presence of multi-scale fractures.

Meanwhile, complex fracture networks are usually created during hydraulic operation using a low viscosity fracturing fluids, where a proppant is injected to support fractures opening. Proppant distribution in shale formation can create different fracture network and might impact gas production. After a proppant injection, it is important to know (1) proppant location, (2) proppant concentration within primary fractures and (3) the conductivity of the propped and partially propped fracture networks which could significantly improve productivity.

Figure 1.6 and Figure 1.7 show different possible proppant transport scenarios. In fact, if the proppant is evenly distributed throughout a large complex fracture network (Case1), it may result with an insufficient proppant concentration in order to impact fracture network conductivity. In other words, there isn't enough proppant in primary and secondary fractures, where fractures could behave as if they were un-propped. On the other hand, the proppant could be concentrated within a single fracture (Case2). This could significantly improve the connection between the fracture network and the wellbore; however the proppant would not disperse into the fracture network. In Case3, the proppant distribution is evenly distributed in pillars. This

scenario could result in a small fracture area propped which would be insufficient to support the closure stress. Production from unconventional shale-gas reservoirs may be dominated by un-propped or partially propped fractures, so it is important to understand the conductivity of these fractures as they could play a crucial role in gas recovery.

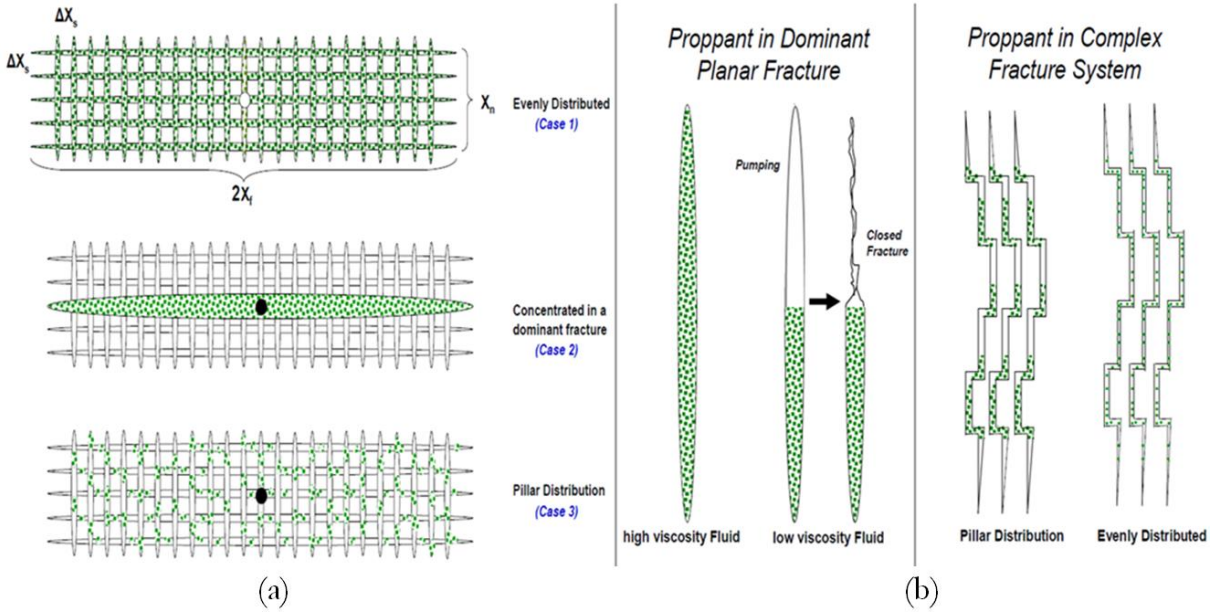

Figure 1.6: Proppant transport scenarios (a) plan and (b) side view; after Cipolla (2008).

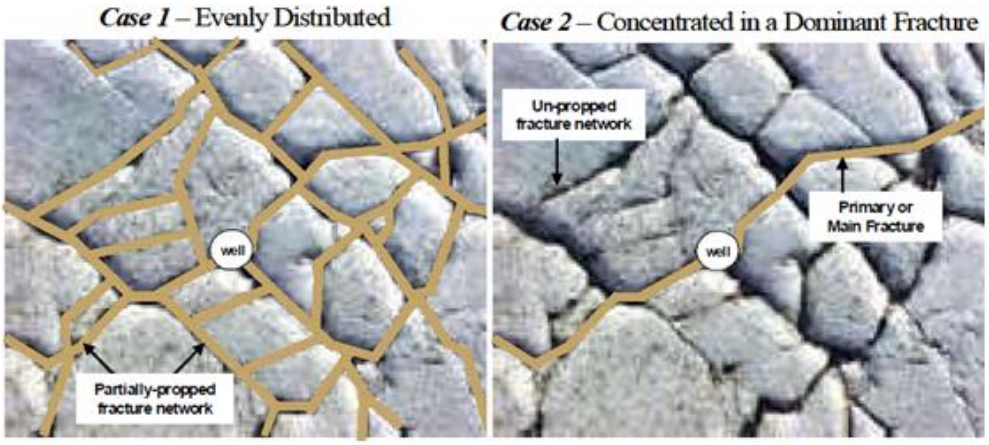

Figure 1.7: Proppant distribution for two different cases; after Cipolla (2009a).

Also, Cipolla *et al.* (2009a) shows that the conductivity of partially and un-propped fractures is approximated as a function of closure stress (defined as the horizontal stress perpendicular to the fracture minus the pressure inside the fracture).

$$Closure\ Stress = \sigma_h - P_f \tag{1.2}$$

where, σ_h is the horizontal stress perpendicular to the fracture and and P_f is the pressure inside the fracture.

Based on the laboratory tests presented by Cipolla *et al.* (2009a), Figure 1.8 summarizes the impact of closure stress on fracture conductivity for two different proppant types. The bottom curve (black curve) represents an un-propped fracture where the two fracture faces are aligned upon closing. Clearly, the conductivity for an un-propped aligned fracture faces can decrease dramatically when the closure stress increases, impacting the gas the production which could be greatly reduced. However, if the fracture is partially propped with 0.1 lbm/ft² of Jordan sand (blue curve) or the fracture faces are displaced un-propped, the fracture conductivity would be improved. Furthermore, the type of the proppant can increase greatly the conductivity of a partially propped fracture (partially propped with 0.1 lbm/ft² of bauxite (orange curve)).

Cipolla *et al.* (2008) investigated the impact of the Young's modulus on the conductivity for un-propped fractures. Figure 1.9 presents fracture conductivity as a function of the closure stress for different Young's modulus. Obviously, the conductivity can drop off dramatically using lower modulus materials. Un-propped fractures will be closed when modulus is lower than 2 Mpsi and the closure stress exceeds 4000 psi.

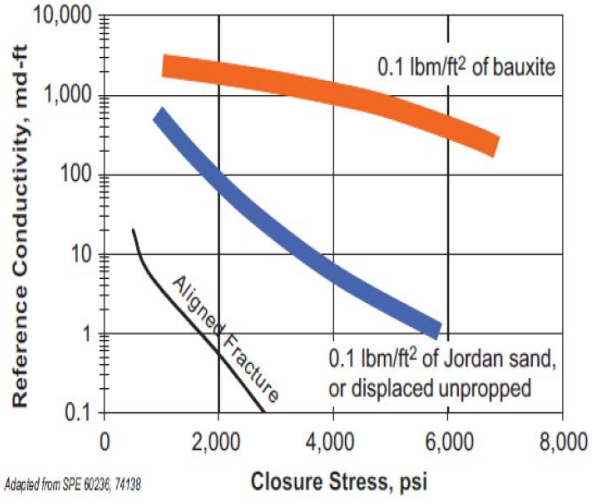

Figure 1.8: Effect of closure stress (effective stress) on un-popped and partially-propped fracture conductivity; after Cipolla (2009a).

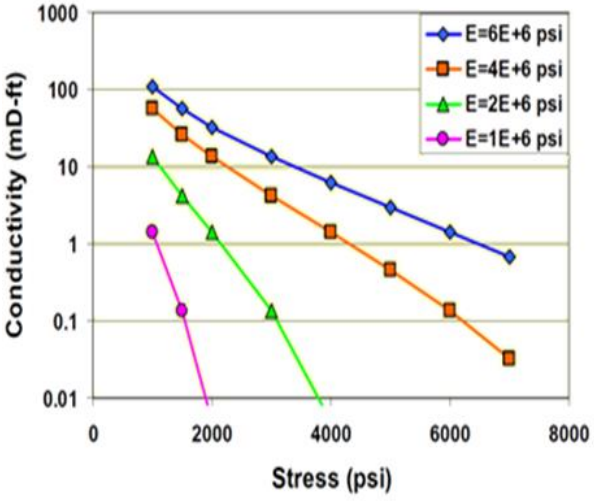

Figure 1.9: Effect of modulus on conductivity of un-propped fractures; after Cipolla *et al.* (2008).

Moreover, Cipolla *et al.* (2010) studied geomechanical aspect on the Marcellus shale. An estimated effect of closure stress on un-propped-fracture conductivity in Marcellus shale for a Young's modulus value of 2 Mpsi is represented in Figure 1.10 (based on previously published work by, Fredd *et al.* (2010); Cipolla *et al.* (2008)). Before production, the initial network-fracture conductivity is 2 mD-ft. The conductivity declines to 0.02 mD-ft, when the pressure in the fracture network decreases to the FBHP (Flowing Bottom-Hole Pressure) of 500 psi.

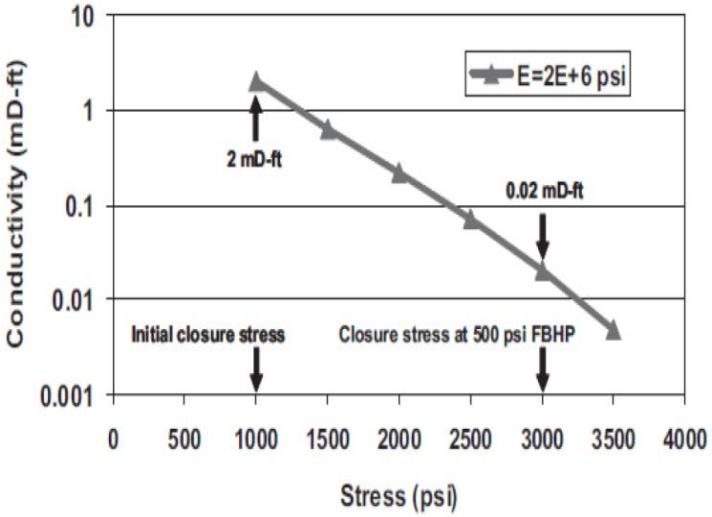

Figure 1.10: Effect of closure stress on un-propped-fracture conductivity, Marcellus shale example; after Cipolla *et al.* (2010).

Meanwhile, due to the extremely low permeability in unconventional reservoirs, many researchers assume that gas flow cannot be described by the Darcy law equation in shale formation (gas flow in nanopores). Processes such as Knudsen diffusion at the solid matrix separate gas flow behavior from Darcy-type flow. Based on this reason, dual-continuum models were known as inaccurate for shale reservoirs simulations. Instead, innovative approaches were proposed, where a coupling of Darcy flow and Fickian diffusion in matrix was taken into consideration. Such dual-mechanism approach was introduced for a better gas flow modelling in coal or shale formation, Ertekin *et al.* (1986); Clarkson *et al.* (2010). Others used the concept of apparent permeability taking into account Knudsen diffusion, gas slippage and advection flow. Javadpour (2009) presents a formulation for gas flow in the nanopores of mudrocks based on Knudsen diffusion and slip flow. Also, it was applied to modelling shale-gas at pore scale by Shabro *et al.* (2011, 2012). Moreover, Civan *et al.* (2010), calculate the apparent permeability

through the flow condition function, function of Knudsen number. Finally, others as Hudson *et al.* (2011, 2012), Yan *et al.* (2013) describe the shale reservoir using four categories; such as, organic porosity, inorganic porosity, natural fractures and hydraulic fractures.

Obviously, referred to the literature; it is remarkable the diversity of physical phenomena applied in shale-gas reservoirs modelling. Simply, due to the requirement to accurately modelling gas production from unconventional reservoirs, critical physics should be taken into consideration which may/could impact gas production from shale reservoirs. Also, facing ultra-low permeability in shale-gas formations with nano-pores, gas slippage effect or Klinkenberg effect may change significantly the formation permeability, especially in low reservoir pressure conditions. Klinkenberg effect is incorporated in the gas flow equation by modifying the gas phase permeability as a function of gas pressure (after, Wu *et al.* (1998)):

$$k_g = k_\infty \left(1 + \frac{b_k}{P_g}\right) \tag{1.3}$$

where, k_∞ is a constant, equal to the absolute gas-phase permeability under very large gas-phase pressure (where the Klinkenberg effect is minimized); and b_k is the Klinkenberg b-factor. Although b_k may change with gas nature and pore/threshold size and it is a function of the pressure, where we can use a constant value for shale-gas flow simulations.

Note that, in tight formations, the matrix permeability is subject to both the Klinkenberg effect and the geomechanical effect, with opposite impacts on results. When pressure decreases, the gas permeability increases because of the Klinkenberg effect, but at the same time decreases because of the geomechanical effect. Besides, Klinkenberg effect modifies only the permeability to gas, whereas the geomechanical effect modifies the absolute permeability for both gas and water flows.

In some gas reservoir, gas could condensate. Modelling liquid-rich shale reservoirs is a complex process. Numerous studies indicate that the PVT (pressure/volume/temperature) phase behavior of fluids in nano-pores of an unconventional reservoir deviates from phase behavior in large pores of conventional reservoirs (see for example, Morishige *et al.* (1997); Shapiro and

Stenby (1997); Zarragoicoechea and Kuz (2004); Singh *et al.* (2009); Travallonia *et al.* (2010); Devegowda *et al.* (2012); Nojabaei *et al.* (2013); Teklu *et al.* (2014); Wang *et al.* (2014)). The deviation in nanopores is a result of large capillary pressure, electrostatic interaction, van der Waals forces, and the fluid structural changes. When the pore size becomes very small, the capillary pressure between the wetting phase and the non-wetting phase becomes significantly large than the conventional reservoirs and affects phase equilibrium pressures. When the pore size is decreased further, the elevated interaction between the fluid molecules and pore walls starts to change the physical properties of the bulk fluid such as critical pressure and critical temperature, density, viscosity, and surface tension. Understanding the production mechanisms from such reservoirs is crucial in the overall effort to increase the ultimate hydrocarbon production.

Teklu *et al.* (2014) models phase behavior by taking into account the presence of high capillary pressure and the modification of critical points. Figure 1.11 shows the simulation of large pores (r_p = infinity) and small pores (r_p = 3 nm and r_p = 10 nm) phase envelopes for Bakken oil (Teklu *et al.* (2014)), where r_p is the pore radius. The thermodynamic properties (PVT) and phase behavior in tight reservoirs (nano-pores or confined pores) differ from the non-confined (large pores) related to conventional reservoirs. The differences are significantly high, and they will impact considerably production behavior for a gas condensate reservoir.

The phase behavior of organic nano-scale pores is very important on oil and gas recovery. Besides, thermodynamic phase behavior of hydrocarbon mixtures in these nano-pores and their effects on flow behavior is not well understood and has been a subject of great interest. Also, facing very tight low permeability in unconventional shale-gas reservoirs, hydrocarbon fluid properties and flow mechanisms is still not well understood. All these add complexities for shale-gas flow simulations.

Gas condensate will also arise some difficulties in numerical simulations. In fact, during production from shale reservoirs as pressure is reduced, the fluid will pass through the dew point where a liquid start to condense. As the reservoir further depletes and the pressure drops, liquid condenses from the gas to form a free liquid inside the reservoir. This is particularly true near the fracture faces, where the matrix pressure is very low and close to the fracture pressure. Thus, the presence of free liquid near fracture faces could decrease highly the gas relative permeability and

impedes gas recovery. Using a large or a small matrix gridblock near the fractures might provide significantly different results.

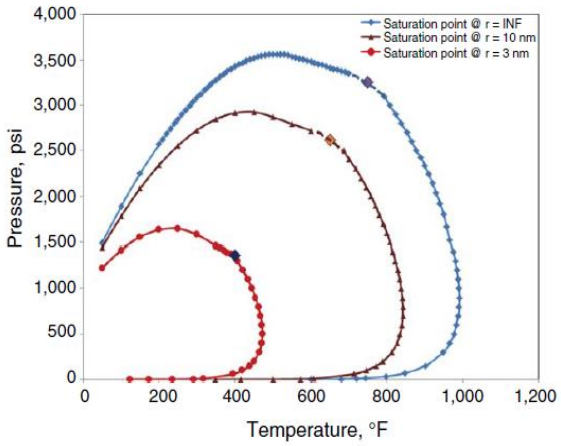

Figure 1.11: Phase envelope of Bakken oil in unconfined (rp = infinity) pores and confined pores (rp = 3 nm and rp = 10 nm); after Teklu (2014).

1.4 Fracturing Fluid Induced Formation Damage

Several mechanisms like, imbibition, relative permeability, gravity segregation and stress-sensitive fractures conductivities will control the behavior of trapped water. Only a part of pumped water can be reproduced during flowback and large quantities of fracturing fluid remained in the formation. High water saturation in the invaded zone near the fracture face will reduce greatly gas relative permeability and impede gas production.

Fracturing fluid induced formation damage has been studied in the literature since a long time; see for example, Holditch (1979), Friedel (2004), Gdanski *et al.* (2006), Wang *et al.* (2009), Ding *et al.* (2013). Recently, the fracturing fluid induced formation damage is particularly discussed in extremely low-permeability shale-gas reservoirs. Li *et al.* (2012) used an analytical model to study fracture-face matrix damage in shale-gas reservoirs. Cheng (2012) investigated formation damage effect with a numerical model. Agrawal and Sharma (2013) used a 3D numerical simulator to study gravity effect. Bertoncello *et al.* (2014) compared with experimental data and studied fracturing fluid induced the formation damage by modelling the flow into a single hydraulic fracture in a shale-gas reservoir. Also, Zanganeh *et al.* (2014) investigated the importance of modelling fracturing fluid and its flowback for better

predictions in hydraulically fractured shale reservoir simulations. For example, considering an area of high oil saturation, where the rock surface is preferentially water-wet and the rock is saturated with oil. In fact, water will imbibe into the smallest pores, displacing oil from the core when the system is in contact with water. The process of water invasion from oil-wet pore to water-wet pore is described in Figure 1.12(a). Firstly, due to high pressure fluid injection water invades into oil-wet pores. Once water remained in the oil-wet pores, water will naturally imbibe into water-wet pores due to high capillary pressures. Moreover, in order to model properly the flow behavior from unconventional reservoirs, the hysteresis of water-oil relative permeability should be considered in back flow and in drilling stage. The oil relative permeability is usually reduced during the period of the back flow. This hysteresis phenomenon is modelled in Figure 1.12(b) by two curves of relative permeability: an imbibition curve for the filtrate invasion during drilling and a drainage curve for flow production during the back flow.

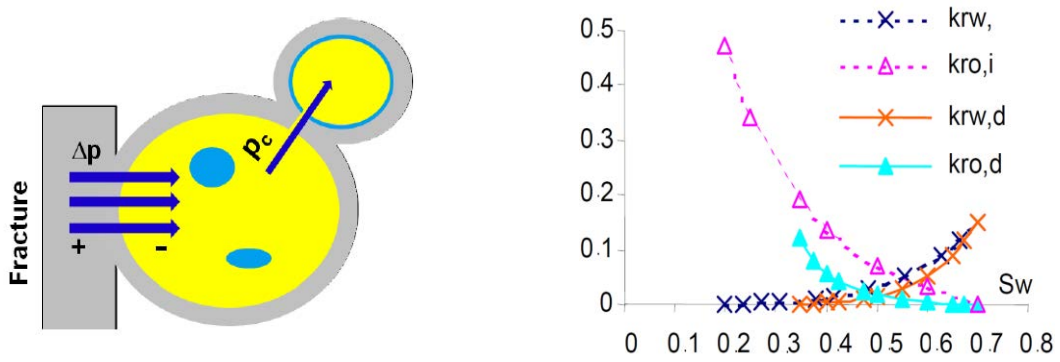

(a) (b)

Figure 1.12: Schematization of (a) naturally water imbibition into water-wet pores due to capillary pressures; after Bertoncello *et al.* (2014) and (b) relative permeability curves used during drilling (dashed line) and back flow (solid line) periods; after Ding *et al.* (2002).

Meanwhile, the capillary pressure is the mostly affecting phenomenon on gas production in tight formation due to the fluid invasion. The capillary pressure effect depends mainly on the interfacial tension and the wettability of the fluid. The wettability term is used to describe the relative adhesion of two fluids with a solid surface. In fact, when two immiscible (gas-fluid or fluid-fluid) fluids are in contact, the fluids are separated by an interface. Usually, at the interface molecules are in tension. Thus, the interfacial tension has the dimension of forces per unit length (newton/meter). However, when the fluid is in contact with the formation, the interface

intersects the rock with an angle Θ. Thus, the fluid wettability can be expressed by θ as a wettability angle, which is a function of the interface tension between the liquid and the solid. This contact angle is described by Young's formula:

$$\cos\theta = \frac{\sigma_{so} - \sigma_{sw}}{\sigma_{wo}} \tag{1.4}$$

where,

σ_{so} = interfacial tension between the solid and oil

σ_{sw} = interfacial tension between the solid and water

σ_{wo} = interfacial tension between water and oil

The capillary pressure, denoted P_c, is defined as the pressure difference at a local scale between two neighboring points on either side of an interface separating two immiscible fluids. The capillary pressure is defined as the pressure difference between the non-wetting and wetting phases:

$$P_c = P_{nw} - P_w \tag{1.5}$$

where, the indices nw and w refer respectively to non-wetting and wetting fluids.

Also, the P_c sign results of an arbitrary convention (here, it is chosen so that the capillary pressure is positive). For both water-oil and gas-oil couples, two capillary pressures can be defined:

$$P_{cw} = P_o - P_w$$
$$P_{cg} = P_g - P_o \tag{1.6}$$

Dealing with a water-oil case, the capillary pressure is not necessarily positive (a rock with an intermediate wettability case, for example). Additionally, the concept of the capillary pressure can be related to that of the saturation. In fact, the capillary pressure is equal to the interface curve multiplied by the interfacial tension. Meanwhile, in shale-gas reservoirs high capillary pressures are taking into account in presence of water due to the very small pore size.

In the literature, many papers studied the impact of water invasion and its impact on gas recovery. For example, Figure 1.13 (Bertoncello *et al.* (2014)), presents the gas rate for three different water invasion depths. Clearly, a decreasing in flow rates occurs at early time of production when water invasion is more important. Actually, fracturing fluid induced formation damage impacts mainly gas production from shale reservoirs at early time. A major concern after a hydraulic fracturing operation is water blocking effect in tight formation due to high capillary pressure and the presence of water sensitive clays. Although some studies were performed in laboratory or at core scale, few works discuss the impact of formation damage in a large SRV on shale-gas productions.

The simulation of fracturing induced formation damage on a SRV scale requires generally a great number of grid blocks and consequently a very large CPU time, which makes the simulation prohibitive.

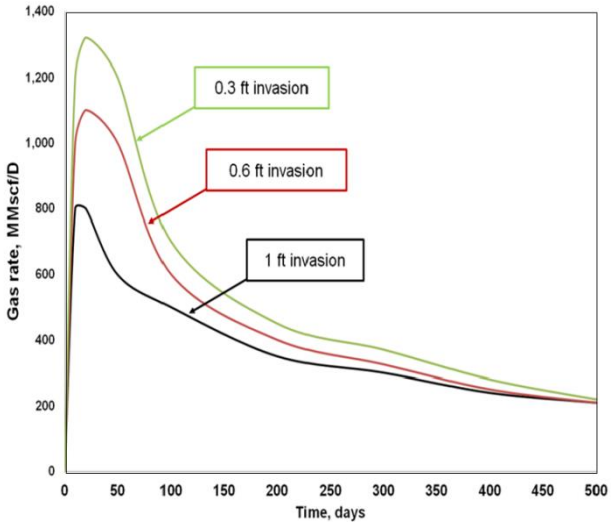

Figure 1.13: Impact of water invasion depth on gas rate; after Bertoncello *et al.* (2014).

In this report, we will study the hydraulic damage, due to fluid invasion into the formation, using a hybrid approach by simulating the full process of fracturing fluid invasion followed by a cleanup of loaded fluid in a complex fracture network in the whole stimulated

reservoir volume. The necessary of full-field information for the hydraulically fractured well simulation has been discussed in the literature; see for example, Ehrl and Schueler (2000); Lolon *et al.* (2007); Fazelipour, (2011); Delorme *et al.* (2013). In shale-gas formations, it is particularly necessary to take into account the presence of complex fracture network and their contribution on gas productions.

1.5 Research Objectives

Clearly, production from unconventional low permeability shale-gas/tight oil reservoirs has become an important source of gas in the world especially in the US. In 2011, gas production from shale formation has reached 30 percent of total production after comprising only 8 percent in 2007 (EIA, 2013). Consequently, the development of a realistic approach for gas flow modelling from shale reservoirs is a topic of an active research worldwide. Thus, researchers make a huge effort for understanding/recognizing the correct physics in order to describe flow transport in nano-porous shale reservoirs.

Usually, to simulate accurately flows in a fractured low permeability reservoir, it is required to explicitly discretize the fracture network and use very fine meshes around the fractures. However, the presence of a complex fracture network in shale reservoirs makes it impossible. In fact, discretizing the Discrete Fracture Network (DFN) make any reservoir simulator too CPU time consuming.

As generally recognized, dual-continuum (dual-porosity and dual-permeability) models are not suitable for simulating gas recovery from shale reservoirs due to the ultra-low formation permeability, large matrix block and a non-linear pressure variation into the matrix grid cell. In fact, the inter-porosity flow is treated by a quasi-steady-state flow formulation with a dual-porosity model. However, dual-continuum models present an efficient computational time comparing to an explicit discretized model, where an enormous grid cells is required to discretize each fracture explicitly. So, an approach combining explicit discretized model and dual-continuum model is extremely needed to make reservoir simulation efficient in terms of flow prediction and CPU time consuming.

First, in this work, a hybrid approach is proposed to model flow behavior from unconventional shale-gas reservoirs. In particular, we propose a hybrid approach associated with

the classic MINC (Multiple INteracting Continua) method in order to improve the matrix-fracture flow exchange known also by the inter-porosity flow. Moreover, this hybrid approach consists in a triple-continuum model, where high conductive fractures (propped) are explicitly discretized and natural, stimulated (non-propped) and non-stimulated fractures in the stimulated reservoir volume (SRV) are homogenized using a standard dual-porosity model. The matrix media of the dual-porosity model is subdivided into nested sub-volumes based on the MINC method taking into account all sorts of fracture distribution.

Furthermore, the efficiency and the ability of the hybrid approach are investigated through several numerical examples, including a small reservoir zone and a large SRV case treating a Warren and Root's fracture network type (regular discrete fracture network). On one hand, the study focuses on flow prediction from unconventional shale-gas reservoirs. On the other hand, the formation damage; due to hydraulic fracturing by simulating the full process of fracturing fluid invasion followed by a cleanup of loaded fluid in the whole SRV, is considered and studied. The ability of this hybrid approach to simulate correctly fracturing fluid invasion and its backflow under hydraulic fracturing between matrix and fractures is discussed.

Later in this work, our hybrid approach based on the classic MINC method is generalized to treat the irregular fracture distribution. The generalized approach is called DFM based on a MINC proximity function. Finally, a complex DFN is studied to quantify the ability and the robustness of our DFM based on a MINC proximity function for unconventional shale reservoirs simulations. A study concerning a shale-gas reservoir and a tight-oil reservoir with the presence of an irregular DFN distribution is presented. Note that, initially our study focuses on modelling flow from unconventional shale gas reservoirs. However, our DFM is also tested on a tight-oil reservoir example in order to test its ability to modelling flow from different types of unconventional reservoirs.

Chapter 2 - RESERVOIRS SIMULATION MODELS

Hydraulic fractures play an important role in gas production from unconventional low permeability shale reservoirs. Additionally, fractures may exist in various scales leading to a complex DFN as shown in Figure 2.1. As recognized, in order to enhance gas production from shale formations, hydraulic stimulation is required. Therefore, a higher heterogeneity with the presence of multi-scale fractures, including hydraulic and natural fractures (stimulated and/or un-stimulated), occurs through the reservoir and makes reservoir simulations and flow modelling from such reservoirs quite challenging. Nevertheless, fluid flow could be modeled by taking into account a single hydraulic fracture or a complex fracture network around the well (see, Figure 2.2).

In order to model properly gas flow from shale-gas reservoirs, different types (propped and/or non-propped, stimulated and/or non-stimulated) of multi-scale fractures must be incorporated in the reservoir simulation model. Usually, a single-porosity or dual-continuum models are used in shale-gas flow simulations. However, a single-porosity model is often too CPU time consuming due to the large number of grid cells and the dual-continuum models are not accurate for unconventional reservoir simulations.

So, in this chapter, a review on different simulation models, such as the single-porosity model with an explicit fracture discretization, the dual-continuum models presented by a single-permeability (2ϕ-1K) or a dual-permeability (2ϕ-2K) approach, the multi-porosity model, the classic MINC method and the discrete fracture model is presented.

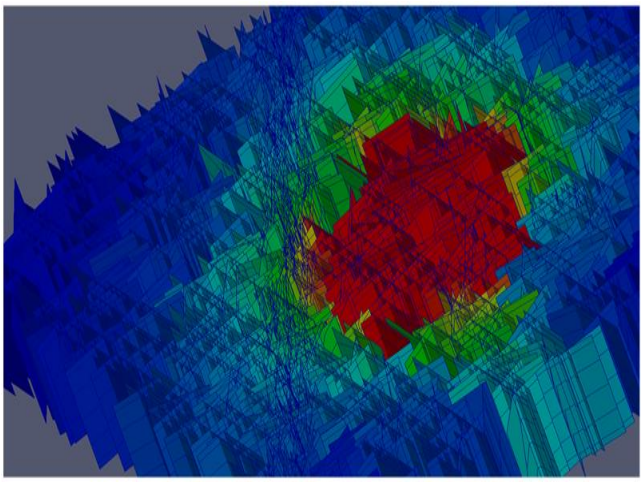

Figure 2.1: A large fracture network with an irregular fractures distribution; after Delorme *et al.* (2013).

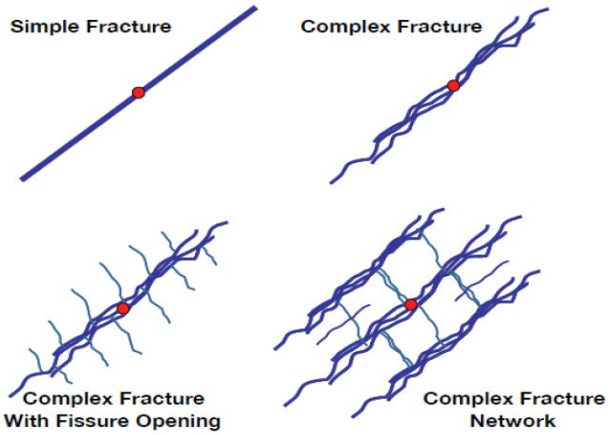

Figure 2.2: Schematic of the level of hydraulic fracture complexities; after Warpinski *et al.* (2008).

2.1 Explicit Fracture Discretization with Single-Porosity Model

As multi-scale fractures have a crucial role in shale-gas reservoir productions, these fractures should be modeled properly for a better gas recovery prediction from shale-gas reservoir simulations. According to the explicit approach; all fractures must be included and explicitly discretized using fine grid cells. Such approach was used by Cipolla *et al.* (2009b), Cheng (2010) in order to simulate shale-gas reservoir where fractures were represented using fine cells.

Moreover, Cipolla *et al.* (2009b), Ding *et al.* (2014a) used an approach known as DK-LS-LGR (Dual-Permeability-Logarithmically Spaced-Local Grid Refinement) which consists in discretizing explicitly the major fractures and refining the matrix media near the fractures by

using a logarithmic spacing for a better flow modelling into and from the fractures (matrix-fracture interaction). This method is a good technique for simulating hydraulic fractures in shale-gas reservoirs where it consists in discretizing all sorts of existing fractures. On one hand, the explicit discretized model with a single-porosity approach presents an advantage where it can model regular fracture network accurately as the fractures are known for their spatial distributions. On the other hand, due to the presence of multi-scale fractures in shale-gas formation, this technique is not a good approach for reservoir simulation as it requires a large number of grid cells and high computational CPU time. Furthermore, facing an irregular fracture distribution, this kind of model is not suitable for shale-gas reservoir simulations where an unstructured mesh is required. Moreover, the problem of CPU time can be bypassed using dual-continuum models such as, dual-porosity, dual-permeability or multi-porosity models.

2.2 Dual-Continuum Models

Originally developed by Barenblatt *et al.* (1960) and Warren and Root (1963), dual-continuum models represent the field with two systems, named matrix and fracture. For a better comprehension of the flow connections from a dual-porosity model, a schematic diagram and fluid flow method is given in Figure 2.3. Since it was proposed by Warren and Root (1963), dual-porosity model in addition to the dual-permeability model are the most commonly approaches used for modelling naturally fractured reservoirs in the petroleum industry. However, due to the ultra-low matrix permeability which emphasizes the transient period, dual-continuum models are not suitable for flow modelling in shale formation.

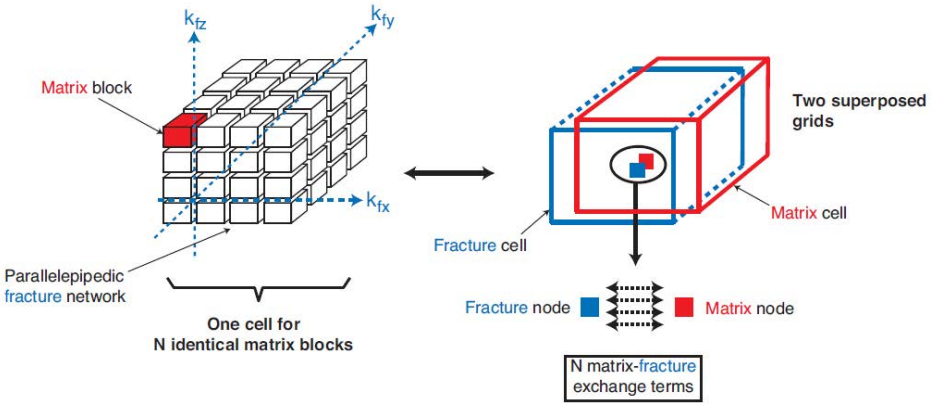

Figure 2.3: Flow connections in the dual-porosity method; after Karsten Pruess (1992).

2.2.1 Shape-Factor

The most commonly challenging problem concerning unconventional reservoir simulations is to modelling properly the matrix-fracture flow exchange. Performing reservoir simulations using dual-continuum models usually require a shape factor in order to calculate the matrix-fracture interaction. Since the dual-porosity model was introduced, many different values for the shape factor have been proposed in the literature.

Firstly, Warren and Root (1963) used the shape-factor concept to model fluid transfer between matrix and fractures. They introduced the following shape-factor:

$$\sigma_{n_d}^{WR} = \frac{4n_d(n_d+2)}{L_{n_d}^2} \tag{2.1}$$

where, $\mathbf{n_d}$ denotes the dimension and $L_{\mathbf{n_d}}$ denotes the matrix block size:

$$L_{1d} = L_x$$

$$L_{2d} = \frac{2L_xL_y}{(L_x+L_y)} \tag{2.2}$$

$$L_{3d} = \frac{L_xL_yL_z}{(L_xL_y+2L_xL_z+L_yL_z)}$$

After Warren and Root, Kazemi (1976) proposed the following shape-factor:

$$\sigma = \alpha \sum_{k=1}^{n_d} \frac{1}{L_k^2} \tag{2.3}$$

with, $\alpha = 4$ and with L_k denoting the matrix block size.

Coats (1989) mentioned that the shape-factor proposed by Kazemi is too low, and suggests a shape factor $\alpha = 8$. Lim and Aziz (1995) published a result similar to Chang (1993), which showed $\alpha = \pi^2$. In fact, they derived an analytical full transient solution of the diffusion equation for the single-phase flow and determined the shape factor under a pseudo-steady-state regime. Chang (1993), Lim and Aziz (1995) confirmed that shape-factor is actually not a constant, but a function of time. Quintard and Whitaker (1996) applied a mathematical technique consisting in averaging, at the overall scale of a matrix block, the single-phase Darcy flow equations describing local flows within the matrix block. Additionally, van Heel and Boerrigter (2006) presented various forms of shape-factor treating different physical phenomena such as diffusion and convection processes.

Table 2.1 summarizes the shape factors most used in the literature, the values in the table corresponds to σa^2, for a cubic block of lateral dimension a ($L_x = L_y = L_z = a$), exchanging fluids for 1D, 2D or 3D flow transfer cases.

Table 2.1: Comparison of Shape factors σa² reported in the literature; after Bourbiaux (1999).

Case	Warren and Root (1963)	Kazemi *et al.* (1976)	Coats (1989)	Lim and Aziz (1995)	Quintard and Whitaker (1996)
1D	12	4	8	π^2 (9.87)	12
2D	32	8	16	2 π^2 (19.7)	28.4
3D	60	12	24	3 π^2 (29.6)	49.6

2.2.2 Dual-Porosity Model (2ϕ-1K)

Due to their simplicity and computational efficiency, most fractured reservoir simulations are based on dual-continuum models, where the matrix-fracture interaction is modeled via a shape-factor. The dual-porosity approach represents the reservoir model with two systems (matrix and fracture). Figure 2.4 shows different concepts of fracture-matrix interactions using dual-continuum models. Figure 2.4(b) shows the concept of a dual-porosity model. Also, we should mention that a dual-porosity model is based on a pseudo-steady state flow regime modelling exchange flow between fracture and matrix continuum. Note that, this kind of model

is not suitable for shale-gas simulations due to the tight reservoir rock with very low matrix permeability (nano-Darcy).

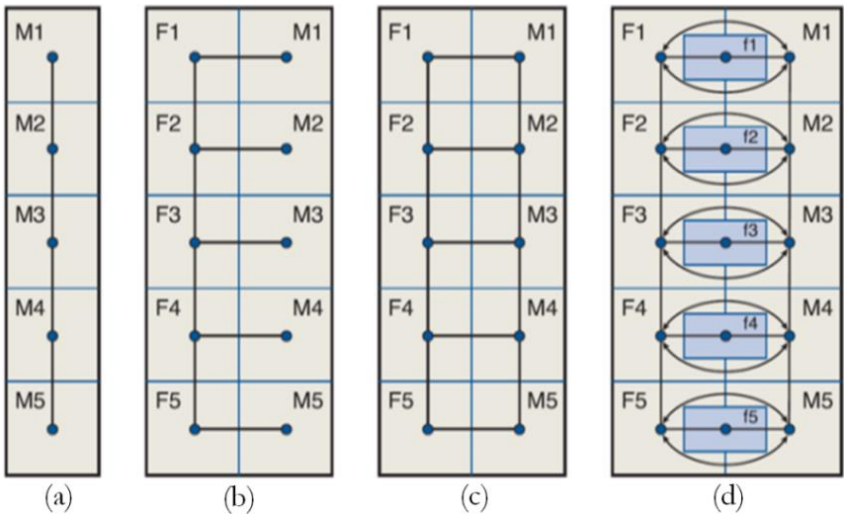

Figure 2.4: Schematic of different conceptualizations for handling fracture-matrix interactions: (a) effective-continuum model, ECM; (b) dual-porosity model; (c) dual-permeability model; and (d) multi-porosity, triple-continuum model. (M=matrix; F=large-fractures; f=small- fractures).

2.2.3 Dual-Permeability Model (2ϕ-2K)

These kinds of models have been incorporated in almost every commercial reservoir simulator, due to their simplicity to implement, and high computational efficiency. Figures 2.4(b) and (c), the difference between dual-porosity and dual-permeability is represented from these two conceptual models. In fact, a dual-permeability model allows matrix-to-matrix flow while a single-permeability one does not. Both models rely on a pseudo-steady-state condition for flow exchange between fractures and the matrix system.

The applicability of the dual-continuum models to unconventional reservoir simulation has been studied in the literature (see for example, Rubin (2010); Ding *et al.* (2014a)), where results show that these models are not able to properly model gas flow from very low permeability fractured shale reservoirs. In fact, the transient period is very long due to the large matrix block size and extremely low matrix permeability, and the conditions of a pseudo-steady-state flow are not satisfied (Wu and Pruess (1988)). However, dual-continuum models are suitable for conventional fractured reservoirs, where fluid transfers can be handled due to higher matrix permeability and the short transient period (see, Kazemi (1969); Wu *et al.* (2004)). In general, the dual-continuum models are no longer applicable to unconventional low permeability reservoirs.

However, the MINC method, which uses nested discretization for the matrix media, could provide a better handling of the inter-porosity flow, where the flow exchange between the matrix and fracture media is treated by a fully transient representation.

2.3 The Multiple INteracting Continua Method

A shale-gas reservoir primarily consists in three main types of porous media: organic matter, inorganic matter and natural fractures; where a fourth type called hydraulic/induced fractures occurs during hydraulic stimulation. It must be mentioned that, gas desorption and diffusion are the dominant physics in the organic matter or kerogen, where the organic content is expressed in term of TOC. Thus, the inorganic matrix contains clay, quartz and calcite particles. Bicheng Yan *et al.* (2013) presented a micro-scale multiple-porosity model for fluid flow in shale reservoirs. As unconventional shale-gas reservoirs present significant heterogeneity depending on multi-scale fractures (hydraulic fractures, stimulated natural fractures, natural fractures, micro-fractures) and matrix continuum, a multiple-porosity as presented in Figure 2.4(d) (or triple/multiple-continuum) is needed. Clearly, in shale-gas reservoirs, a large number of micro, medium and large fractures exist together with a heterogeneous matrix. All these media cannot be lumped into an averaged by one medium. However, the standard triple-continuum model proposed by Wu *et al.* (2004) is suffering from the same requirement of the pseudo-steady-state flow assumption as the dual-porosity model. If such pseudo-steady-state condition is not satisfied, the multiple-continuum model should be used in combination with the MINC concept to handle heterogeneity, as well as long lasting transient flow in the matrix system.

MINC stands for "Multiple INteracting Continua", originally developed by Pruess *et al.* (1982) and Pruess and Narasimhan (1985) to model heat and multiphase fluid flow in fractured porous media. This concept is able to describe gradients of pressures, temperatures, or concentrations near matrix surface and inside the matrix by further subdividing individual matrix blocks into one or multidimensional strings of nested meshes. Also, MINC is particularly suitable to media where the fractures are well connected (fracture network), so that a continuum treatment of flow in the fracture can be made. This method is a generalization of the dual-porosity (DP) concept.

The main difference between MINC method and a DP model is in the matrix-fracture exchange known also by "inter-porosity flow". The DP method simulates matrix-fracture exchange on the basis of a pseudo-steady state flow, while MINC method treats the problem entirely by numerical methods in a fully transient way. In other words, MINC method consists in a fully transient representation of the inter-porosity flow. Global flow in a fractured-porous media will flow through the fractures while matrix blocks can exchange fluid with the fractures. In general, the MINC model provides a better numerical approximation for transient fracture-matrix interactions than the dual-porosity model. Also, this technique was applied to various studies of fractured reservoirs (see, Nanba (1991); Farhadinia and Delshad (2010)).

Additionally, the concept of MINC method consists in partitioning of the matrix blocks into a sequence of nested volume elements as schematically shown in Figure 2.5(a), where a MINC6 model is presented and continuums # 1, 2, 3, 4, 5 and 6 represent the subdivision of the matrix media. Also, Figure 2.5(b) is a representation of MINC5, where 5 refers to the number of subdivisions in matrix media. This technique presents a solution concerning the matrix-fracture flow exchange, which seems suitable and more efficient than a standard dual-porosity model. Additionally, in case of multi-phase (gas and water) flow simulations, very fine subdivisions near fracture are required for a better simulation of fluid invasion and its backflow after a hydraulic operation, which can be modeled and accurately simulated using MINC method. Furthermore, the application of MINC method in partitioning the matrix media into nested volumes based on the distance from the fracture is not limited to a regular fractured network but can also be applied to an irregular network as shown in Figure 2.5(b).

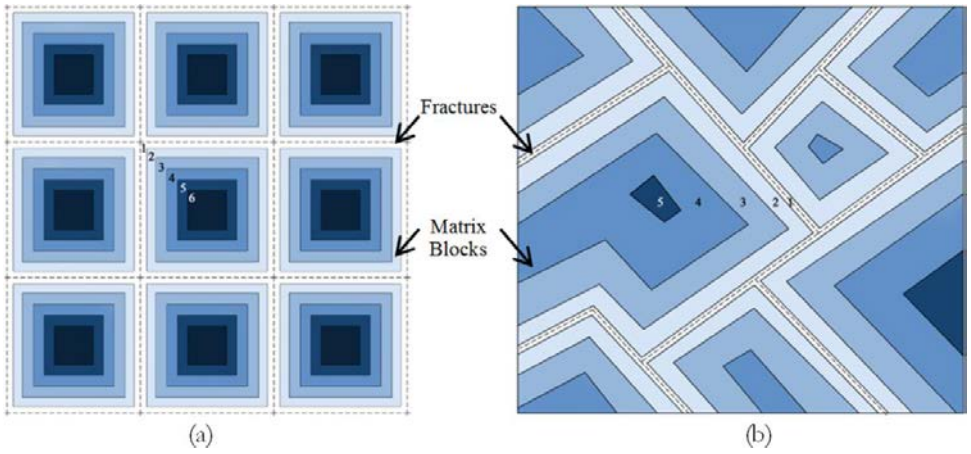

Figure 2.5: Schematic of the MINC concept for (a) a regular fractures network; after Pruess and Narasimham (1983) and (b) for an arbitrary fractures distribution; after Pruess (1982 and 1992).

2.4 Discrete Fracture Models (DFMs)

Usually, shale-gas formations are naturally fractured and fractures are irregularly distributed through the reservoirs. Such characteristics from shale formation increase the heterogeneity and the complexity of the reservoir simulation. Lately, to model a realistic reservoir fracture network, a new type of model called discrete fracture models (DFMs) has received a great attention. In fact, these kinds of models consist in discretizing complex fracture networks (hydraulic, reactivated, induced, micro-fractures, etc.). Early, Lee *et al.* (2001) proposed a Hierarchical Fracture Model (HFM) to model fluid flow from natural fractured reservoirs taking into account multi-length scaled fractures. Their concept consists in discretizing explicitly long fractures as major fluid conduits while short and medium fractures were homogenized. In fact, Homogenized fractures contribute in increasing the effective matrix permeability. Many techniques using DFMs were tested and studied in the literature (see, for example, De Dreuzy *et al.,* (2013)). Most applicable models called by Unstructured Discrete-Fracture Model (USDFM), Embedded Discrete-Fracture Model (EDFM) and iDFM (integrate Discrete Fracture Model), see for example, Karimi-Fard *et al.* (2004, 2006), Moinfar *et al.* (2011 and 2013b), Norbeck *et al.* (2014). Actually, most DFMs rely on unstructured grids to conform the geometry and location of the fracture network. These approaches are a new class of models which can accurately simulate fluid flow from naturally fractured reservoirs.

Karimi-Fard *et al.* (2004, 2006) developed a USDFMs based on an unstructured control-volume finite-difference formulation, where the rock matrix is modeled by 3D polyhedral cells and the fracture network is represented by a subset of the 2D interfaces separating grid cells. Figure 2.6(a) depicts a 2D example of fracture network defined in a physical domain. The physical domain is discretized using unstructured grids, where the matrix is represented by 2D control volumes and the fractures by 1D control volumes. The thick line segments in the grid domain represent the fractures. Also, as shown in Figure 2.6(b), each control volume is associated with a node. It must be mentioned that, this type of DFMs could be implemented in any reservoir simulator to accurately capture the complexity of a fractured reservoir. Otherwise, generation of such grid for an arbitrary fracture network can be a substantial challenge.

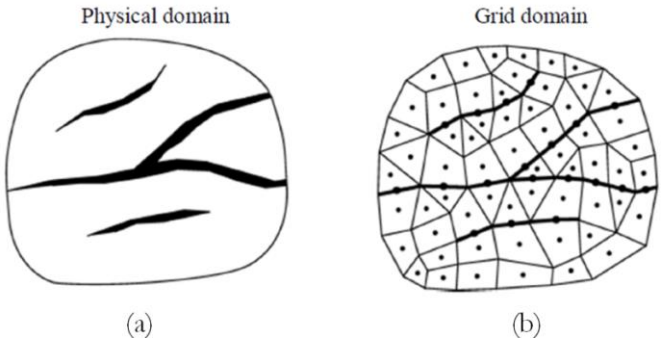

Figure 2.6: Illustration of a (a) 2D example of a fractured porous medium and (b) an unstructured model consisting in a control-volume finite-difference formulation; after Karimi-Fard *et al.* (2004).

Moinfar *et al.* (2011 and 2013b) introduce a new type of discrete fracture models called EDFMs. Generally, EDFMs consist in modelling fractures embedded in a structured matrix grid. Also, Norbeck *et al.* (2014) presents an iDFM where a numerical model was developed, aiming to capture the dynamic behavior of fractured reservoir systems in which both the properties of individual fractures and the connectivity of fracture networks are expected to evolve over time. The approach proposed by Jack Norbeck *et al.* (2014) consists in coupling fluid flow in fractures to mechanical deformation of the fractures. Thus, the fracture mechanics and propagation calculations are done using the strategy introduced by McClure (2012). Also, to incorporate matrix-fracture mass exchange into geomechanical model, the HFM approach was adopted from Lee *et al.* (2001).

Furthermore, using DFMs present several advantages. Actually, these types of models use a structured grid representing the matrix media, while the flow exchange is done through transmissibility calculation depending on fracture intersection with the matrix grid. The approach proposed by Moinfar *et al.* (2013b), employed a structured grid bypassing entirely the challenges associated with unstructured gridding required for other discrete fracture models. In fact, this approach consists in modelling fractured reservoirs using two completely different domains, matrix and large scale fractures. Hence, it offers a computational efficiency while simulating fluid flow in natural fracture reservoirs. So, using discrete fracture models, a structured grid is usually used to represent the homogenized matrix media, where the intersection between fractures and the matrix grid should be quantified. Here some possible intersections between the two domains are schematized in Figure 2.7.

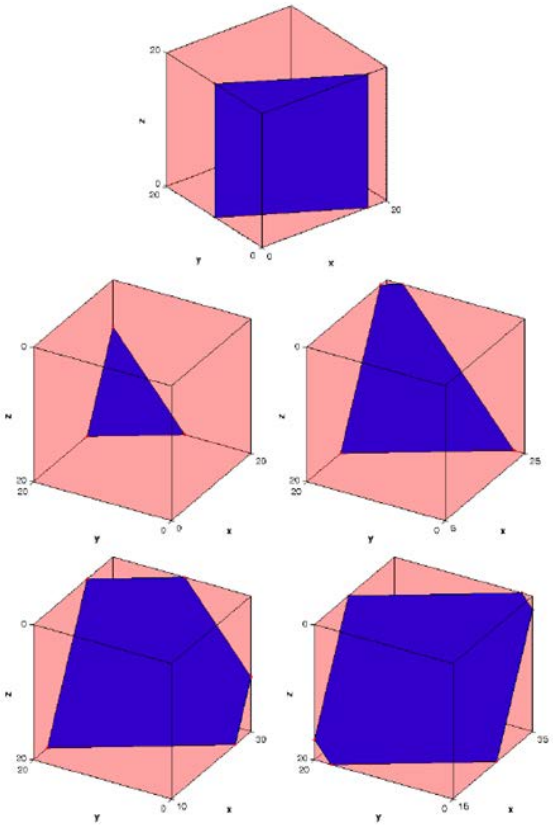

Figure 2.7: Possible intersections of vertical, an inclined fracture plane and a matrix gridblock, which can be rectangle, triangle, quadrilateral, pentagon, hexagon; after Ali Moinfar (2013a).

A non-neighboring connection (NNC) is generally required for the DFM approach. Moinfar *et al.* (2013) represents three possible types of NNCs (see, Figure 2.8), which are required to implant in the reservoir modelling the different connections between (a) a fracture cell and its neighboring matrix grid cell, (b) two intersecting fractures and (c) two cells of an individual fracture crossing through two matrix grid cells.

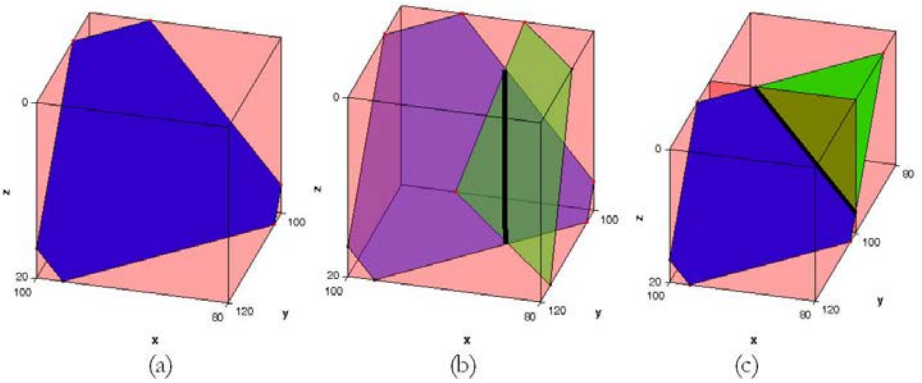

Figure 2.8: Three possible connections in DFMs; after Moinfar (2013a).

Hence, after identifying the possible connections between fractures and matrix media, transmissibility must be calculated.

In the literature, Hajibeygi *et al.* (2011) presents an appropriate approach using an analytical method to calculate the average distance between fracture and its neighboring rock matrix. The average distance between a matrix cell and a fracture cell is donated by $< d >$, which can be calculated by Equation (2.4). Furthermore, analytical expressions of particularly cases and different possible 2D scenarios are presented in Figure 2.9.

$$< d > = \frac{\int_V d(x')\, dx'}{V} \tag{2.4}$$

Most DFMs rely on analytical expressions concerning the mean distance. However, naturally fractured reservoirs present very complex fractures network. Obviously, the approach based on analytical expressions may not be applicable, especially when several fractures present in the same matrix cell. So, other techniques are required to be studied for efficient transmissibility calculations.

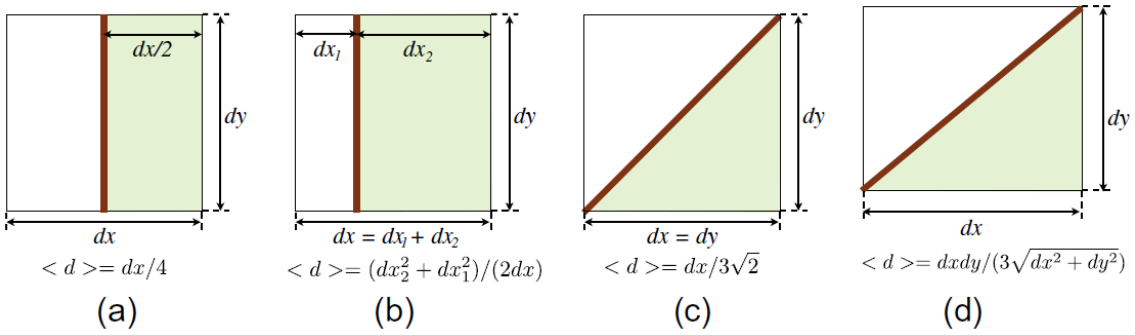

Figure 2.9: Different analytical expressions of <d> for some selected 2D scenarios; after Hajibeygi *et al.* (2011).

2.5 Governing Equations

As presented above, both single-porosity and dual-porosity models can be used in reservoir simulations. In case of dual-porosity model, two continua (matrix and fracture) should be considered. The general equations governing three-phase, multi-component, three-dimensional flow in naturally fractured reservoirs with a dual-porosity model, are written in the

follows. The mole conservation for each component c in a dual-permeability system is expressed as:

$$\frac{\partial}{\partial t}\left[\emptyset^f \sum_p \left(\rho_p^f C_{cp}^f S_p^f\right)\right] + div\left[\sum_p \left(\rho_p^f C_{cp}^f \vec{u}_p^f + \vec{j}_{cp}^f\right)\right] - Q_{cp}^{mf} - \sum \rho_p^f C_{cp}^f q_p^f = 0 \qquad (2.5)$$

and

$$\frac{\partial}{\partial t}\left[\emptyset^m \sum_p \left(\rho_p^m C_{cp}^m S_p^m + v_{sg}\right)\right] + div\left[\sum_p \left(\rho_p^m C_{cp}^m \vec{u}_p^m + \vec{j}_{cp}^m\right)\right] + Q_{cp}^{mf} - \sum \rho_p^m C_{cp}^m q_p^m = 0 \qquad (2.6)$$

where the superscript f refers to the fracture, superscript m to the matrix and subscript p to the phase. $\emptyset^m$, $\emptyset^f$ are the matrix and fracture porosity, respectively. C_{cp}^M is (for medium $M = f, m$) the mole fraction of component c in phase p and S_p^M (for medium $M = f, m$) the saturation of the phase p. ρ_p^M is the mole density of phase p in medium $M = f, m$. v_{sg} corresponds to the gas sorption term, and it appears only in the gas component conservation equation in the matrix media. $\vec{u}_p^M$ is the velocity of phase p in medium $M = f, m$. $\vec{j}_{cp}^M$ is the molecular diffusion and dispersion flux of component c in phase p in medium $M = f, m$. Also, q_p^M is the sink/source term of phase p per unit volume of formation in medium $M = f, m$. Q_{cp}^{mf} is the matrix-fracture mass flow rate of component c in phase p per unit bulk volume of reservoir.

The phase velocity is expressed in both media as usually with the Darcy equation:

and $$\vec{u}_p = -k\frac{k_{rp}}{\mu_p}\overline{grad}(\Phi_p) \qquad (2.7)$$

$$\Phi_p = P_p - \rho g Z$$

where Z is depth (positive, increasing downwards), g is the algebraic value of gravitational acceleration projection on z axis. k is the absolute permeability tensor of the medium, P_p the pressure of phase p, μ_p the viscosity of phase p, k_{rp} the relative permeability of phase p. Full tensor permeabilities are often required to describe complex reservoirs, especially fractured reservoirs.

For simplicity, let us consider a gas-water two-phase flow problem. It is assumed that the gas and water components are present only in their associated phases and adsorbed gas is within the solid phase of rock. Also, molecular diffusion and dispersion flux of component are neglected. In this case with a dual-continuum model, the mole conservation is applied to each component p ($p = g$ for gas and $p = w$ for water) in both matrix and fractured media, and Equations (2.5) and (2.6) are simplifies by:

$$\frac{\partial}{\partial t}\left(\emptyset^f \rho_p^f S_p^f\right) + div\left(\rho_p^f \vec{u}_p^f\right) - Q_p^{mf} - q_p = 0 \tag{2.8}$$

$$\frac{\partial}{\partial t}\left(\emptyset^m \rho_p^m S_p^m + v_{sg}\right) + div\left(\rho_p^m \vec{u}_p^m\right) + Q_p^{mf} - q_p = 0 \tag{2.9}$$

In a dual-porosity model, if the single-permeability concept is applied, the term $div\left(\rho_p^m \vec{u}_p^m\right)$ in Equation (2.9) is ignored. In the following, we will discuss how to simulate the specific shale-gas flow physics with the above model and the numerical discretization aspects that are involved in the implementation of that model.

Although gas desorption from kerogenic media has been studied extensively in coalbed methane reservoirs, and several models have been developed for such reservoirs (Clarkson and Bustin (2010)), the sorption properties of shale are not necessarily analogous to coal (Leahy-Dios

et al. (2011)). The most commonly used empirical model describing sorption onto organic carbon in shales is analogous to that used in coalbed methane and follows the Langmuir isotherm (Langmuir (1916)).

The sorption term in Equations (2.6) or (2.9) is calculated by:

$$v_{sg} = (1 - \emptyset^m - \emptyset^f)\rho_{sc}\,\rho_r V_s \tag{2.10}$$

where V_s is the volume of adsorbed gas in standard conditions per unit mass of solid, ρ_r is the solid rock density, and ρ_{sc} is the gas mole density at standard condition.

The system equations Equations (2.8) and (2.9) are discretized in space using a control-volume method. Time discretization is carried out using a backward, first-order, fully-implicit, finite-difference scheme. In this section, we will particularly study spatial discretizations for the flow term across an interface between two neighboring cells (transmissibility calculation) and for the matrix-fracture exchange in a dual-porosity model and with the MINC approach. The analysis for the transmissibility calculation is particularly useful for explicit discretization of fractures with a single-porosity model. The investigation of MINC method and study new techniques is helpful to improve the calculation of matrix-fracture exchange in a dual-porosity model (see, Figure 2.10).

For simplicity, we consider only the discretization of the transport equation for a single-porosity model. This equation is very similar to the transport equation of the matrix media Equation (2.9) in the dual-porosity model. By neglecting the sorption term and the matrix-fracture exchange term, the discretization of Equation (2.9) on a cell i with a control volume method is given by:

$$\left[\left(\emptyset^m \rho_p^m S_p^m\right)_i^{n+1} - \left(\emptyset^m \rho_p^m S_p^m\right)_i^n\right]\frac{V_i}{\Delta t^{n+1}} - \sum_{j \in N_i} F_{p,ij}^{n+1} - q_{p,i} = 0 \tag{2.11}$$

where the superscript $\mathbf{n}$ denotes the previous time step, and $n+1$ the current time step to be solved; Δt^{n+1} is the timestep size; V_i is the volume of the cell i; N_i contains the set of direct neighboring cells j of cell $\mathbf{n}$; $F_{p,ij}$ is the flow term between cells i and j; and $q_{p,i}$ is the sink/source term in cell i.

The flow terms F_{ij} in the above equation are mole fluxes by advective processes. When Darcy's law is applicable, this term is written as:

$$F_{p,ij} = -\int_{\Gamma_{ij}} \lambda_p k \frac{\partial \Phi}{\partial n} d\sigma \tag{2.12}$$

where Γ_{ij} is the interface between cells i and j, λ_p is the mobility term of phase p, k is the absolute permeability, Φ is the potential, and $\mathbf{n}$ is the normal direction at the interface Γ_{ij}. Taking a simplified two point flux approximation scheme, the discretization of the flow term is given by:

$$F_{p,ij} = \lambda_{p,ij} T_{ij} (\Phi_{p,j} - \Phi_{p,i}) \tag{2.13}$$

where $\lambda_{p,ij}$ is calculated with an upstream scheme; T_{ij} is the transmissibility between cells i and j, calculated with a weighted harmonic average for a two-points scheme (Figure 2.11):

$$T_{ij} = A_{ij} \frac{k_i k_j}{D_i k_j + D_j k_i} \tag{2.14}$$

where A_{ij} is the area of the interface between cells i and j; D_i and D_j are respectively the distances from the cell centers i and j to their interface; k_i and k_j are respectively the absolute permeabilities in cells i and j in the direction orthogonal to their common interface.

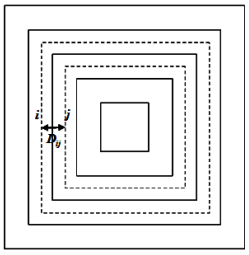

Figure 2.10: Connection transmissibility calculation using MINC method.

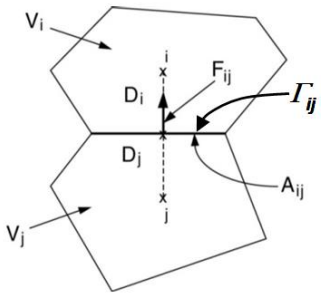

Figure 2.11: Transmissibility calculation using a two points flux approximation scheme.

Meanwhile, in a dual-porosity model, the flow exchange term between coupled matrix and fracture cells is calculated by:

$$Q_{cp}^{mf} = C_{cp}^{mf} \lambda_p^{mf} \sigma (\Phi_p^m - \Phi_p^f) \tag{2.15}$$

where λ_p^{mf} is the mobility term to phase p; Φ_p^m and Φ_p^f are the matrix and fracture potential respectively; σ is the shape factor, characterized by the geometry of matrix block(s) and the matrix permeability under pseudo-steady-state flow.

However, as the matrix permeability in the shale-gas reservoir is very low, the flow can be in transient regime during several years before stabilizing in a pseudo-steady-state regime. Therefore, the dual-porosity model is generally not accurate enough for flow simulations in the shale-gas reservoir using a shape factor obtained under pseudo-steady-state condition. Nevertheless, the MINC method could improve the matrix-fracture flow exchange by introducing an entirely a transient solution based on a numerical approach.

In the MINC approach, the matrix block is subdivided according to a criterion based on the distance from the fracture in order to build a pattern of nested meshes. The flow transport is governed by Equations (2.8) and (2.9) in the fractures and the matrix media, respectively. The discretization for inter-porosity flows in subdivision cells is still written in the form of Equation (2.11) with flow exchange between two neighboring cells calculated by Equation (2.12) or Equation (2.13). The key point of the MINC method is the approximation of the flow term F_{ij} between two neighboring nested meshes expressed by Equation (2.12). Considering a square matrix block (2D problem) and assuming the matrix permeability k_m is constant, the discretization form of the flow F_{ij} between two neighboring sub-cells i and j is still given by Equation (2.13) with the transmissibility T_{ij} given by:

$$T_{ij} = k_m \frac{A_{ij}}{D_{ij}} \tag{2.16}$$

where, A_{ij} is the area of the interface between these two sub-cells and D_{ij} is the average distance between the two sub grids. This approach is reasonably accurate, if the potential is constant in each ring (dashed lines in Figure 2.10). It is generally true for sub-cells near the boundary, especially in early-time. But it is less accurate for fluid flow approximation near the matrix block center. Ding *et al.* (2014a) propose an approach based on iso-potential lines for matrix block subdivisions and for the transmissibility calculation to improve the MINC method. This approach improves the MINC method for single-phase flow simulations.

Chapter 3 - HYBRID APPROACH BASED ON THE CLASSIC MINC METHOD

The objective of this work is to propose a simulation technique in order to model properly the gas flow from low permeability unconventional shale-gas reservoirs. However, improving the flow modelling of the matrix-fracture interaction especially for multi-phase flow problems in shale-gas reservoirs remains the main objective.

In this chapter, a hybrid approach for unconventional shale-gas reservoir simulations is proposed. This hybrid approach model consists in a triple-porosity model associated with the classic MINC method. Moreover, this model treats the fractures in a hierarchical way, where the fractures are classified based on a conductivity criterion. Note that, high conductive fractures such as hydraulic fractures are explicitly discretized while low conductive fractures (natural and un-propped) are homogenized within a standard dual-porosity model. However, the matrix medium is subdivided based on the concept of the MINC method.

The ability and the efficiency of our hybrid approach to model properly flow from unconventional shale-gas reservoirs is also tested. Our hybrid approach is compared to an explicit discretized model with a single-porosity approach set as a reference solution. Note that, the explicit model consists in very fine grid cells where all sort of fractures are explicitly discretized taking into account a LGR (Local Grid Refinement) technique.

In this chapter, the numerical results for both single and two-phase flow simulations with a regular fracture network are presented. The impact of fracturing fluid invasion on gas recovery from shale-gas reservoirs is discussed.

3.1 Methodology

In general, unconventional gas reservoirs are naturally fractured with low reservoir permeability. Furthermore, the presence of multi-scale fractures increases the heterogeneity and complexity of reservoir simulations. In fact, simulations where fractures are explicitly discretized using a single-porosity model requires very fine grid cells as fracture width is small. This kind of approach can give us a very accurate flow modelling into and from fractures. However, it involves a large number of cells which is not suitable for the reservoir simulations due to the high CPU time. Moreover, the commonly used dual-porosity approaches based on pseudo-steady-state flow regime are inadequate for solving fluid flow from such reservoirs facing tight reservoir rock with nano-Darcy permeability. Lately, new type of models called discrete fracture model (DFM) have received a great attention. These models consist in discretizing reservoirs fractures, and need efficient transmissibility calculation between fractures and matrix cells.

In this part, we will present our hybrid approach based on the concept of MINC method for a regular fracture distribution. In other words, we will study the ability of this approach on Warren & Root fracture type.

The MINC approach was investigated by Ding *et al.* (2014a) for the single-phase flow simulation in shale-gas reservoirs. The purpose of the MINC method implementation is to improve the two-phase flow simulations via the matrix-fracture interaction in extremely low-permeability fractured reservoirs. Note that, for a two-phase flow simulation, fine grids around the fractures are needed in order to quantify the presence of fluid near fracture faces. However, using a standard dual-continuum approach, this matter is not possible.

As flow modelling from shale reservoirs is very complicated due to the presence of a complex multi-scale fracture network. In order to overcome the complexity of flow simulation from unconventional reservoirs, we propose to treat the reservoir into three different zones. In other words, our fractures will be classified using a hierarchical technique based on fracture conductivity. Lee *et al.* (2001) presented a hierarchical approach based on fracture length. In this work, a criterion on fracture conductivity will be taken into account.

Once our fractures are created, a classification between high and low conductive fractures will be done. Firstly, in the SRV zone a standard dual-porosity approach is applied. So, low conductive densely natural and micro fractures are homogenized as one fractured media in the

SRV zone. However, high conductive hydraulic fractures are explicitly discretized, and the interaction between high conductive hydraulic fractures and the homogenized fractured media and considered.

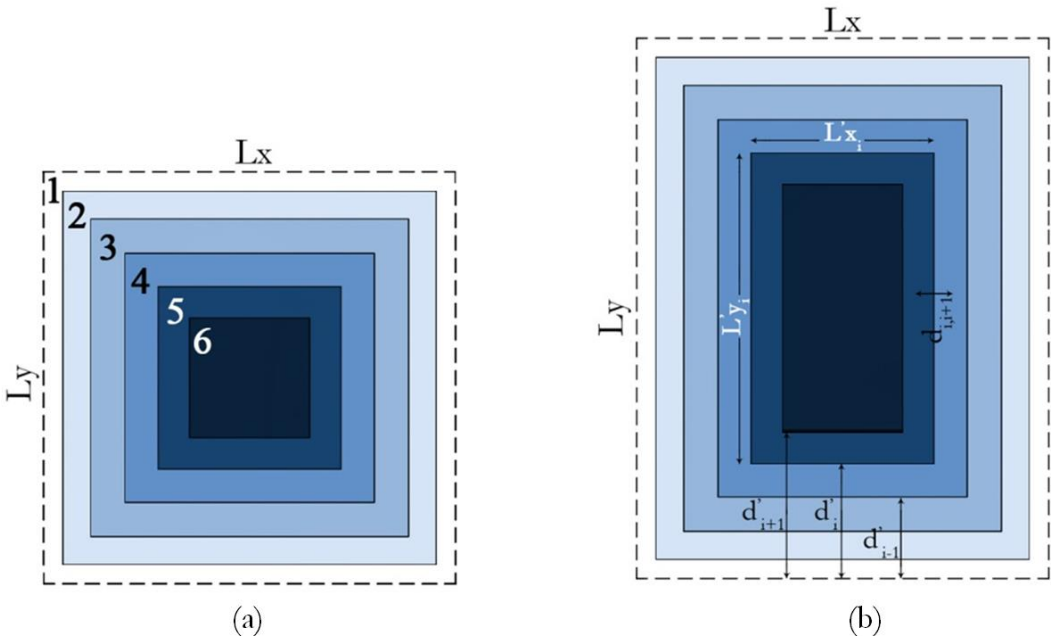

Figure 3.1: A MINC6 model (a) for a 2D square case Lx = Ly and (b) for a 2D rectangular case where Lx ≠ Ly.

The MINC method is applied to the flow exchange between the matrix and the homogenized fractures. Note that, for a squared matrix block where the block dimensions in x and y directions are equal with $L_x = L_y = L$ as shown in Figure 3.1(a), the formulas presented by Pruess and Narasimhan (1985) are taken into consideration. However, if a rectangular Warren and Root's fracture type case is faced we propose to calculate the exchange area and the average distance between sub grids cells of the MINC method differently. An illustration of an example where the grid block dimensions are different ($L_x \neq L_y$) is presented in Figure 3.1(b).

The calculation of the average distance between subdivisions will be described hereafter. In fact, the user is able to define the number of matrix refinement and the fraction volume of each subdivision. In other words, the volume of each subdivision is known. Let's suppose the 2D example presented in Figure 3.1(b) with L_x and L_y representing the grid dimensions in x and y

direction respectively. The main objective here is to calculate an equal distance d_i' from the fractures for each subdivision.

For example, let's consider L'_{x_i} and L'_{y_i} are the dimensions of a subdivision i. So, the volume of subdivision i defined by fraction volume f_i is written by Equation (3.1):

$$L'_{x_i} L'_{y_i} = f_i * L_x L_y \tag{3.1}$$

where,

$$L'_{x_i} = L_x - 2d_i' \qquad L'_{y_i} = L_y - 2d_i' \tag{3.2}$$

Combining Equations (3.2) and (3.1):

$$(L_x - 2d_i')(L_y - 2d_i') = f_i * L_x L_y \tag{3.3}$$

$$4d_i'^2 - (2L_x + 2L_y)d_i' + (1 - f_i) * L_x L_y = 0$$

$$d_i'^2 - \frac{(L_x + L_y)}{2} d_i' + \frac{(1 - f_i)}{4} * L_x L_y = 0 \tag{3.4}$$

Solving this second order polynomial of d_i', the distance d_i' of each subdivision from the fractures (dashed lines in Figure 3.1) is calculated using the fraction f_i of each matrix subdivision. Once the distances from the fractures to each subdivision face are known, then the average distance $d_{i,i+1}$ between two consecutives subdivisions could be calculated. Moreover, the surface exchange $A_{i,i+1}$ and the transmissibility $T_{i,i+1}$ between two consecutives matrix subdivisions i and $i + 1$ are calculated by the following equations:

$$A_{i,i+1} = 2\left(L'_{x_i} + L'_{y_i}\right) * Z_{Depth} \tag{3.5}$$

$$T_{i,i+1} = \frac{k_m A_{i,i+1}}{0.5 * d_{i,i+1}} = \frac{2 * k_m A_{i,i+1}}{d_{i,i+1}} \tag{3.6}$$

where, Z_{Depth} corresponds to the depth of the studied grid cell.

Furthermore, a single-porosity model is applied to the non-SRV region (matrix formation). As two different zones are presented, SRV and non-SRV zones, a transition zone which connect these two media exists. In order to model properly the flow between the two zones, we suggest to apply a refinement on the border of the SRV. In fact, a LGR technique is taken into consideration connecting the non-SRV/SRV regions using a 1D MINC approach (see, Figure 3.2 and Figure 3.3) in order to improve the flow exchange between these two regions. It must be mentioned that, concerning the transition area, matrix media on the border of the SRV zone is connected with the homogenized (DP/MINC) fracture media inside the SRV.

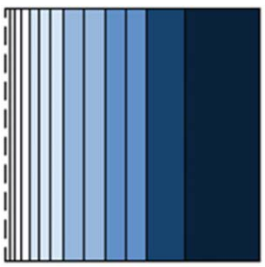

Figure 3.2: One-dimensional (a) fracture model in y-direction and (b) its optimization using the MINC method.

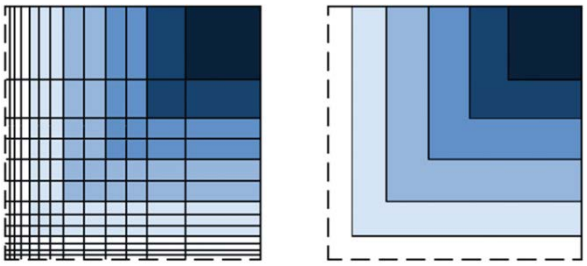

Figure 3.3: Two-dimensional fracture model for (a) a discretized model and (b) the MINC optimization with nested sub-grids.

The transmissibility between a high conductive hydraulic fracture and the fractured media (DP/MINC) inside the SRV zone needs to be correctly calculated, for example, using an integral approach (Ding *et al.* (2014b)). In this chapter, for hydraulic fractures oriented along the grid axes as show in the example of Figure 3.4, the following equation is used:

$$T_{Hydraulic/Homogenized\ Fractures} = \frac{k_{Bperx} * k_F * (d_{Bfrac} + d_F)}{k_{Bperx} * d_F + k_F * d_{Bfrac}} * \frac{A_{exchange}}{d_{Bfrac} + d_F} \approx \frac{k_{Bperx} * A_{exchange}}{d_{Bfrac}} \tag{3.7}$$

where, k_{Bperx} is the homogenized block permeability in the x-direction, k_F is the fracture permeability, d_{Bfrac} is half length of the block size in x-direction, d_F is the half aperture of the hydraulic fracture and $A_{exchange}$ represents the exchange area between these two media.

The benefits from using a hybrid approach are numerous. Firstly, this approach reduces the number of grid cells comparing to a reference solution where fractures are explicitly discretized. In fact, decreasing the number of grid cells will result in decreasing the computational time. Performing simulations using the hybrid approach takes seconds or minutes rather than hours or days comparing to an explicit discretized model on the same hardware. Secondly, this approach is accurate for shale-gas reservoir simulations, where a similar trend could be found with a minimum time which is benefit for petroleum companies and research studies.

Hereafter in this work, we will present a comparison between this new approach and a reference solution (simulation with an extremely refined grid with an explicit fracture discretization using a single-porosity model) for different fracture spacing. Additionally, various physical processes could be tested with this hybrid model, for example, adsorption/desorption, geomechanics effect, Klinkenberg aspect, etc.

The main purpose is to improve matrix-fracture flow exchange. Based on the MINC approach, the matrix media is subdivided into several nested volumes, and this is more suitable than a dual-porosity/permeability method to modelling matrix-fracture interaction and handling the physics of such flow. Moreover, the MINC concept could be a solution of the inter-porosity flow, where this approach can treat this problem entirely by a fully transient representation. In fact, the stimulated fracture network could be represented by regular fracture geometry with a uniform spacing in the SRV. As explained before, a standard MINC method (2D approach) was used inside SRV, together with a single-porosity approach in the non-stimulated zone. In the

transient area between SRV and non-stimulated volume, a 1D MINC approach by using nested fine cells around the fracture in x/y-direction (see, Figure 3.4).

Furthermore, a reservoir example discussing the impact of hydraulic damage due to fracturing fluid invasion into a tight formation by simulating the full process of fracturing operation in a complex fracture network from shale-gas reservoirs is presented. To simulate correctly fracturing fluid invasion and its backflow, very fine cells are required near the fractures for fracture-matrix interaction simulations as fluid invasion is generally shallow in the tight formation. Additionally, for a better gas flow modelling fluid transport should be considered in multi-scale fracture network.

The proposed hybrid approach associated with the concept of MINC method is perfectly suitable for simulation of this kind of problems. This hybrid approach provides a solution for a better reservoir simulation in shale formations. Furthermore, the hybrid model explicitly describes the dominant role of primary fractures (or flow conduits), as well as it offers a computational efficiency where the number of grid cells is greatly reduced.

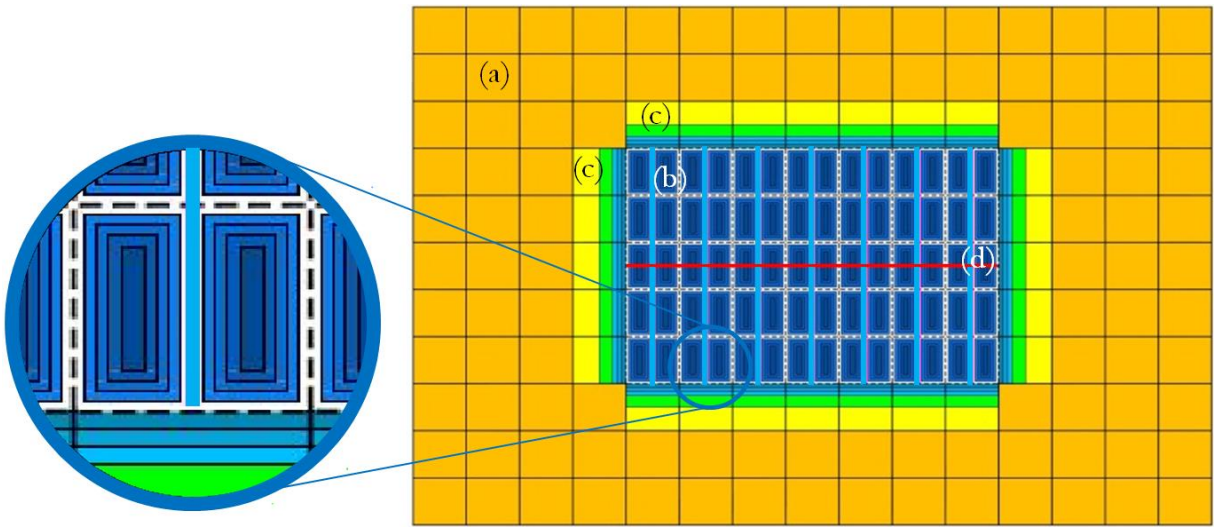

Figure 3.4: Illustration of the proposed hybrid approach, where (a) a non-SRV region, (b) a SRV region where the Classic MINC method is applied, (c) a transition zone where a refinement using 1D MINC method is applied on the border of the SRV region and (d) a horizontal well.

3.2 Small Reservoir Zone

In this part, a simple case considering a single squared matrix block of 200 ft in x and y directions is studied. Figure 3.5(a) presents the explicit discretized model where the fractures are represented by dashed lines and surrounded the matrix grid block. On the other hand, Figure 3.5(b) presents the 2D dimensional MINC optimization. . The net thickness of the reservoir in z direction is of 300 ft. In this study, the permeabilities are defined as 0.0001 mD in the matrix and 2 D in the fractures. The fracture aperture is fixed at 0.005 ft. Furthermore, the porosity of the matrix media is 0.05.

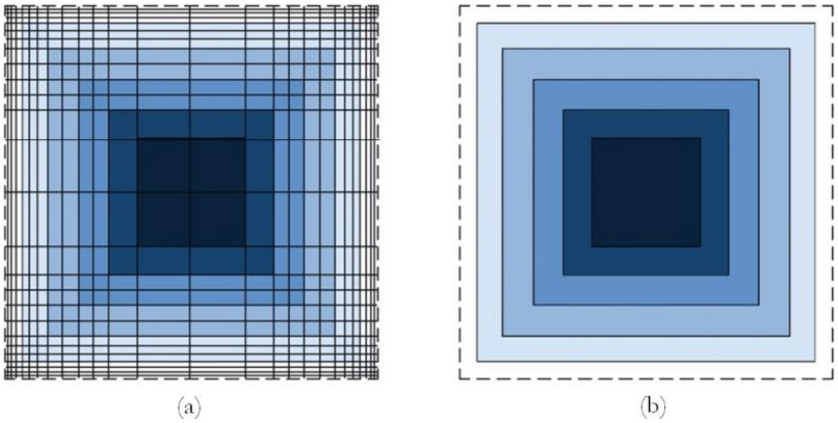

Figure 3.5: Illustration of (a) the explicit discretized model and (b) the classic MINC method for a grid cell of 200 ft in x and y direction.

According to the explicit discretized model (single-porosity approach), the fractures are discretized explicitly. In fact, very fine grid cells are used for the discretization of matrix media around the fractures. On the other hand, concerning the dual-porosity model, the problem was illustrated using a grid cell of 200 ft in x and y-direction. Note that, using a dual-porosity model the flow exchange between the matrix and fracture media is controlled by a shape factor. Additionally, a third model using the MINC method is also tested. This technique, based on the subdivisions of the matrix media into nested volume, is performed in order to study the ability of MINC method and its impact on the inter-porosity flow. The subdivision of the matrix block is controlled in a way so that the grid cell widths are identical to those in the explicit discretized model in the perpendicular direction towards the fracture. Only single phase (gas only) flow simulation is performed to compare these different simulation models. The fluid invasion due to the hydraulic fracturing will not be taking into consideration in this part. The initial reservoir

pressure is 3800 psi. A horizontal well is connected to the fracture, and the bottom hole well flowing pressure is 1000 psi.

The cumulative gas production for different simulation models are shown in Figure 3.6 for 800 days of production. Obviously, the dual-porosity model greatly underestimates the gas production, while MINC method is very accurate comparing to the explicit discretized model set as the reference solution. Note that, a MINC6 model was applied and seemed sufficient for a single-phase simulation. Based on the simulation results, clearly the dual-porosity model is not suitable for flow simulations in very low permeability reservoirs, and the MINC method presents very satisfactory result comparing to the explicit discretized model. Moreover, the explicit discretized model consists in 1369 grid cells while using the MINC6 approach decreases the number of grid cells to 7 (continuum #1 refers to the fracture and continuums #2, 3, 4, 5, 6 and 7 refer to the matrix media on Figure 3.5). The MINC technique decreases greatly the CPU time to 3 seconds comparing to the explicit model which took 25 seconds to be performed. Hence, the MINC method provides a numerical solution and an efficient improvement concerning the matrix-fracture flow exchange. Based on the above results, the applicability of MINC method for shale-gas reservoirs modelling was approved for a single-phase flow simulation.

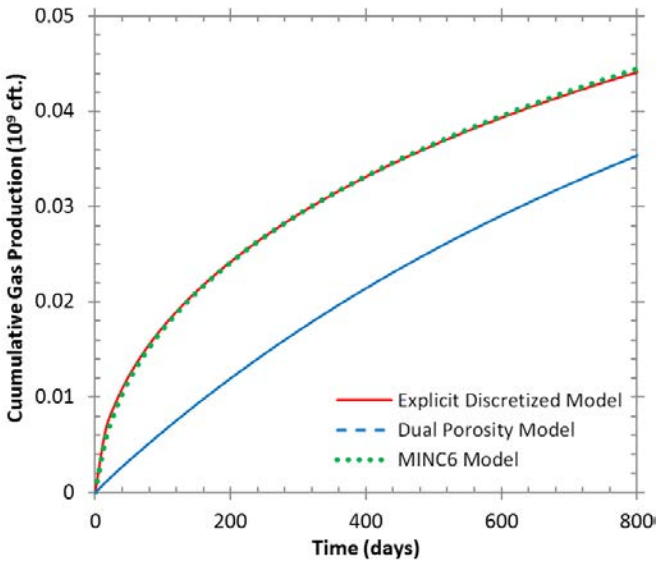

Figure 3.6: Cumulative gas production comparing different simulation models.

The following example will discuss the applicability of the hybrid method on a larger case considering two regions; a stimulated region (SRV zone) and a non-stimulated one, for two-phase flow simulations by considering fracturing fluid induced formation damage.

In order to study the efficiency and the applicability of our approach for reservoir simulation in low permeability reservoirs, simulations are performed in a SRV around a single hydraulic fracture for a regular fracture distribution.

3.3 Flow Modelling beyond the SRV Region

In order to study the impact of fracturing fluid induced formation damage in shale-gas reservoirs, a two-phase flow (gas and water) model is simulated. In order to validate the hybrid approach on this synthetic large SRV case, simulations are first performed for a single-phase (reservoir water is not mobile) to compare different simulation methods. Once the hybrid approach is validated for single-phase flow, fracturing fluid induced formation damage and its impact on gas recovery from shale-gas reservoirs will be investigated. Table 3.1 summarizes the reservoir properties.

Table 3.1: Reservoir properties.

Property / Parameter	Value	Unit
Matrix Permeability	0.0001	mD
Hydraulic Fracture Permeability (during hydraulic fracturing)	200	D
Hydraulic Fracture Permeability (during production)	2	D
Induced-fracture Permeability (during hydraulic fracturing)	40	D
Induced-fracture Permeability (during production)	0.5	D
Fracture Thickness	0.01	ft
Induced-fracture Thickness	0.001	ft
Reservoir Net Thickness	300	ft
Top of the Reservoir	5800	ft
Initial Reservoir Pressure	3800	psi
Bottom Hole Well Pressure	1000	psi

A horizontal well (red line in Figure 3.7) in the x-direction is placed in the middle of the reservoir, where 7 multi-stages hydraulic fractures perpendicular to the well along the y-direction are created. With hydraulic fracturing, high pressure injection and pumping fluid can also stimulate natural fractures and induced secondary fractures. After a hydraulic operation, two areas will exist in the reservoir, the SRV and the non-SRV region. The SRV has a volume of 1400×1000×300 cft and centered in the model. Apart from the high conductive hydraulic

fractures, all other fractures, including stimulated and un-stimulated natural fractures, are homogenized in the SRV.

The natural fracture densities are generally uncertain and they are reservoir-dependent. So, we will study three cases with different fracture spacing: 100 ft (Case1), 50 ft (Case2) and 25 ft (Case3). Note that, in all cases, 7 hydraulic fractures (solid blue line in Figure 3.7) perpendicular to the well direction are created. Inside the SRV zone, for Case1, the induced/stimulated and un-stimulated natural fractures can be approximated by a fracture network with a spacing of 100 ft in x and y-directions. This network is schematically represented in Figure 3.7(a) by 15 fractures (7 hydraulic and 8 induced fractures) in y-direction and 11 induced fractures in x-direction. For Case2 (see, Figure 3.7(b)), 7 hydraulic fractures in addition to 22 induced fractures in y-direction with a spacing of 50 ft together with 21 reactivated fractures in x-direction are created. Finally, for Case3, 57 fractures (7 hydraulic and 50 induced fractures) in y-direction and 41 induced-fractures in x-direction with a spacing of 25 ft are incorporated.

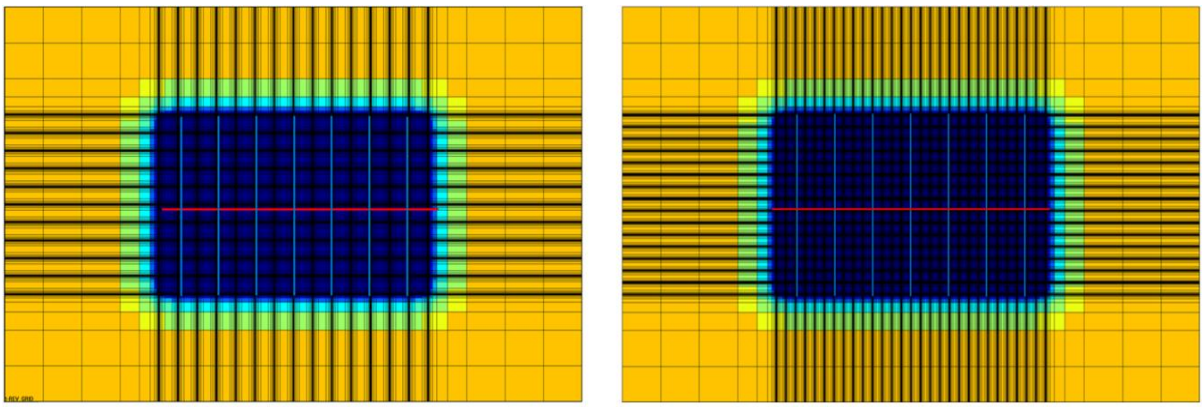

Figure 3.7: Illustration of the explicit discretized model for (a) Case1 and (b) Case2.

Outside the stimulated reservoir volume, a single-porosity medium is considered. For all the performed cases, the hydraulic fracture half-length is 500 ft (total length of 1000 ft in y-direction), and the total length of a secondary fractures is 1400 ft in x-direction.

A base model named "Explicit discretized model" (using single porosity approach) explicitly discretized hydraulic and natural fractures, using a local grid refinement logarithmically spaced around each fracture, is considered as a reference solution.

Our reservoir model presents different scale of fractures in x and y-directions dedicated to hydraulic and induced fractures, where grids which are donated to the hydraulic fractures presented in y-direction have a width of 0.01 ft and a permeability of 2000 mD, while the stimulated natural fractures are presented in x and y-directions with a thickness of 0.001 ft and a permeability of 500 mD. The top of the reservoir is at a depth of 5800 ft.

The dual-porosity model is also considered with a grid block size of 200 ft in x and y directions. This study will compare the dual-porosity model and the hybrid approach to the reference solution. Concerning the DP model, the SRV region will consist in discretizing explicitly the hydraulic fractures and the stimulated natural fractures will be homogenized using a dual-porosity approach. Care was taken to be consistent in the calculation of the effective fracture permeability and porosity for the DP model, and the shape factor σ for calculating matrix-fracture exchange in the DP model is given by:

$$\sigma = \frac{10}{a^2} + \frac{10}{b^2} \tag{3.8}$$

where, **a** and **b** are the matrix block dimensions (in x and y directions).

Concerning the hybrid approach, through the SRV region in order to improve the flow exchange between stimulated fractures and the matrix media, the MINC 2D approach (see, Figure 3.3) will be applied. However, as said before through the transition zone between SRV and non-SRV medias (see, Figure 3.4) a MINC 1D approach (see, Figure 3.2) is taken into account. In fact, as we have fractures surrounding our SRV region, a grid refinement must be done into the transition zone in order to capture the flow behavior through this region.

Firstly, single-phase flow simulation is treated. Later in this work a two-phase (gas and water) flow model will be considered to simulate fracturing fluid induced formation damage. We assume that the hydraulic fractures are already created, and also we do not consider the geomechanics effects for the fracture generations in our simulations.

Table 3.2 summarizes the three different cases of fracture spacing. Figure 3.8 presents the pressure distribution (grid system used) at the end of production (5000 days) for the standard dual-porosity model and the hybrid approach based on the MINC method for Case1 (fracture spacing of 100 ft).

The formation damage related to the fracturing fluid invasion is not considered by performing a single-phase flow simulation. So, we assume that gas is the only mobile phase in the reservoir and will be directly produced from the complex fracture network.

Table 3.2: Representation of HF (Hydraulic Fractures), NFx and NFy (stimulated Fractures in x and y directions) for each case of the explicit discretized model.

Case	Fracture Spacing	Number of HF (perpendicular to the well direction)	Number of NFx (stimulated fractures parallel to the well direction)	Number of NFy (stimulated fractures perpendicular to the well direction)
Case1	100 ft	7	11	8
Case2	50 ft	7	21	22
Case3	25 ft	7	41	50

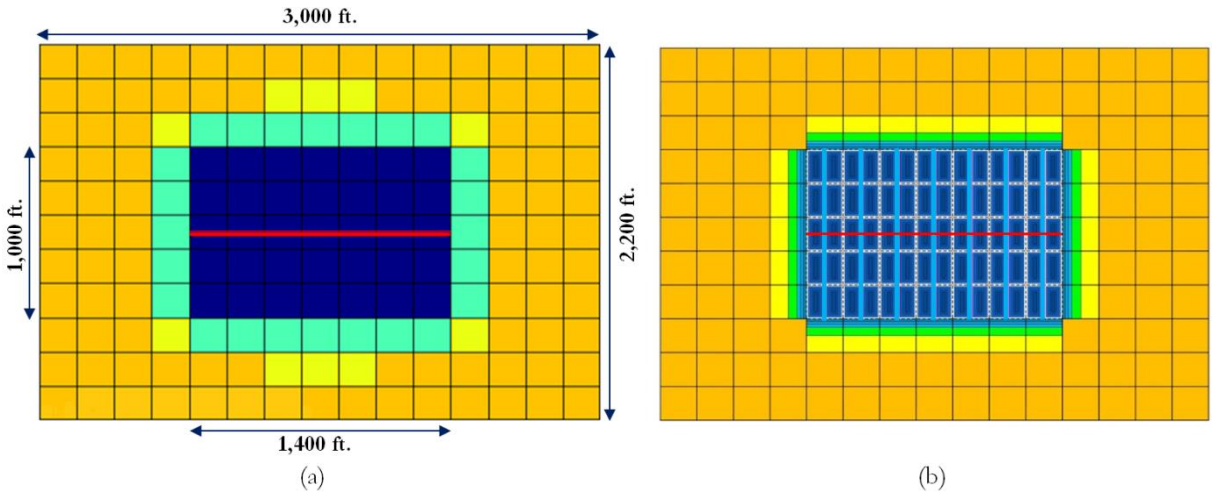

Figure 3.8: Illustration of (a) the dual-porosity model and (b) the hybrid approach model based on the classic MINC method for Case1.

3.3.1 Single Phase Flow Simulation

The three simulation models (explicit discretized model, dual-porosity and hybrid approach) are compared for Case1 and Case2. It must be mentioned that, the hybrid approach is based on a MINC6 model (1 continuum for the fracture and 6 continuums for the matrix media)

in the SRV zone. In fact, subdividing the matrix into 6 continuums (number of refinement is set at 6) for a single-phase flow simulation seems sufficient. Moreover, to improve the connection between the SRV region and the non-SRV one, a grid refinement through the matrix on the border of the SRV zone is added.

First, this study concerns only Case1 in order to show the efficiency of the hybrid method by testing different number of matrix refinement such as; 1 (DP Model), 2 (MINC2 Model), 4 (MINC4 Model), 6 (MINC6 Model) and 14 (MINC14 Model). Note that, the DP model is a particular case of the MINC method where the matrix refinement is 1. Hereafter, Figure 3.9 shows the convergence of the cumulative gas production of the hybrid approach model for different matrix refinement. A comparison to the explicit discretized model which is considered as a reference solution is done. Figure 3.9(a) describes the cumulative gas production for 5000 days, where Figure 3.9(a) presents the cumulative curves for 1000 days of production. On one hand, increasing the order of refinement for the hybrid approach improves the gas production and makes the result more accurate. However, using a MINC6 or MINC14 model gave us nearly the same results which are very accurate compared to the reference solution. On the other hand, it is clear that beyond a MINC6 there is no more need to refine and a MINC6 model is sufficient for a single phase flow case.

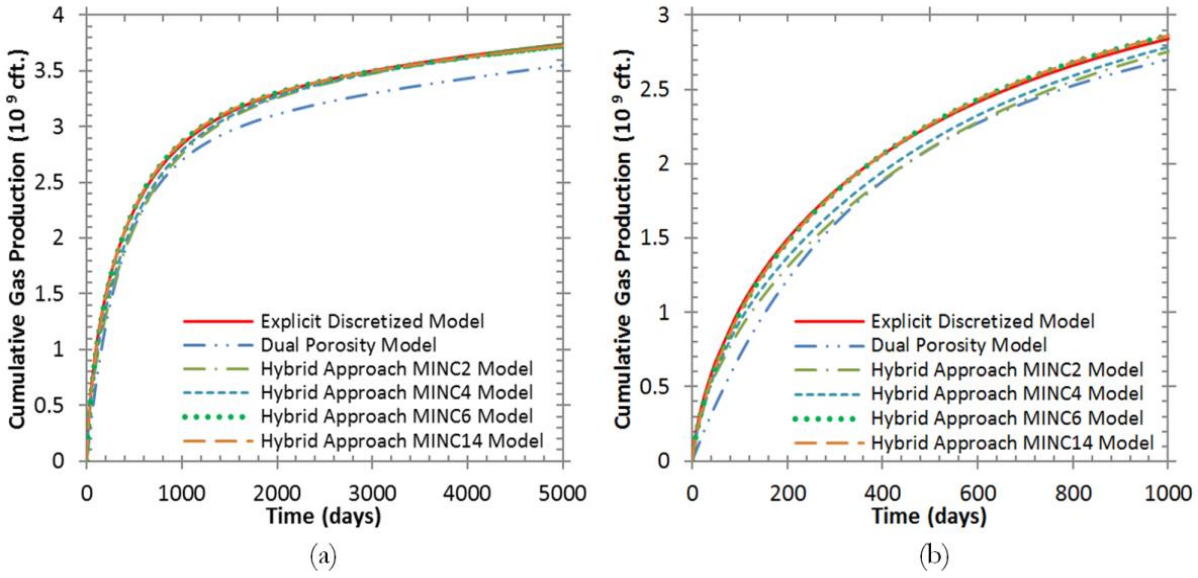

Figure 3.9: Comparison of different order of refinement for the MINC method to the reference solution and the dual-porosity model for (a) 5000 days and (b) 1000 days for Case1.

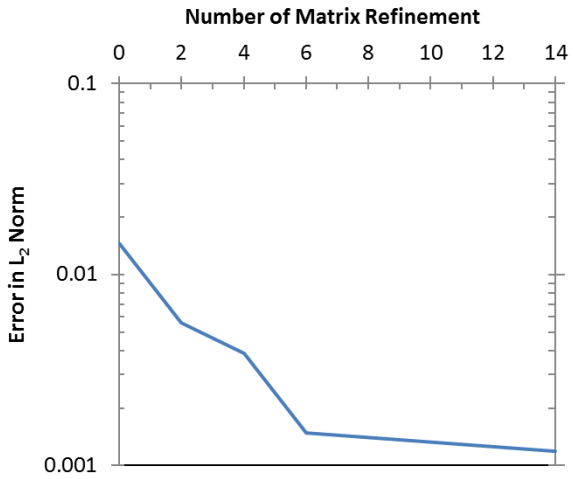

Figure 3.10: The L2 norm error of the cumulative gas production for a single phase flow concerning Case1 function of number of matrix refinement.

Also, Figure 3.10 presents the L_2 norm error function of number of refinement using a semi-log concerning the norm error Y-axis for a single-phase flow simulation. The L_2 norm error is defined as:

$$L_2 = \sqrt{\frac{1}{N_p}\sum_{i=1}^{N_p} \varepsilon_i^2} \tag{3.9}$$

where, N_p refers to the number of points taking into the calculation, ε represents the difference between the hybrid approach and the reference solution and i corresponds to the time index. In our case, N_p = 100.

In the following, three simulation models (the explicit discretized model, the dual-porosity model and the hybrid approach using a MINC6 model) are performed. Figure 3.11(a) and (b) presents the cumulative gas production for Case1 and Case2 for 5000 days respectively. Clearly, the dual-porosity model underestimates the gas production. On the other hand, the hybrid approach based on the concept of MINC method provides a much better result than the dual-porosity model and can match accurately the explicit discretized model (reference solution). Furthermore, the hybrid approach works very well independently from fracture spacing (100 ft

and 50 ft). These simulations show the ability of the hybrid approach to predict gas production from unconventional fractured shale-gas reservoirs, while a dual-porosity model is inaccurate for such problems. As the hybrid approach is quite accurate, in order to investigate the impact of fracture spacing on gas production from shale-gas reservoirs, Case3 (fracture spacing of 25 ft, presenting a higher fracture density than Case2 and Case1) was only simulated using the hybrid model.

Figure 3.12 compared the cumulative gas production from these three cases using a hybrid approach for a single-phase flow simulation. In fact, a higher fractures density decreases the fracture spacing and clearly enhances gas production. As we expected, higher gas production is observed (Figure 3.12) for Case3 than Case2 and Case1. Using the hybrid approach with a MINC6 model for the whole SRV region seems to be sufficient and efficient for a single-phase flow simulation. Based on these simulation results, we conclude that a standard dual-porosity model is not suitable for shale-gas simulations.

The hybrid approach using the hybrid techniques proves its accuracy for the application on shale-gas reservoirs, at least for single-phase flow problems. The hybrid method improves significantly the capability to predict inter-porosity flow exchange. In fact, discretizing the matrix blocks into a sequence of volume elements can handle much better the transient flow from the matrix into the fractures during the whole production period.

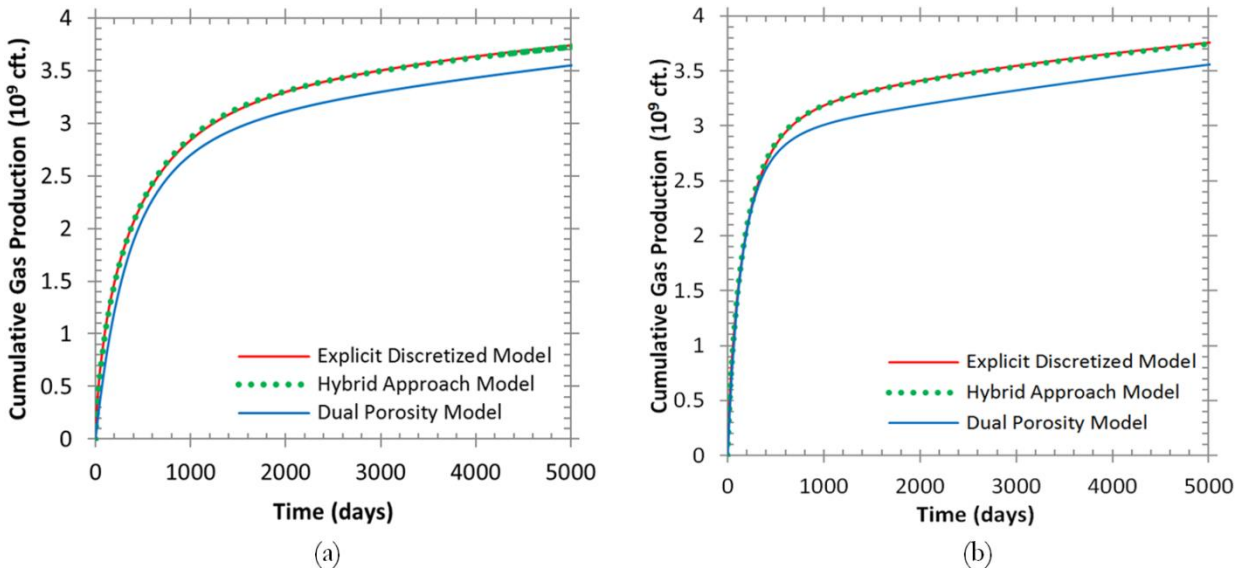

Figure 3.11: Comparison of different simulation models for (a) Case1 and (b) Case2.

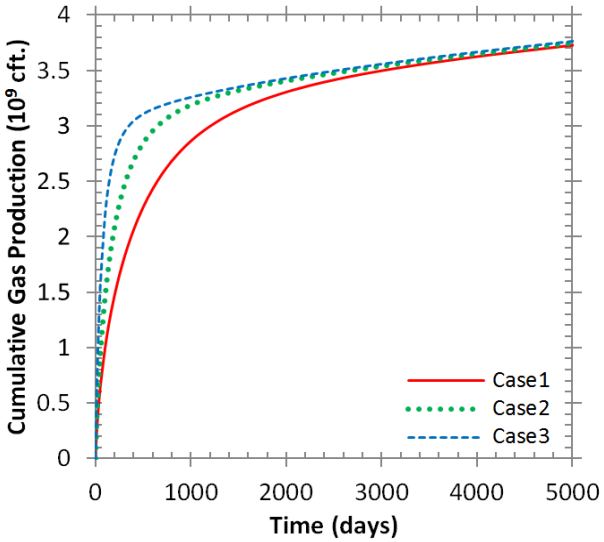

Figure 3.12: Comparison of gas production for different fracture spacing's.

3.3.2 Two-Phase Flow Simulation

In order to improve gas production from shale-gas reservoirs by enhancing matrix permeability, hydraulically fracturing operation is widely required in shale-gas formations. A huge amount of water (thousands of barrels) is injected to create multi-stage hydraulic fractures in a purpose to have an economic production from unconventional gas reservoirs. We should mention that only a part of the injected water is reproduced during a long period, while a significant percentage of water remain in the reservoir and get trapped near the fracture face due to capillary effects. In this part, simulation of a two-phase (gas and water) flow problem is performed to investigate the impact of fracturing fluid invasion induced formation damage after a hydraulic stimulation.

Water is injected to simulate the creation of the hydraulic fractures. A water volume of 25000 bbl is pumped into the horizontal fractured well (7 fracture stages) during 5 hours. Due to the high pressure water injection during hydraulic fracturing, we assume that the fracture conductivity is very high. So, the permeability is assumed to be 200 D in the hydraulic fractures and 40 D in the stimulated natural fractures using hydraulic operation. Later on, during production, the permeability is set to 2 D in the hydraulic fractures and 500 mD in the stimulated natural fractures. As the reservoir model contains both matrix and fracture media, gas/water relative permeabilities in both medium in addition to the capillary pressures between gas and water in the matrix medium are needed to be incorporated in the reservoir model. Figure 3.13

and Figure 3.14 show respectively, fracture/matrix relative permeabilities and the capillary pressures between gas and water versus water saturation. No capillary pressure presents in the fracture. Furthermore, we consider the initial water saturation in this shale-gas reservoir equals to the irreducible water saturation set at 0.35 (Sw_{ini} = Sw_{ir} = 0.35).

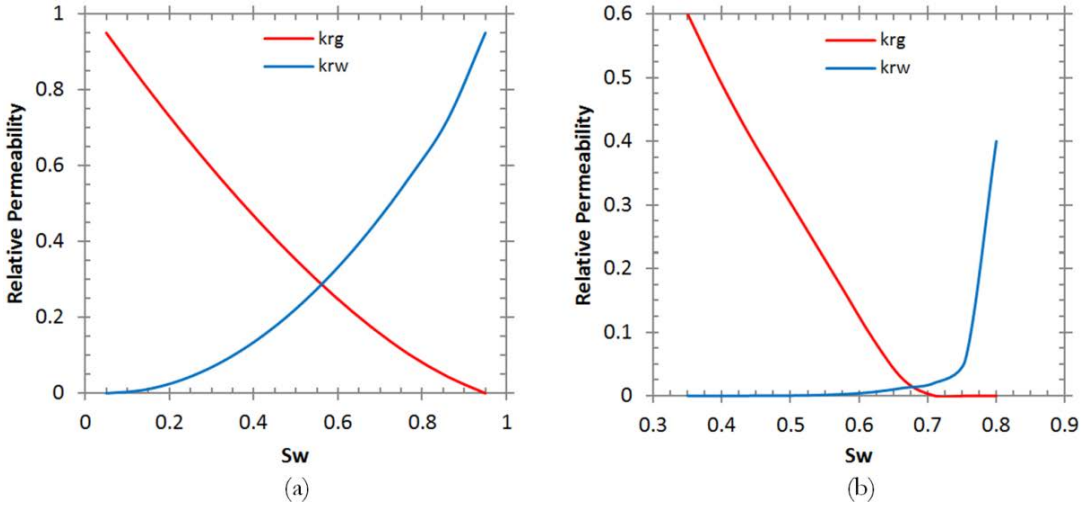

Figure 3.13: Relative permeability curves for (a) the fracture media and (b) for the matrix media vs. water saturation.

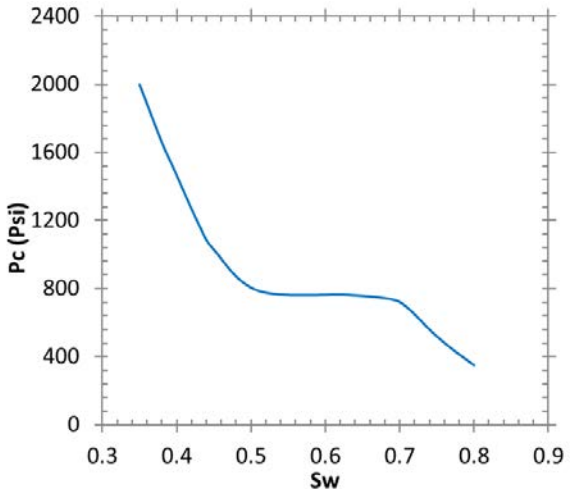

Figure 3.14: Gas-Water capillary pressures vs. water saturation.

Dealing with two-phase flow simulation, MINC6 model was not sufficient to handle fluid invasion and its backflow, as the depth of water invasion is in order of 1 or 2 inches. To compare the hybrid method with the explicit discretized single-porosity model, the cell sizes near the fracture in the hybrid approach are controlled in a way so that their block sizes in the direction perpendicular to the fracture are identical to those in the single-porosity model. Table 3.3

describes the mesh discretization with block size from the fracture to the matrix block center for different simulation models (explicit or hybrid approach). The first value (0.01 ft) refers to the fracture aperture.

Table 3.3: Meshes description for an explicit discretized model compared to a hybrid approach using MINC6 and MIN13 model.

Simulation Models	Mesh Discretization (ft)						
Explicit Discretized Model (in x and y directions)	0.01 (fracture) 0.16 5	0.02 0.2 8	0.03 0.4 14	0.04 0.7 15.1	0.06 1 50	0.08 2	0.12 3
Hybrid Approach MINC6 Model	0.01 (fracture)	0.02	0.03	0.04	5	20	74.9
Hybrid Approach using MINC13 Model	0.01 (fracture) 0.16	0.02 0.2	0.03 0.4	0.04 0.7	0.06 2	0.08 20	0.12 76.2

To simulate correctly water invasion into the matrix formation, smaller grid cells are needed around the fractures. In order to improve the accuracy for a two-phase flow simulation, we decided to increase the number of nested volumes related to the matrix media, by using a MINC13 model (1 continuum for the fracture and 13 continuums for the matrix media), instead of a MINC6 model (single-phase case). In fact, in order to select a reasonable MINC for two phase flow simulations, we performed several MINC tests for Case 1, where a 100 ft of fracture spacing is considered. The convergence of the two-phase flow simulation with different MINC refinement (MINC 4, 8, 10, 13 and 14) is presented in Figure 3.15. It is obvious that, by adding supplement continuum from 4 to 8 to 10 to 13 the results of cumulative gas production are more accurate. It should be mentioned that beyond MINC13 there is no need to refine more. Clearly, MINC14 provides nearly the same result as MINC13. This claim could be explained also based on the results of the L2 norm from Figure 3.16. In fact, Figures 3.16(a) and (b) present the L2 norm error function of different number of refinement for the cumulative gas production and for the cumulative water production, respectively, concerning a two-phase flow for Case1. Based on the results from Figure 3.16, the L2 norm error is decreasing by increasing the number of matrix subdivision for both the cumulative gas production (Figure 3.16(a)) and the cumulative water production (Figure 3.16(a)). It must be mentioned that, a MINC13 model is sufficiently accurate for this simulation case and it is selected for our hybrid approach model for the two-phase flow simulations in the following.

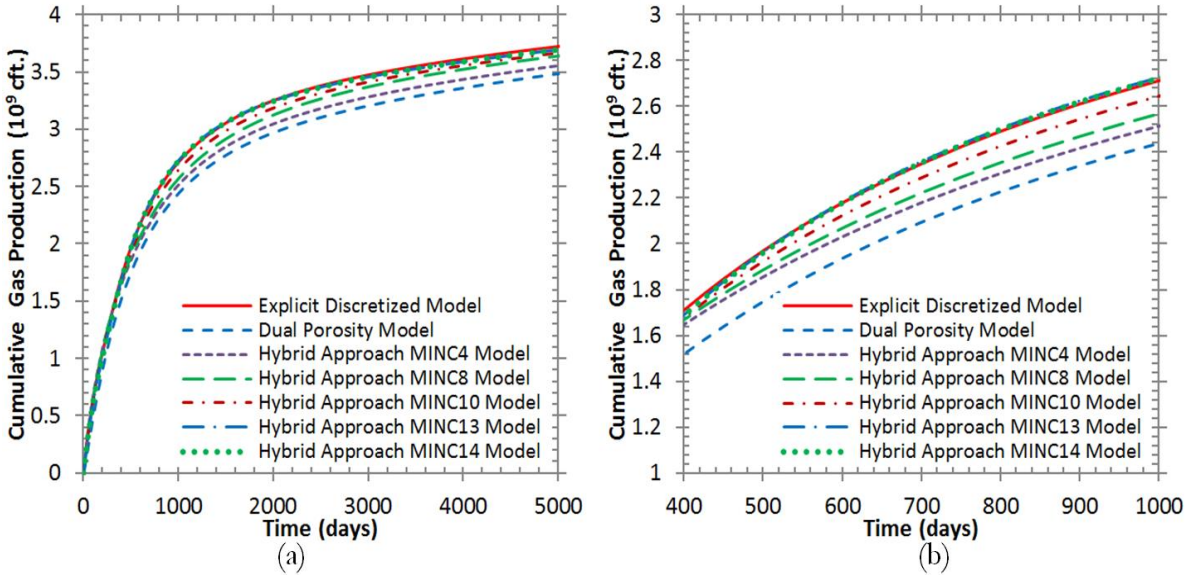

Figure 3.15: Comparison of different order of refinement for the MINC method to the reference solution and the dual-porosity model for (a) 5000 days and (b) from 400 to 1000 days for Case1.

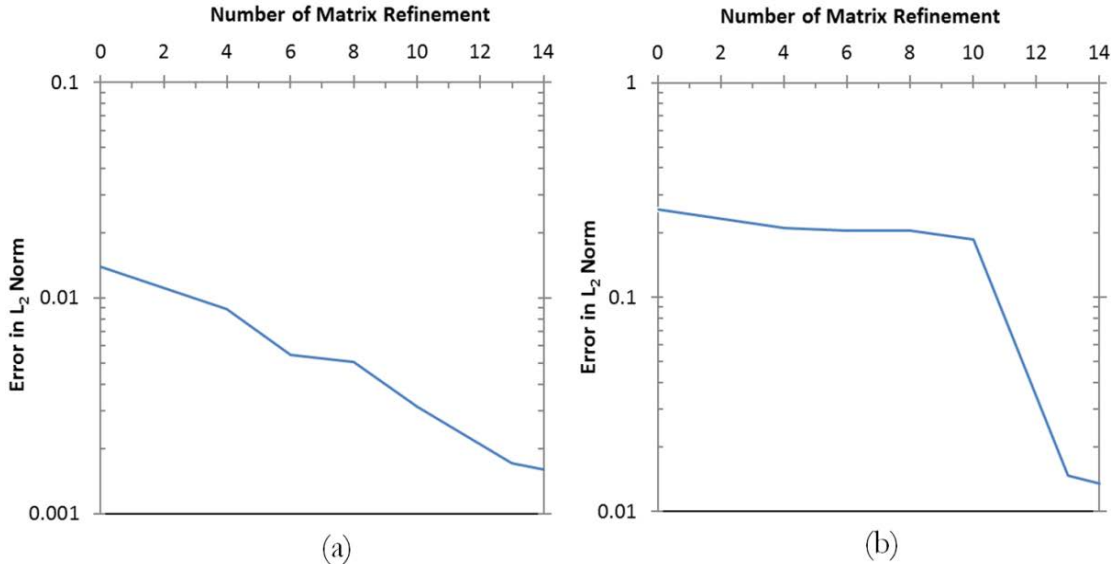

Figure 3.16: The L2 norm error function of number of refinement concerning a two-phase flow (a) for the cumulative gas production and (b) the cumulative water production for Case1.

3.3.2.1 Fracture Spacing of 100 ft – Case1

Simulation results from fracture spacing of 100 ft (Case 1) are presented in Figure 3.17. Different simulation models: dual-porosity and the hybrid approach (MINC13 model) are compared to the explicit discretized model (reference solution). Figures 3.17(a), (b), (c) and (d)

represent respectively the results of the water cut, the daily gas rate, the cumulative water production and the cumulative gas production for a two-phase flow simulation taking into account the same reservoir model as defined previously (see, Figure 3.7, Figure 3.8).

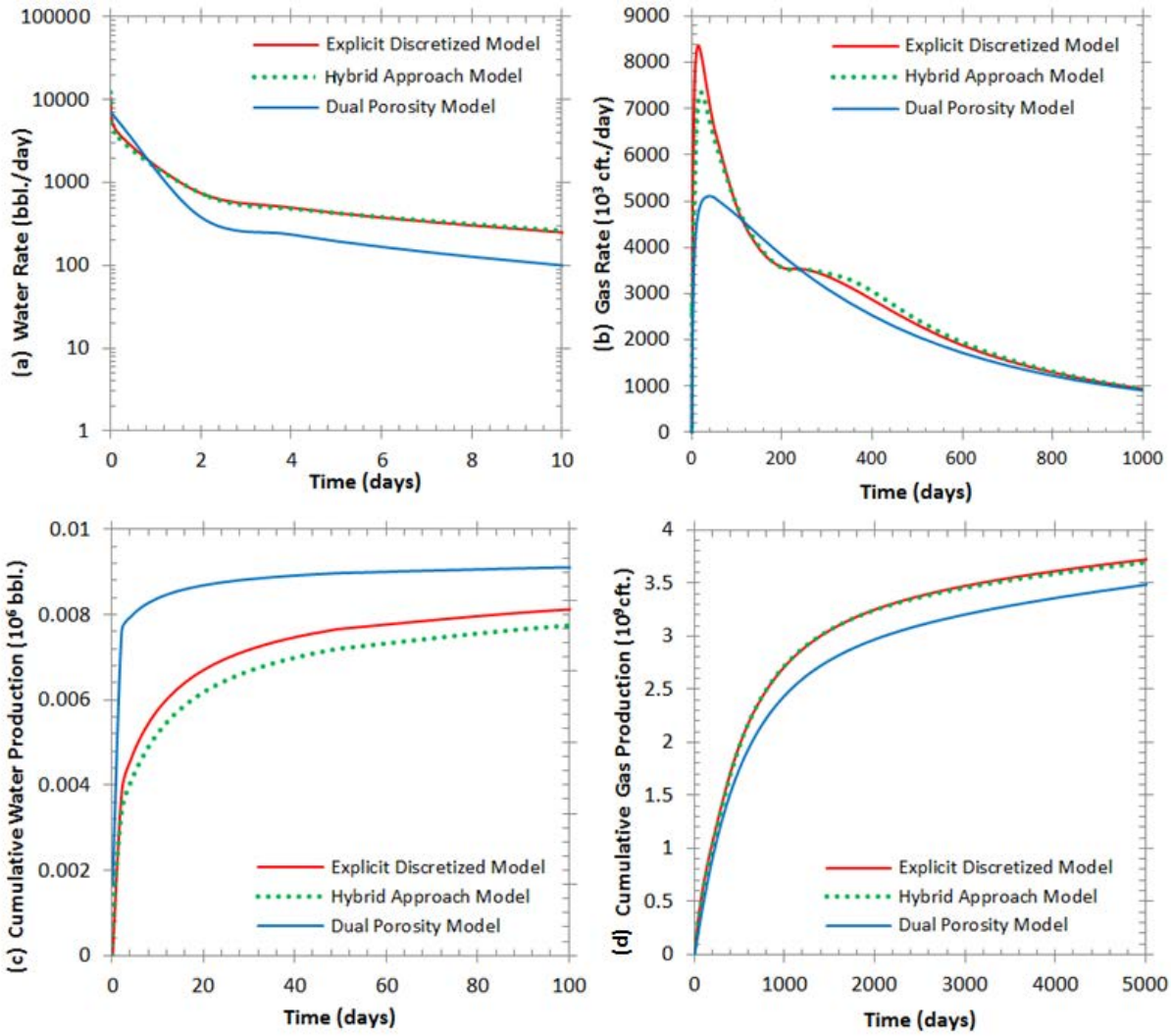

Figure 3.17: Simulation results of Case1 for different simulation models for a two-phase flow problem (a) water rate, (b) gas rate, the cumulative (c) water and (d) gas production.

Figure 3.17(a) presents the daily water rate production during the first 10 days. Also, Figure 3.17(b) shows the daily gas rate during the first 1000 days. The gas rate is impacted by the presence of fracturing fluid during the cleanup period. The hybrid method is very close to the reference solution and it is much better than the dual-porosity model. Figure 3.17(c) presents the cumulative water production curves during the first 100 days. The explicit discretized model and the hybrid (dotted green curve) produce around 8000 bbl of water on 100 days, while the dual-

porosity model produces a volume close to 9000 bbl Only around 30% of injected water is produced, and the rest of water remains in the tight formation and needs a very long time to be cleaned. The hybrid approach gives approximately a similar water production as the explicit discretized model, and the dual-porosity model is not accurate. If we are interested in long-term production, based on Figure 3.17(d) which presents the cumulative gas production for 5000 days**,** the hybrid method is always very accurate and the dual-porosity model still not suitable.

3.3.2.2 Fracture Spacing of 50 ft – Case2

The following simulations are carried out for Case2 with fracture spacing of 50 ft. Results are presented in Figure 3.18. Figure 3.18(a) presents the daily water rate at early time for 10 days of production, and Figure 3.18(b) presents the daily gas rate for 1000 days. Also, the cumulative water production during the first 100 days is shown in Figure 3.18(c). In this case, water production is reduced to 6500 bbl by the explicit discretized model and hybrid approach. Clearly, facing a higher natural fracture density in Case2 (comparing to Case1 with a fracture spacing of 100 ft), the contact area between the fractures and the matrix formation is much greater. Note that the total injected water volume is fixed at 25000 bbl for fracturing the whole SRV in both cases. Little water invades into the matrix formation per unit of fracture surface in Case2 than Case1. So only a small quantity of water can be removed, due to the water blocking effect and the presence of a high capillary pressure (2000 psi). In other words, working with a smaller fracture spacing (higher fracture density) the exchange surface with the matrix media will be more important and therefore the water invasion is extended to a very larger area and the water backflow is reduced. Furthermore, the simulation using the hybrid approach in Case2 is very accurate. Moreover, the shorter transient period due to small block sizes also helps to improve the hybrid simulation accuracy. On the contrary, the dual-porosity model highly overestimates the water production and is not accurate. Figure 3.18(d) shows the cumulated gas production for 5000 days. The hybrid method is very accurate in both early time and long term periods. The dual-porosity model is not suitable for the two-phase flow simulation.

The simulations of these two cases (fracture spacing of 100 ft and 50 ft) allow us to confirm that our hybrid approach is accurate and can be used as a reference solution for further simulations. In the following, we will use the hybrid approach to simulate the Case3 with a fracture spacing of 25 ft to study the effect of fracturing fluid induced formation damage.

Based on our simulation results, the hybrid technique can match the explicitly discretized fracture model simulation which is considered as a reference solution. Furthermore, results also show that this kind of problem cannot be handled by a dual-porosity model. Our hybrid approach proved the possibility to accurately modelling the matrix-fracture exchange even for a multiphase flow model independently from fracture spacing.

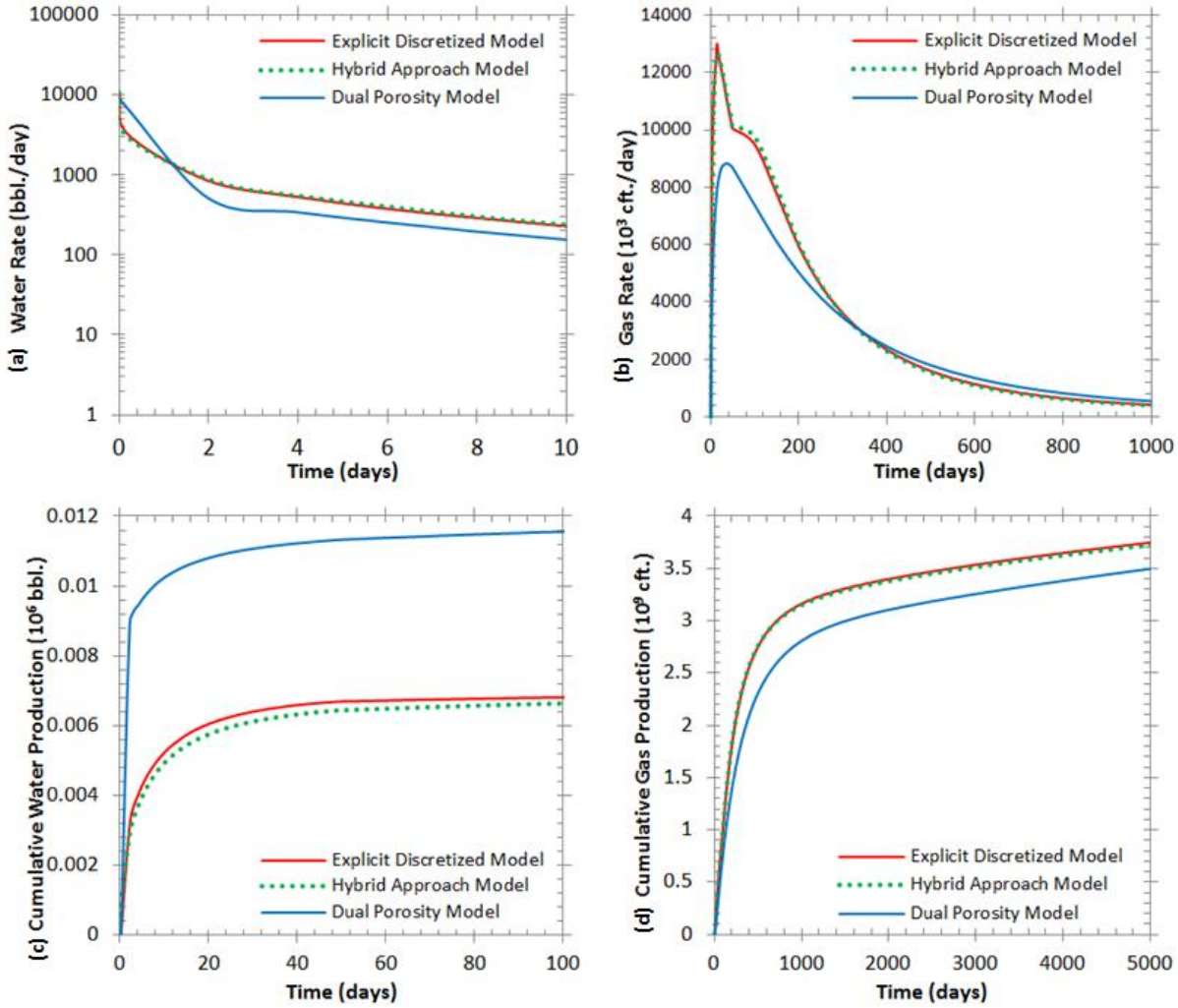

Figure 3.18: Simulation results of Case2 for different simulation models for a two-phase flow problem (a) water rate, (b) gas rate, the cumulative (c) water and (d) gas production.

3.3.2.3 Impact of Fracturing Fluid Invasion on Gas Production

Under the high pressure fluid injection, water will invade through matrix media. Unproduced fracturing water leading to a blocking effect in tight formation due to high capillary pressures impedes gas production. The presence of water sensitive clays could damage the

formation and unfortunately will reduce gas relative permeability and may also impact gas production from shale-gas reservoirs.

In order to illustrate the impact of the fracturing fluid invasion, Figure 3.19 shows the water saturation remaining in the reservoir for Case2 (a zoom was made near fractures cells). These snapshots illustrate the water saturation (fracturing fluid) at the end of injection after 5 hours (see, Figure 3.19(a)) and after 50th days (see, Figure 3.19(b)) of production. After 5 hours of water injection, fracturing fluid invades around 0.15 ft into the matrix formation due to very low matrix permeability. However, after 50 days of gas production, water still remains in the reservoir with an average saturation around 0.65 in the tight formation near the fracture faces. The remaining water is difficult to be removed and may rest during the whole production time.

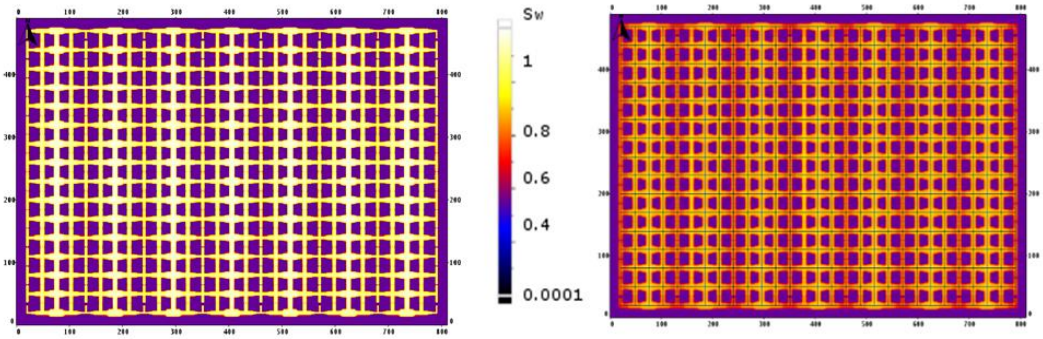

Figure 3.19: Water saturation distribution (Fracture Spacing of 50 ft).

Figure 3.20 shows the impact of fracturing fluid induced formation damage by comparing the single-phase flow simulation, where no formation damage is considered, and the two-phase flow simulation, where the formation damage due to fracturing fluid invasion is taken into account. The formation damage effects are also compared for different fracture spacing of 100 ft (Case 1), 50 ft (Case 2) and 25 ft (Case 3). We notice that gas production from single-phase flow simulations (no formation damage) are higher than those from two-phase flow simulations (fracturing fluid induced formation damage), because of the water blocking effect and capillary trapping in the two-phase flow. Therefore, the hybrid approach can be used to evaluate quantitatively the effect of fracturing fluid induced formation damage.

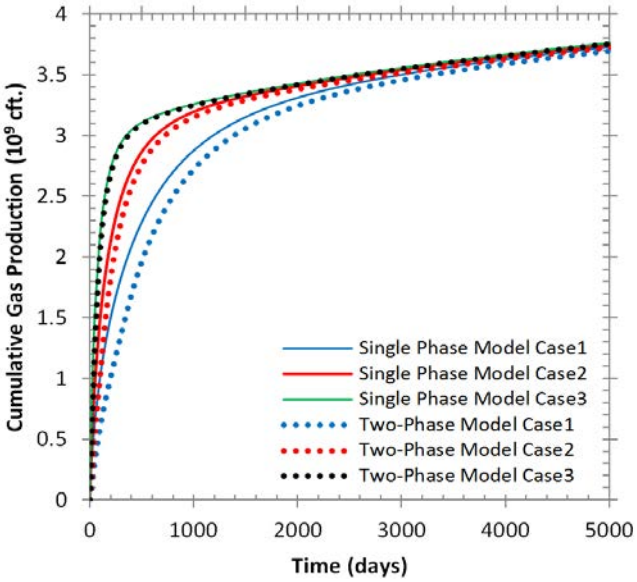

Figure 3.20: Impact of water invasion on gas production for Case1, Case2 and Case3.

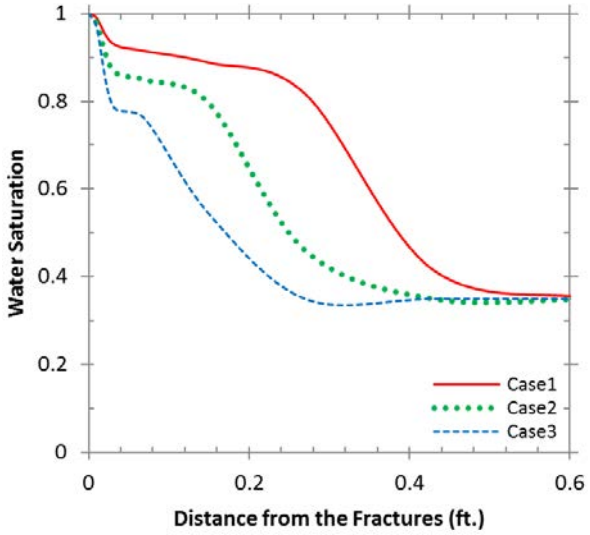

Figure 3.21: Water saturation around the fractures for Case1, Case2 and Case3.

The formation damage in Case1 is more important than Case2 at the earlier time (several years) of production, while it can almost be neglected in Case3. Treating a higher natural fracture density (decreasing the fracture spacing) case, the impact of the fracturing fluid invasion on gas production from unconventional shale-gas reservoirs becomes less important. This result can be explained by the formation damage through water invasion depth. When fracture spacing decreases, the number of fractures increases. So, when fractures are dense the volume of water invasion into the matrix formation by unit fracture surface becomes small. Once the fluid

invasion is shallow, the impact of water invaded through the formation on gas production will be insignificant. This claim can be explained by Figure 3.21 where the water saturation near the fracture as a function of the distance from the fractures is plotted for Case1, 2 and 3. Clearly, the formation for Case1 is more damaged than Case2 and Case3 and it explains the impact on the cumulative gas production in Figure 3.20.

A summary of the numerical simulation results is presented in Table 3.4, including, the number of grid cells used in the simulation, CPU time, average water invasion depth, and the smallest grid cells volume concerning single and two-phase flow simulations. Table 3.4 compares the CPU time between the explicit discretized model and the hybrid approach for single and two-phase flow simulations for each case. For single phase flow simulations, the explicit discretized model takes 7841 and 28702 seconds respectively for Case1 and Case2, while the hybrid approach with MINC6 takes only 8 seconds and uses 1039 grid cells for the same cases independently from the fracture spacing. It has to be mentioned that we tried to simulate Case3 with an explicit dicretized model, but the simulation was not achieved due to the high number of grids cells (1.5 millions grids approximately) and small block sizes leading to an istability issue. So, the hydbrid apppraoch based on a MINC6/MINC13 model were taken as the refernece solution concerning Case3 for single/two-phase flow model. Furthermore, concerning the two-phase flow simulation, much higher CPU time is required to achieve such simulations using an explicit discretized fracture model, for example, 20262 and 84211 seconds respectively for Case1 and Case2. The hybrid approach is much more efficient and faster than the explicit model one. The CPU time is reduced to 12 seconds for all the three cases with a MINC13 for the hybrid model (1529 meshes for a two-phase flow simulation independently from fracture spacing). This approach decreases significantly the number of grid cells and the CPU time compared to an explicit discretized model. Also, the accuracy of the hybrid method does not depend on the fracture spacing. It is clear that an explicit discretized model takes a lot of CPU time. The large number of grid cells required to an explicit model increase the CPU time in solving the system at one-time step, and the smallest grid cells volume used in the simulation constrains the time steps (need to use very small time steps). Table 3.4 shows the smallest grid volume for each case for different simulations. The smallest cell volume for the hybrid approach is 6 orders of magnitude greater than that of the explicit model (0.0003 cft for the explicit discretized model and 120 cft, 240 cft and 480 cft, respectively for Cases 1, 2 and 3 with the hybrid approach). As expected,

small grid volumes impact greatly numerical stabilities in flow simulations, especially for two-phase flow problems.

Concerning the average depth of fracturing fluid invasion, it is 0.27 ft for the large fracture spacing of 100 ft. This depth is reduced to 0.15 ft for the fracture spacing of 50 ft and reduced to only 0.07 ft for the small fracture spacing of 25 ft. This observation confirms the simulation results in Figure 3.20. For Case1, water invasion is deeper, and the impact of fracturing fluid induced formation damage lasts several years.

Table 3.4: Comparison of the numerical results between the explicit discretized model and the hybrid approach for each case.

		Single Phase Flow Simulations		Two-Phase Flow Simulations			
Simulation Model	Case	N° of Grid Cells	CPU Time (secs.)	N° of Grid Cells	CPU Time (secs.)	Invasion Depth (ft)	Smaller Grid Volume (cft)
Explicit Discretized Model	Case1	147063	7841	147063	20262	0.27	0.0003
	Case2	396579	28702	396579	84211	0.15	
	Case3	Not Simulated		Not Simulated			
Hybrid Approach	Case1	1039 MINC6	8.0	1529 MINC13	12.0	0.27	120
	Case2					0.15	240
	Case3					0.07	480

The accuracy of the hybrid method for large reservoir simulations was demonstrated. Also, the hybrid method can be used for both single-phase and two-phase flow simulations, where it takes much less CPU time comparing to an explicit discretized model. Moreover, the hybrid method can be used to study the effect of fracturing fluid induced formation damage. We believe that it can also be used to simulate other physics such as three phase flow (gas/oil/water) with phase changes due to pressure drop.

As field cases are almost impossible to be simulated using an explicit discretized model with a single-porosity approach, we believe that our hybrid approach can be applied to field applications with the presence of a large SRV. On hand our hybrid approach is able to accurately model propery flow from unconventional shale-gas resrvoirs for bothe single and two-phase

flow. On the other hand, this model is very efficient in term of CPU time consuming. So, in the following a generalization of our hybrid approach to take into account the general discrete fracture network is presented.

Chapter 4 - EXTENSION OF THE HYBRID APPROACH TO THE DISCRETE FRACTURE MODEL

To model a realistic reservoir fracture network, a new type of model called discrete fracture models (DFMs) has received a great attention. In fact, these kinds of models consist in discretizing complex fracture networks (hydraulic, reactivated, induced, micro-fractures, etc...). However, this method is usually too CPU time consuming. Besides, some DFMs rely on unstructured grids to conform the fracture geometry and location, where all types of fractures are explicitly discretized, leading to a complicated and often non tractable numerical system to solve. To overcome these limitations, Embedded Discrete Fracture Models (EDFM) propose a hierarchical method to easily deal with these problems (see, Karimi-Fard *et al.* (2004, 2006), Moinfar *et al.* (2011 and 2013b), Norbeck *et al.* (2014) and Delorme *et al.* (2013).). However, the matrix-fracture interaction is not properly handled within the EDFM due to the very low matrix permeability and the large matrix grid cells.

In this chapter, to improve DFMs, an extension of our hybrid approach to a DFM based on a MINC proximity function is proposed. The fractures are considered within a triple-continuum model, where the propped fractures (high conductivity fractures) are explicitly discretized and other sorts of fractures (low conductivity) are homogenized. Also, note that the MINC proximity function is computed by taking into account all discrete fracture network. In other words, in order to improve the flow exchange between the matrix and fractures, the matrix media is subdivided according to the fractures distribution in each grid cell based on the MINC proximity function.

Our DFM is first validated on some simple cases. Then, a validation is performed on a large regular fracture network with Warren and Root's type on a uniform and a non-uniform SRV zone.DFM Based on MINC Proximity Function

One of the critical issues in numerical modelling for low permeability reservoir is how to handle fluid flows in the presence of a complex fracture network and the interaction between tight matrix formation and fractures (see, Figure 4.1). Therefore, proposing an approach to model fluid flow from a Discrete Fracture Network (DFN), taking into account a complex fracture network with existing multi-scale fractures, is needed. We will particularly present the MINC proximity function to handle the inter-porosity flow, where the matrix and fracture interaction can be treated entirely by a fully transient representation.

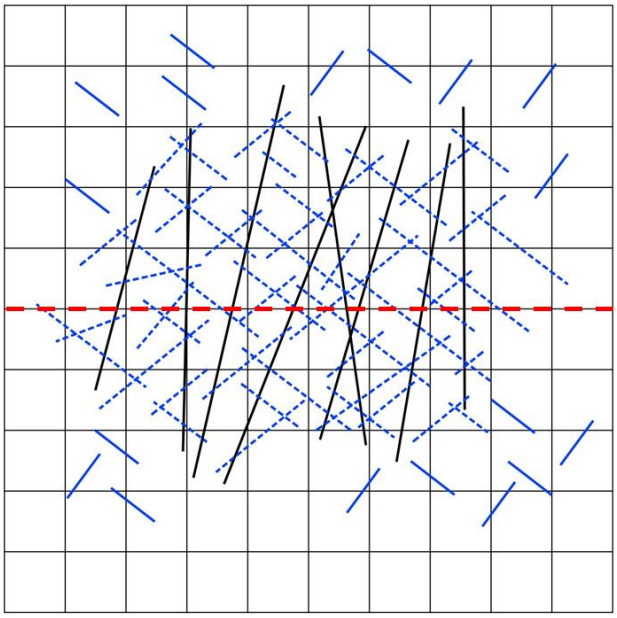

Figure 4.1: Illustration of the hierarchical fractures model with multi-scales fractures: (a) hydraulic fractures (black solid lines), (b) stimulated natural fractures connected creating a DFN (blue dashed lines) and (c) non stimulated natural fractures (blue solid lines).

In shale formations, a hydraulic stimulation using a horizontal well (dashed red line in Figure 4.1) is generally needed. After hydraulic fracking operations, multi-scale fractures are present such as: hydraulic fractures, stimulated natural fractures/non-stimulated and micro-fractures. All these types of fractures are connected to each other leading to a very complex DFN. This proposed approach takes into consideration a triple continuum media: (a) matrix media, (b) homogenized fracture media and (c) highly conductive fractures which are explicitly

discretized. The MINC method is used to model flow exchange between the matrix media and the fractures (all sort of fractures).

In fact, two types of fractures should be considered: (a) hydraulic fractures and fractures with presence of proppant with high conductivity (black solid lines in Figure 4.1) and (b) natural fractures stimulated with very low conductivity compared to hydraulic fractures as shown in Figure 4.1 (dashed and solid blue small lines). In order to treat the heterogeneity, a hierarchical method to model fluid flow in a reservoir with multiple-length scaled fractures is proposed. Here, we suggest to classify fractures using a hierarchical method based on a conductivity criterion.

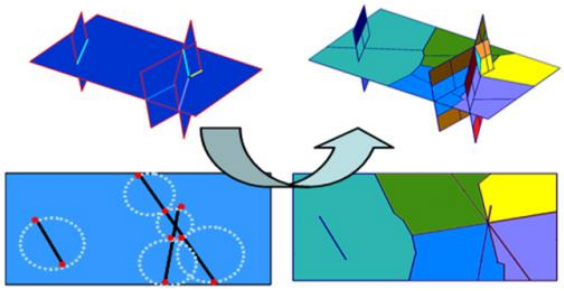

Figure 4.2: Discretization of the fracture intersections; after Delorme *et al.* (2013).

So, hydraulic and highly conductive fractures are explicitly discretized, and stimulated/non-stimulated natural fractures are homogenized, where the equivalent porosity ϕ^* and permeability k* (k') are required.

This approach is appropriate for describing a large reservoir for the reason that it treats multi-scale fractures and takes into consideration flow modelling between all existing media. The purpose of this work is to explicitly discretized hydraulic and highly conductive fractures, due to their very important role in the production of natural gas. All sorts of other fractures are homogenized. The conductive fractures are discretized using the nodes of the fracture intersection (see, Figure 4.2, after Delorme *et al.*, (2013)). The fractures porosity and surface exchange are assigned to each fracture node. Furthermore, homogenized fractures will be assigned with another representative node presented with a blue node on Figure 4.3. Finally, the matrix media will be represented with a third node connecting with the homogenized fractures through the blue node. In the matrix media the MINC proximity function will be applied taking into account all sort of fractures existing in the grid cell. It must be mentioned that, among all the interactions the modelling of flow exchange between matrix and fracture is extremely important,

because of low matrix permeability induced long transient period. Hereafter, the connections between different media and transmissibility calculations will be described and detailed.

4.1 Interaction Between Different Medias

4.1.1 Flow Between High Conductive Hydraulic Fractures

Modelling the flow in high conductive path way is important in reservoir simulations. As known, highly conductive fractures have more dominating influence on fluid flow than short and medium fractures. Thus, the flow between highly conductive fractures should be taken into consideration and is explicitly discretized. So, in our model we intend to model explicitly every hydraulic fracture using the fractures nodes only. In fact, each intersection of two (or more) high conductive or hydraulic fractures (black lines in Figure 4.3) will be assigned with a fracture node (red node in Figure 4.3).

The fracture volumes and the exchange surfaces are assigned to the fracture nodes and are estimated using Voronoï mesh in each fracture plane (see, Delorme *et al.* (2013)). Here, for the simplification of the problem, a 2D formulation is presented.

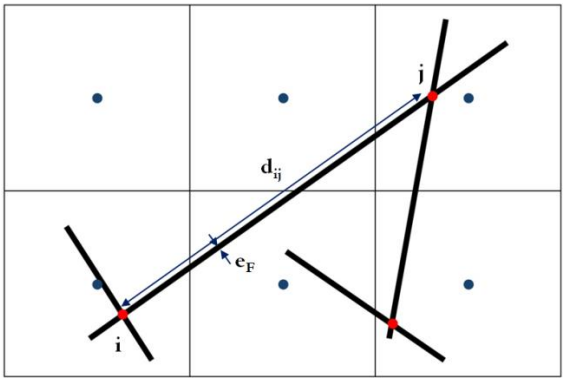

Figure 4.3: Illustration of intersections between hydraulic fractures, where each intersection is assigned by a red fracture node.

The connection between the fracture nodes for 2D problem in XY plane is done by:

$$T_{Frac\ node_i/Frac\ node_j} = A_F * \frac{k_F}{d_{ij}} \tag{4.1}$$

and

$$A_F = e_F * Z_F$$

where k_F corresponds to the fracture conductivity, A_F to the fracture exchange area and d_{ij} represents the distance between the two fracture nodes, respectively node i and j. Also, e_F corresponds to the hydraulic fracture aperture and Z_F to the fracture depth in z direction.

4.1.2 Exchange Between High Conductive and Homogenized Fractures

To connect the hydraulic fractures to the homogenized media, the transmissibility can be calculated in different ways. In this section, we present two formulas, one based on the linear pressure distribution around the fractures and the other based on the a more realistic pressure distribution given by an integral representation. For the linear approach, the transmissibility is computed using the following equation:

$$T_{ij} = \frac{k'_{fi} * k_F\,(d_i + d_j)}{k'_{fi} * d_j + k_F * d_i} * \frac{A_F}{d_i + d_j} \approx \frac{k'_{fi}}{d_i} * A_F \tag{4.2}$$

where, i corresponds to a homogenized fracture grid cell, j corresponds to a hydraulic fracture node, A_F corresponds to the hydraulic fracture exchange surface of the $node_j$ within the homogenized grid cell i, k'_{fi} corresponds to the homogenized fractures permeability. The distance d_i corresponds to the average distance from the grid cell to the hydraulic fractures.

The distance is calculated using a stochastic approach based on a randomly method (randomly points inside the grid cell). Firstly, the cell grid is discretized into n sub-domains and a

point is randomly selected in each sub-domain (see, Figure 4.4). Using random point may avoid biased distance distribution computation for fractures of type Warren and Root, where the fractures are parallel to the grid axes. Once the distance to the fractures is calculated, the average distance from the homogenized grid cell to the hydraulic fractures is obtained:

$$< d_i >= \frac{1}{p}\sum_{k=0}^{p-1} d_{k(pt-frac)}) \tag{4.3}$$

where, p is the number of sample points launched into the studied grid cell and $d_{k(pt-frac)}$ corresponds to the distance from each sample point to the nearest fracture inside the grid cell.

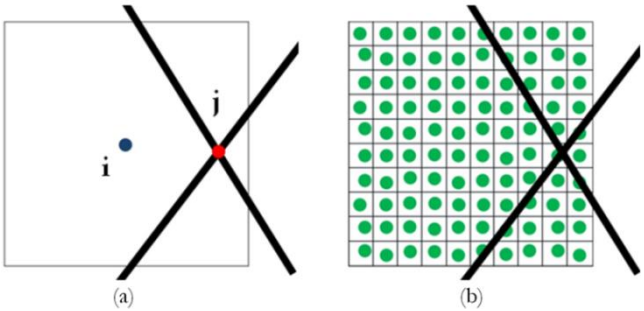

Figure 4.4: Illustration of (a) a connection between hydraulic fractures (red node j) and homogenized fractures (blue node i) (b) the homogenized grid cell is discretized into p sub-domains and p points were launched randomly.

On the other hand, an homogenized grid cell could connect to more than one fracture node (see, Figure 4.5). In fact, once a hydraulic fracture intersects with an homogenized grid cell, a transmissibility must be calculated between the fracture node and the homogenized grid cell node depending on the hydraulic fracture surface intersecting with the homogenized cell associated to the considered fracture node.

Taking this example below, homogenized fracture node m (blue node) will connect with both hydraulic fractures node i and i' respectively. For example, the transmissibility calculation $T_{mi'}$, between fracture node i' and homogenized fracture node m, will take into consideration the exchange surface of the hydraulic fractures intersecting with the homogenized grid cell (red

dashed fracture). On the other side, the connection between fracture node i and matrix node m take into account the green dashed hydraulic fracture surface (see, Figure 4.6).

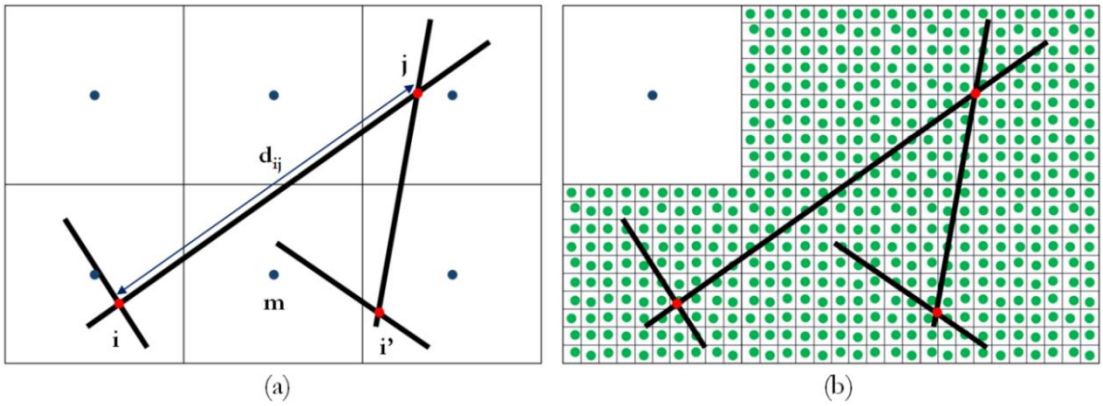

Figure 4.5: Illustration of (a) the intersection of hydraulic fractures with one or more homogenized natural fractures grid cells and (b) the distance distribution computation where p points were launched in each homogenized grid cell intersecting with a hydraulic fracture.

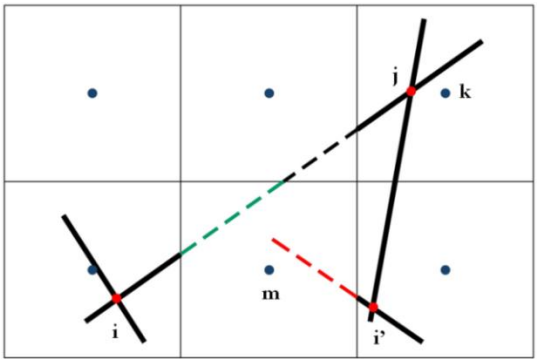

Figure 4.6: Illustration of a homogenized grid cell m connecting to two fractures nodes i and i'.

The transmissibilities can also be determined using a steady-state (or pseudo-steady-state) pressure field around the explicitly discretized fractures. The pressure field can be represented using the integral approach (see, Ding *et al.* (2014b)). Once the pressure field around the fracture is known, the transmissibility between the homogenized fracture cell and the hydraulic fractures is corrected by the following formula:

$$T_{kj} = \frac{Q_{kj}}{P_j - P_k} \tag{4.4}$$

where, P_j is the node j of the discrete fracture, P_k is the average pressure on the homogenized fracture cell k, Q_{ij} is the flow rate from the cell k to the fracture node j through the exchange surface A_F. All these variables are computed using the integral method (see, Ding *et al.* 2014b). These two different transmissibility formulas will be compared through some examples hereafter.

4.1.3 Flow Between Homogenized Low Conductive Fractures

The low conductive fractures are homogenized. Concerning an isotropic 3D case, a steady state flow is described by:

$$k_f\left(\frac{\partial^2 P}{\partial x^2}+\frac{\partial^2 P}{\partial y^2}+\frac{\partial^2 P}{\partial z^2}\right)=q \tag{4.5}$$

Otherwise, for an anisotropic case, the equation can be given by:

$$k_{fx}\frac{\partial^2 P}{\partial x^2}+k_{fy}\frac{\partial^2 P}{\partial y^2}+k_{fz}\frac{\partial^2 P}{\partial z^2}=q \tag{4.6}$$

where, P is the pressure, k_{fx}, k_{fy}, and k_{fz} are the fracture permeability in x, y and z direction respectively.

However, using the following transformation:

$$\begin{cases} x'=\dfrac{(k_{fx}k_{fy}k_{fz})^{\frac{1}{6}}}{k_{fx}^{\frac{1}{2}}}x=ax \\ y'=\dfrac{(k_{fx}k_{fy}k_{fz})^{\frac{1}{6}}}{k_{fy}^{\frac{1}{2}}}y=by \\ z'=\dfrac{(k_{fx}k_{fy}k_{fz})^{\frac{1}{6}}}{k_{fz}^{\frac{1}{2}}}z=cz \end{cases} \tag{4.7}$$

Equation (4.6) becomes an isotropic case:

$$k'_f \left\{ \frac{\partial^2 P}{\partial x'^2} + \frac{\partial^2 P}{\partial y'^2} + \frac{\partial^2 P}{\partial z'^2} \right\} = q \tag{4.8}$$

where,

$$k'_f = \sqrt[3]{k_{fx} k_{fy} k_{fz}}$$

The connection between two grid cells of homogenized low conductivity fractures, assigned by a blue node in the Figure 4.7, is calculated using Equation (4.9):

$$T_{ij} = A_{ij} * \frac{k'_{fi} * k'_{fj}}{d_i k'_{fj} + d_j k'_{fi}} \tag{4.9}$$

where, A_{ij} correspond to the exchange surface between the two homogenized grid cells in the isotropic space, k'_{fi} and k'_{fj} correspond to the homogenized fractures permeabilities, respectively to node i and node j. The distances d_i and d_j correspond to the distance from the center of the cell to the exchange surface in the transformed isotropic space.

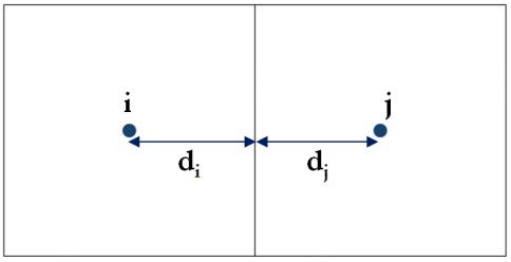

Figure 4.7: Illustration of two homogenized grid cells node i and j.

For the cells near the discrete fractures, the transmissibility can also be computed using the integral approach, because it can give more realistic pressure distribution around the fractures. In that case, the transmissibility can be corrected by:

$$T_{ij} = \frac{F_{ij}}{P_j - P_i} \tag{4.10}$$

where, P_j and P_i are average pressures on the homogenized fracture cells i and j, given with the integral representation (see, Ding *et al.* (2014b)). F_{ij} is the flow exchange between these two gridblocks, also computed with the integral formula, which corresponds to the pressure normal directive on the exchange surface.

In this chapter, examples will be presented to compare the transmissibility calculation from the linear approach (Equation (4.9)) to the transmissibility from the integral approach (Equation (4.10)). In other words, the integral approach could be explained by Figure 4.8. where a hydraulic fractures intersects with a homogenized grid cell (node j). In order to connect the two homogenized grid cells node i and node j, the integral approach Equation (4.10) uses P_i and P_j which are considered as the average pressure of cell i and j taking into consideration the presence of the hydraulic fracture..

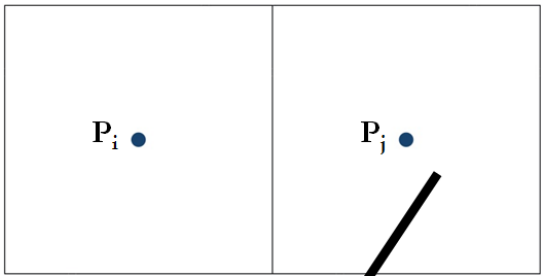

Figure 4.8: Illustration of two homogenized grid cells, with the presence of a hydraulic fracture in grid cell j.

4.1.4 Interaction Between Matrix and All Sort of Fractures

Hereafter, the description of the connection between homogenized fractures cells and matrix will be detailed. The MINC proximity function is applied to compute the matrix and fracture exchange, and the connection between the subdivisions of the matrix media using the MINC proximity function is discussed. Note that, a detailed description of the MINC proximity function is presented in Appendix B - MINC Proximity Function.

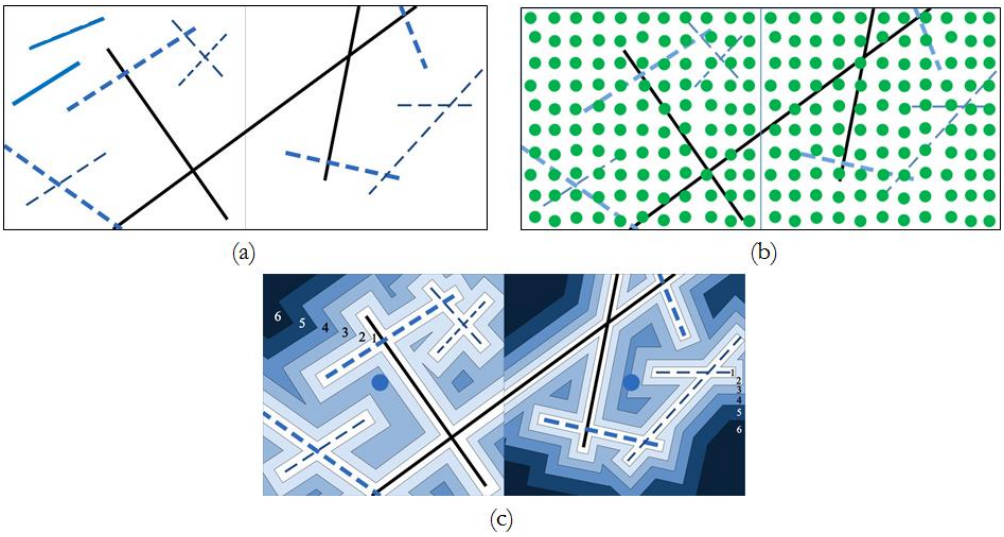

Figure 4.9: Illustration of (a) an irregular fracture distribution (connected and isolated), (b) computing the MINC proximity function only on the connected network and (c) a MINC6 model is applied.

Inside the SRV, a connection between the fractures and the matrix media must be handled. The calculation of the exchange surface of all sorts of fractures intersecting with a grid cell is considered. In other words, hydraulic, stimulated and non-stimulated natural fractures are taken into account in order to apply the MINC proximity function for matrix-fracture exchange modelling (see, Figure 4.9). To do so, a number of points is randomly launched, as explained earlier. Thus, a point distribution versus the distance from the fractures can be plotted for each grid cell, corresponding to density function or a cumulative distribution function (see, Figure 4.10).

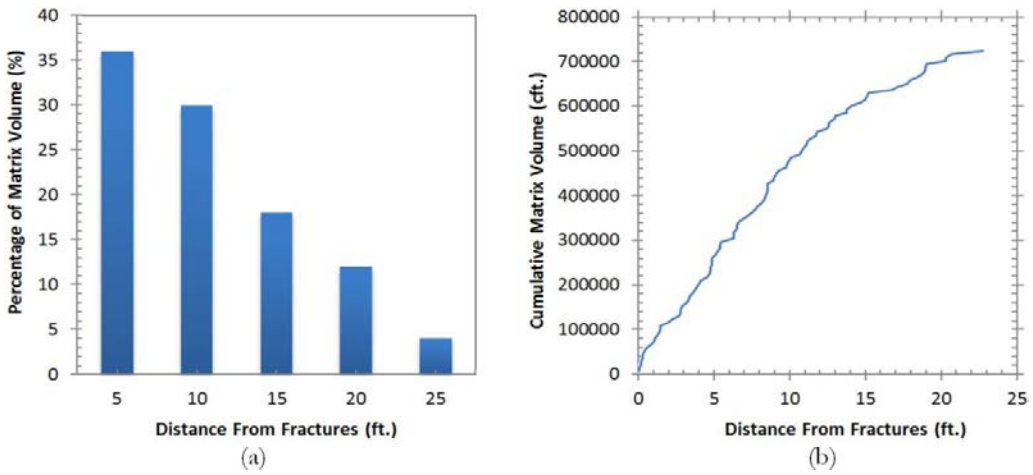

Figure 4.10: Illustration of an example representing (a) a distribution function and (b) the cumulative matrix volume distribution function.

Using the density or the distribution function, the matrix cell is subdivided relatively to the distance from the fractures. For example, the volume from the fracture to a given distance d1 consists in the first continuum (#1) of the MINC method of the matrix media. So, this matrix volume is connected to the homogenized fracture cell using Equation (4.9):

$$\left.\begin{aligned} T_{frac-hom/mat} &= \frac{k_f' * k_m}{d_{frac-hom}K_m + d_{mat}k_f'} * A_{All\ sort\ of fractures} \\ &= \frac{k_f' * k_m}{d_{mat} * \left(\frac{d_{frac-hom}}{d_{mat}}k_m + k_f'\right)} * A_{All\ sort\ of fractures} \\ &\approx \frac{k_m}{d_{mat}} * A_{All\ sort\ of fractures} \end{aligned}\right\} \quad (4.11)$$

where, $A_{All\ sort\ of\ fractures}$ corresponds to the surface taking into account all sort of fractures within this grid cell, k_f' is the permeability of homogenized fracture cell, $d_{frac-hom}$ corresponds to the half average fracture aperture, k_m correspond to the matrix permeability and d_{mat} to the average distance from the first continuum (# 1) of the matrix media (see, Figure 4.9).

The MINC proximity function is computed using a random approach. Usually, the sub-domains are constrained by a given percentage of the total volume, defined by the user. So, we can consider the volumes are known. Instead, we need to determine the distances which separate two sub-domains. This is not a difficult task. The biggest challenge in this work is to calculate the area of an interface between two sub-domains. One solution is to approximate the exchange surface with the derivative of the cumulative function with respect to the distance as follow:

$$A_{exchange\ i,i+1} = \frac{dV}{dx} = \frac{V_{i+1} - V_{i-1}}{d_{i+1} - d_{i-1}} \quad (4.12)$$

where, the distance d_{i+1} corresponds to the average distance from volume V_{i+1} to the fratures and d_{i-1} is the average distance of V_{i-1}. The volumes V_{i+1} and V_{i-1} correspond to the cumulative volume of grid cells $i+1$ and $i-1$ respectively.

Once the exchange area is known, the connection transmissibility between the matrix subdivisions is calculated by:

$$T_{mat/mat} = k_m \frac{A_{exchange}}{d_{ij}} \tag{4.13}$$

where, d_{ij} corresponds to the average distance between two successive matrix subdivisions.

4.1.5 Connection Between SRV and Non-SRV Matrix Media

Concerning the connection between SRV matrix media (MINC subdivision) and the non-SRV matrix transmissibility must be calculated in order to modelling properly the contribution of fluid flow from outside the SRV zone. Let's take the example of the Figure 4.11.

In this example, a non-SRV matrix media (node j) should connect with the matrix media of the MINC subdivision inside the SRV. So, a transmissibility calculation must be done between continuum #1, 2, 3, 4, 5, 6 and the non-SRV grid cell. In Chapter 3, we presented a MINC approach for the regular Warren and Root's fracture network modelling. In this part, we will present a different strategy to handle general discrete fracture networks.

To do so, hereafter the calculation of such transmissibility is detailed. First, the exchange surface $A_{non-SRV/\#i}$ between the non-SRV grid cell and each SRV matrix subdivision $\#i$ must be calculated. This exchange surface could be computed numerically. The idea consists in launching p (here p=20, see, Figure 4.11.) points on the exchange surface $A_{non-SRV/SRV}$. For example, the surface exchange between the non-SRV grid cell (node j) and the matrix continuum #6 of the SRV grid cell (node i) $A_{non-SRV/\#6}$ is calculated by the following equation:

$$A_{non-SRV/\#6} = p_6 \frac{A_{non-SRV/SRV}}{p} \tag{4.14}$$

where, p_6 is the number of points near the surface contained in subdivision #6 (here p_6=7).

The exchange area between a non-SRV grid cell and a subdivision i is written:

$$A_{non\ SRV/\#i} = p_i \frac{A_{non-SRV/SRV}}{p} \tag{4.15}$$

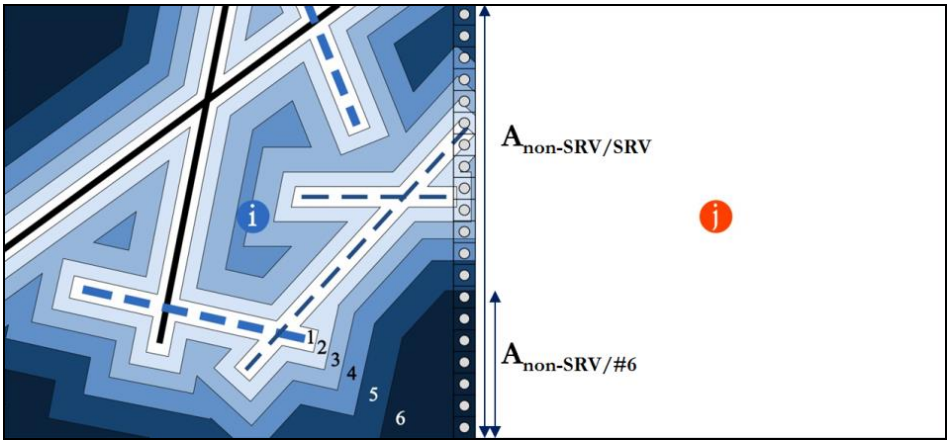

Figure 4.11: Illustration of the random points launched near to the exchange surface between a SRN and a non-SRV grid cells.

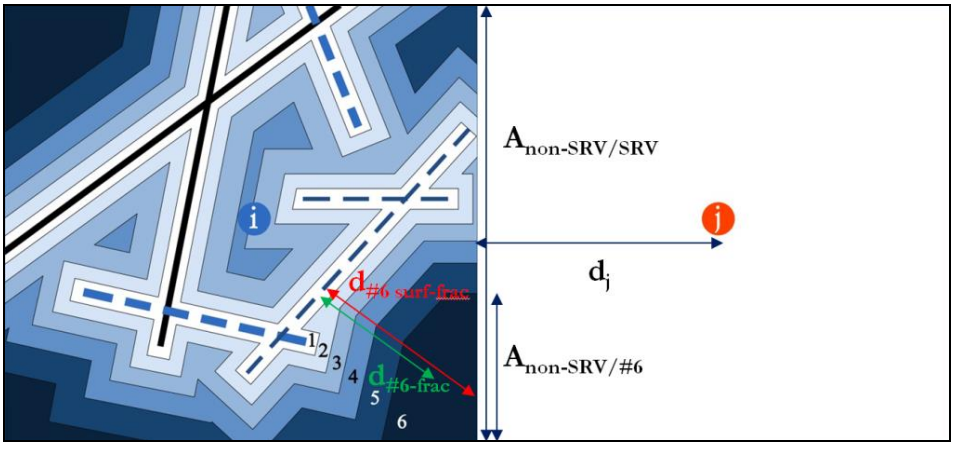

Figure 4.12: Illustration of the connection between a SRV (node i) and a non-SRV (node j) grid cells.

Once the exchange area is determined, the transmissibility is calculated by Equation (4.16). For simplicity, here a homogeneous matrix permeability k_m is taken into account. Thus, the transmissibility is written as follow:

$$T_{non\ SRV/\#i} = \frac{k_m}{d_{non\ SRV/\#i}} A_{non\ SRV/\#i} \tag{4.16}$$

where, $d_{\text{non SVR}/\#i}$ represents the distance between these two media, given by:

$$d_{non\ SRV/\#i} = d_j + d_{\#i}$$

and (4.17)

$$d_{\#i} = d_{\#i\ surf-frac} - d_{\#i-frac}$$

where, d_j correspond to the distance from the center of the continuum of the non-SRV cell to the surface separating the two grid cells and $d_{\#i}$ corresponds to the difference of the average distance $d_{\#i\ surf-frac}$ from the exchange surface $A_{non\ SRV/\#i}$ to the fractures and the average distance $d_{\#i-frac}$ of the MINC subdivision $\#i$ towards the fractures (see, Figure 4.12). Note that we use only positive distance, that is, if $d_{\#i} < 0$, then we define $d_{\#i} = 0$, so $d_{non\ SRV/\#i} = d_j$.

4.1.6 Intersection Between Hydraulic Fractures and the Well

Concerning the connection between a horizontal well (red dashed line in Figure 4.13) and a hydraulic fracture, note that the intersection between the well and the hydraulic fracture is defined by a node (green node on Figure 4.13). Transmissibility must be calculated between red and green nodes using Equation (4.16).

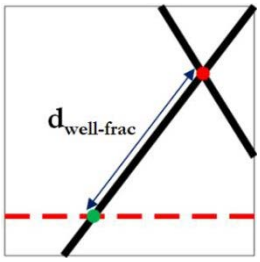

Figure 4.13: Illustration of the intersection between a horizontal well and a hydraulic fracture.

$$T_{well-Frac} = \frac{k_F}{d_{well-Frac}} A_F \tag{4.18}$$

where, k_F is the fracture permeability, A_F corresponds to the exchange surface ($A_F = e_F * Z_F$) and $d_{well-Frac}$ correspond to the average distance between the two nodes (red and green nodes). To take into account the radial flow behavior towards the well, a numerical PI is used for the flow modelling inside the fracture plane to connect the calculated well node pressure and the true wellbore pressure (see, Ding (1996)).

4.2 Validation Test on Simple Examples

In this part, several simple cases treating a single phase flow are studied in order to validate our DFM based on a MINC proximity function. For each example, three simulation models (a reference solution, a dual-porosity model and our DFM) are performed. It must be mentioned that, using a DP model the block size cannot be properly determined for some kinds of fracture distributions. So, the dual-porosity model presented for examples #2, 3, 4 and 5 corresponds to our DFM without any matrix refinement. As mentioned before, a DP model is a particular case of the MINC method where the matrix subdivision is set at 1.

4.2.1 Example 1 – Cross Fractures

The following example consists in a matrix block of 65 ft in x and y directions with the presence of two hydraulic fractures with a fracture aperture fixed at 0.04 ft placed in the center of

the block as shown in the Figure 4.14(a). The permeabilities are defined as 0.0001 mD and 2000 mD, in the matrix and fracture media respectively. The porosity of the matrix media is 0.05.The depth of the block is 330 ft in z direction. A horizontal well is placed into the formation. The intersection of the well with the hydraulic fracture (dashed line) is illustrated by the green dot in Figure 4.14(a).

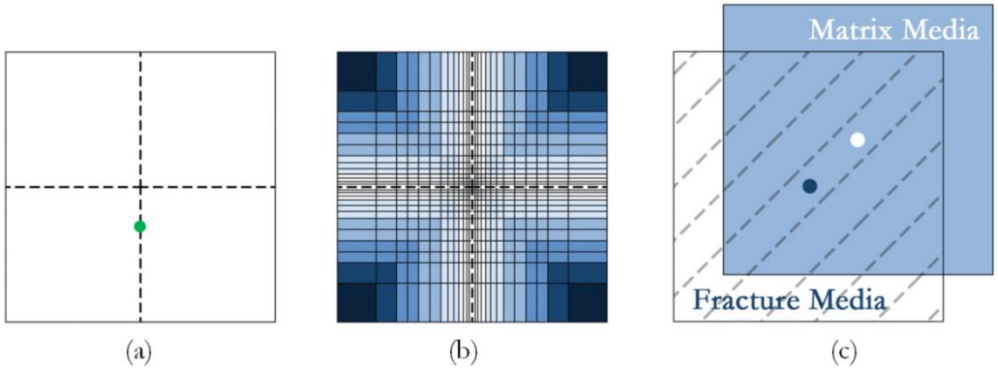

Figure 4.14: Illustration of (a) a cross fracture model, (b) the explicit discretized model and (c) the standard dual-porosity model.

Three simulation models are performed. An explicit model which explicitly discretized the fractures using a local grid refinement (LGR) around the fractures is applied. This model uses very small grid cells and it will be set as a reference solution (Figure 4.14(b)). A standard dual-porosity (DP) model using a block of 50 ft is performed and illustrated in Figure 4.14(c). Care was taken in the calculation of the effective fracture permeability and porosity for the DP model. On the other hand, a discrete fracture model based on a MINC proximity function using a randomly points distribution is performed (see, Figure 4.15(a)). An illustration of our DFM where a red dot is assigned to the intersection between the fractures is presented in Figure 4.15(b). In fact, the domain Figure 4.15(a) is discretized into p equal volumes and then a randomly point is selected in each discretized volume. For example, here our matrix block is subdivided into p = 100 sub-domains (10 subdivisions in each direction), where a random point which belongs to each subdomain is selected. Moreover, the DFM based on a MINC6 model is presented in Figure 4.15(b).

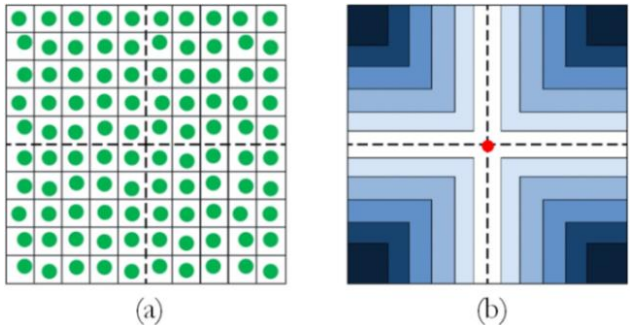

Figure 4.15: An illustration of (a) the stochastic approach for a regular distribution of p points, where the volume is discretized into p equal volume (cubic or rectangular) sub-domains and then a randomly point in each discretized domain is selected and (b) the optimization of the MINC proximity function.

Figure 4.16 illustrates the cumulative distribution function using 100 points (Figure 4.16(a)) and 1000 points (Figure 4.16(b)). In practice, we should limit the number of sampling points in the numerical approach due to CPU time constraint. However, working with a high number of sample points provides a better distribution function as shown in Figure 4.16(b), and it gives us a much accurate result. In fact, as much as the number of randomly points is high, as much as the calculation of the transmissibility is precise and our DFM is accurate comparing to reference solution. To test the robustness of our approach, here the number of random points is limited at 100 points.

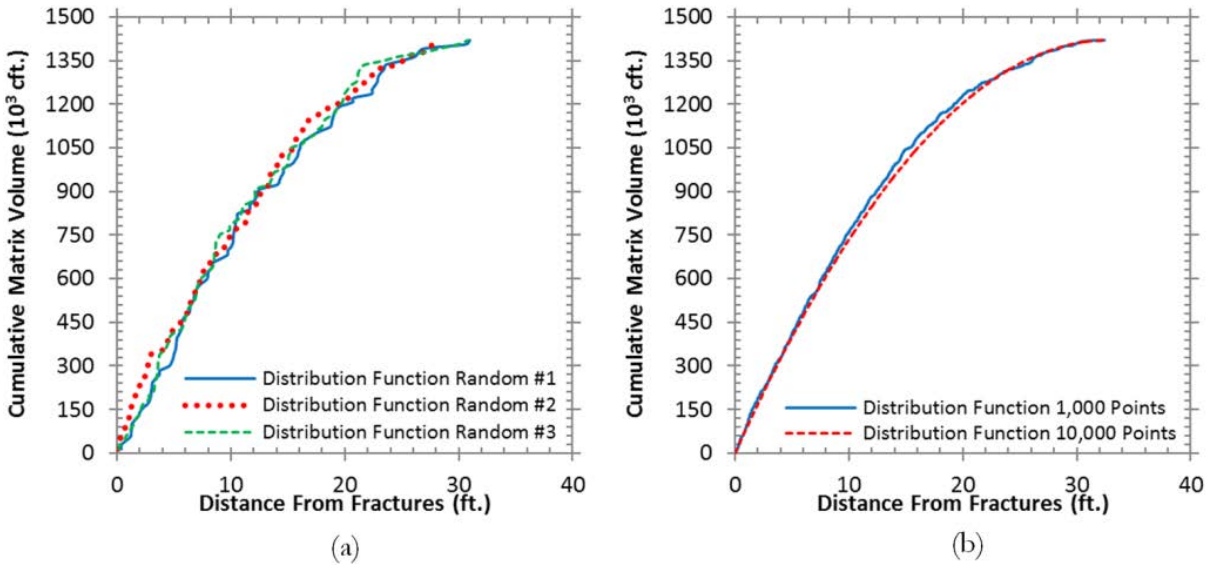

Figure 4.16: Illustration of the cumulative distribution function for (a) a sample of 100 points and (b) 1000 points using the randomly discretized technique for the block of 50ft.

In this part three different simulation models are performed, the explicit discretized model, the dual-porosity model and our DFM based on a MINC6 model. Moreover, in order to study the ability of our DFM approach, three sets of random points (Random #1, Random #2 and Random #3) are generated for the case presented in Figure 4.14 to compute the MINC6 proximity function. Only a single phase (gas only) flow simulation is performed. A horizontal well is connected to the fractures. The initial reservoir pressure is 3800 psi and the bottom hole well flowing pressure is 1000 psi.

The cumulative gas production using different simulation models are presented in Figure 4.17. Clearly, the DP model is not accurate comparing to the explicit discretized model. On the other hand, using our DFM with different random point distributions shows a little impact on the simulation results comparing to the explicit model. All these three DFM simulations are very close to the reference solution.

Clearly, the results shown in Figure 4.17 proves the efficiency of our DFM using only 100 sample points comparing to the DP model which is not accurate. Finally, we can conclude that our DFM based on a MINC proximity function could handle the matrix-fracture exchange with a very good accuracy.

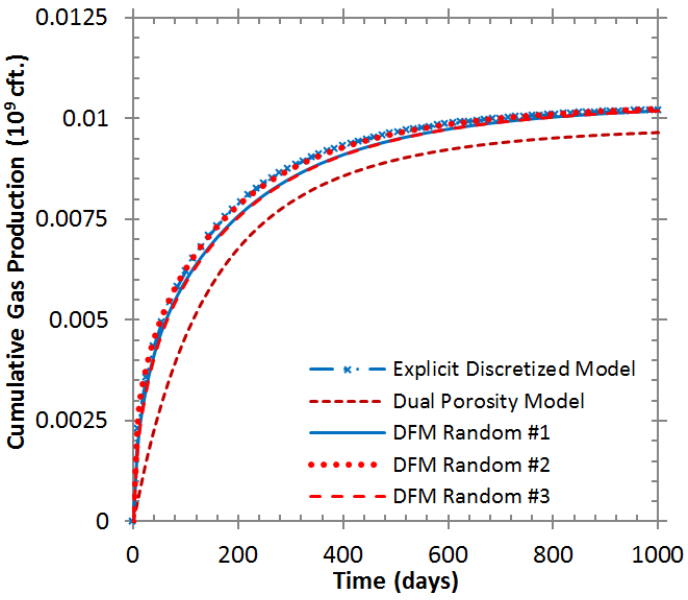

Figure 4.17: Comparison of the cumulative gas production using different simulation models

4.2.2 Example 2 – Isolated Fracture

In this part, an isolated fracture aligned with the coordinate axes is tested with a single phase flow case (only gas) in order to study the ability of our approach. The following example consists in a grid block of 50 ft in x and 100 ft in y directions with the presence of a single hydraulic fracture, with a fracture aperture fixed at 0.01 ft, as shown in the Figure 4.18. The net thickness of the block is 330 ft. The permeabilities are defined as 0.0001 mD and 2 D in the matrix and fractures medias, respectively. The porosity of the matrix media is 0.05.

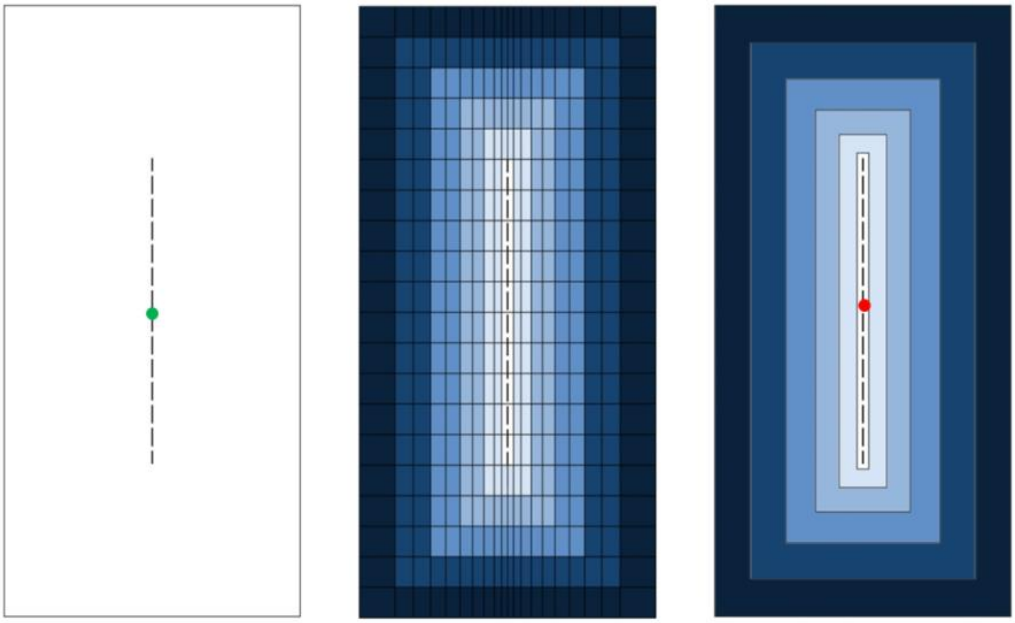

Figure 4.18: Illustration of (a) an isolated fracture, (b) the explicit model and (c) the DFM based on the MINC method.

First, an explicit discretized model is performed. This model requires a lot of fine grids cells. For the fine-grid simulation, the grid is 85×20×1 cells in the x, y, and z directions respectively. The cell dimensions are uniform in y and z directions, while they are non-uniform in x direction to accommodate refinement near fractures. The grid description is presented in Table 4.1. This model is set as a reference solution. A dual-porosity model (no matrix refinement) is also performed.

Moreover, the improved discrete fracture model with the MINC proximity function using a stochastic process is performed for a MINC6 using one grid matrix cell of 50 ft, 100 ft and 20

ft for x, y and z respectively (see, Figure 4.18). Initial reservoir pressure is at 3800 psi and the BHP is set as 1000 psi.

Table 4.1: Grid description of the reference for the example presented in Figure 4.18(b).

Case	Axis	Grid Description
Isolated Fracture	ΔX, ft	5.505 3 2 1 0.95 0.9 0.85 0.8 0.75 0.7 0.65 0.6 0.55 0.5 0.48 0.46 0.44 0.42 0.4 0.38 0.36 0.34 0.32 0.3 0.28 0.26 0.24 0.22 0.2 0.18 0.16 0.14 0.12 0.1 0.09 0.08 0.07 0.06 0.05 0.04 0.03 0.02 0.01 0.02 0.03 0.04 0.05 0.06 0.07 0.08 0.09 0.1 0.12 0.14 0.16 0.18 0.2 0.22 0.24 0.26 0.28 0.3 0.32 0.34 0.36 0.38 0.4 0.42 0.44 0.46 0.48 0.5 0.55 0.6 0.65 0.7 0.75 0.8 0.85 0.9 0.95 1 2 3 5.050
	ΔY, ft	20 x 5.0
	ΔZ, ft	20.0

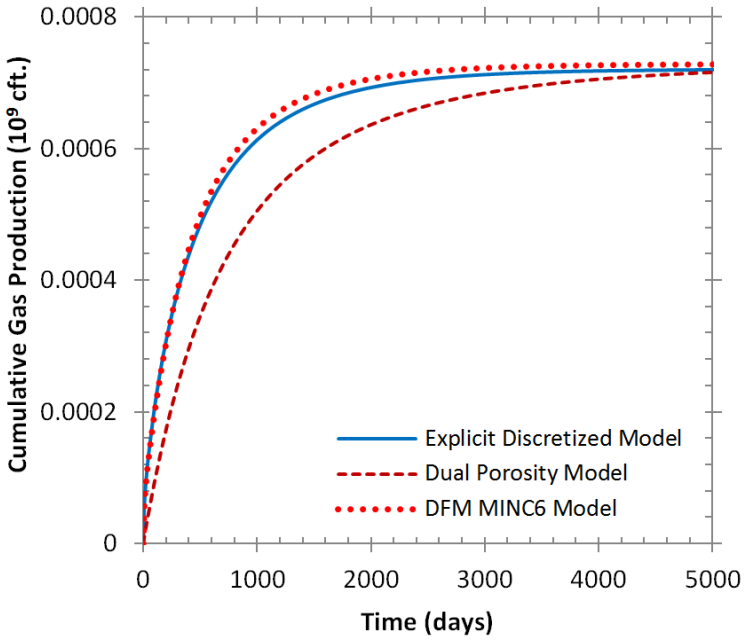

Figure 4.19: Cumulative gas production vs. time for example 2.

The results of the simulations are illustrated in Figure 4.19. The reference solution (Explicit Discretized Model) is presented with the blue solid line. A dual-porosity model is not accurate because of the transient period which could not be model by a DP model. However, the implementation of the MINC method could present a solution to this problem due to the fine

sub-grid continuum near the fractures faces which are able to handle much better the transient flow from the matrix into the fractures during the whole production period. Furthermore, Figure 4.19 presents a comparison of the gas production between these three different simulation models for 5000 days and confirms the accuracy of our discrete fracture model. The computational times for the DFM and the explicit discretized model were 0.7 and 30 seconds, respectively. Due to the MINC method, a very good agreement between both models (the DFM and the fine-grid explicit-fracture model) is found.

4.2.3 Example 3 – Orthogonal Fractures

Figure 4.20 represents a 2D fractured reservoir containing three fractures. The following example consists in a grid block of 50 ft in x and 100 ft in y directions. Also, the fracture apertures are fixed at 0.01 ft. The net thickness of the block is 20 ft. The permeabilities are defined as 0.0001 mD and 2 D, for matrix and fractures medias respectively. The porosity of the matrix media is 0.05. Note that, all fractures are vertical and aligned with the coordinate axes in order to perform a reference solution using very fine grid, where the fractures are explicitly discretized using a LGR technique as shown in Figure 4.20. For the fine-grid simulation, the grid is 95×170×1 cells in the x, y, and z directions respectively. The grid description for the reference solution is given in Table 4.2. One cell of 20 ft defines the reservoir thickness in z direction. However, cell dimensions are non-uniform in x and y to suit refinement near fractures.

Table 4.2: Grid description of the reference solution performed for the model shown in Figure 4.20(b).

Case	Axis	Grid Description
Isolated Fracture	ΔX, ft	5 3 2 1.81 0.95 0.9 0.85 0.8 0.75 0.7 0.65 0.6 0.55 0.5 0.48 0.46 0.42 0.4 0.38 0.36 0.34 0.32 0.3 0.28 0.26 0.24 0.22 0.2 0.18 0.16 0.14 0.135 0.12 0.1 0.09 0.08 0.07 0.06 0.05 0.04 0.03 0.02 0.01 0.02 0.03 0.04 0.05 0.06 0.07 0.08 0.09 0.1 0.12 0.135 0.14 0.16 0.18 0.2 0.22 0.24 0.26 0.28 0.3 0.32 0.34 0.36 0.38 0.4 0.42 0.46 0.48 0.5 0.55 0.6 0.65 0.7 0.75 0.8 0.85 0.9 0.95 1.81 2 3 5
	ΔY, ft	5 5 3 2 1.81 0.95 0.9 0.85 0.8 0.75 0.7 0.65 0.6 0.55 0.5 0.48 0.46 0.42 0.4 0.38 0.36 0.34 0.32 0.3 0.28 0.26 0.24 0.22 0.2 0.18 0.16 0.14 0.135 0.12 0.1 0.09 0.08 0.07 0.06 0.05 0.04 0.03 0.02 0.01 0.02 0.03 0.04 0.05 0.06 0.07 0.08 0.09 0.1 0.12 0.135 0.14 0.16 0.18 0.2

	0.22 0.24 0.26 0.28 0.3 0.32 0.34 0.36 0.38 0.4 0.42 0.46 0.48 0.5 0.55 0.6 0.65 0.7 0.75 0.8 0.85 0.9 0.95 1.81 2 3 3 2 1.81 0.95 0.9 0.85 0.8 0.75 0.7 0.65 0.6 0.55 0.5 0.48 0.46 0.42 0.4 0.38 0.36 0.34 0.32 0.3 0.28 0.26 0.24 0.22 0.2 0.18 0.16 0.14 0.135 0.12 0.1 0.09 0.08 0.07 0.06 0.05 0.04 0.03 0.02 0.01 0.02 0.03 0.04 0.05 0.06 0.07 0.08 0.09 0.1 0.12 0.135 0.14 0.16 0.18 0.2 0.22 0.24 0.26 0.28 0.3 0.32 0.34 0.36 0.38 0.4 0.42 0.46 0.48 0.5 0.55 0.6 0.65 0.7 0.75 0.8 0.85 0.9 0.95 1.81 2 3 5 5
ΔZ, ft	20.0

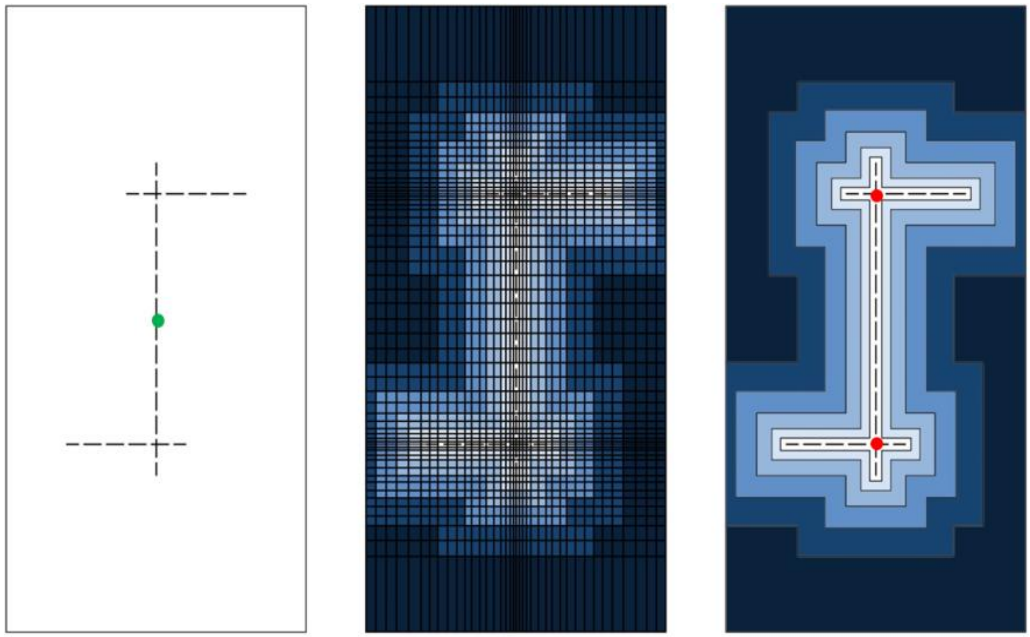

Figure 4.20: Illustration of (a) three orthogonal fractures, (b) the explicit discretized model and (c) the DFM based on the MINC method.

Three simulation models, an explicit discretized model, a dual-porosity model (no matrix refinement) and our DFM, were performed for this case. The results of the simulations are illustrated in Figure 4.21. The reference solution (explicit discretized model) is presented with the blue solid line. A dual-porosity model is not accurate because of the transient period which could not be model by a DP model. However, our DFM is able to handle much better the transient flow from the matrix into the fractures during the whole production period due to the MINC method. Our DFM using MINC6 gives satisfactory results comparing to the reference solution.

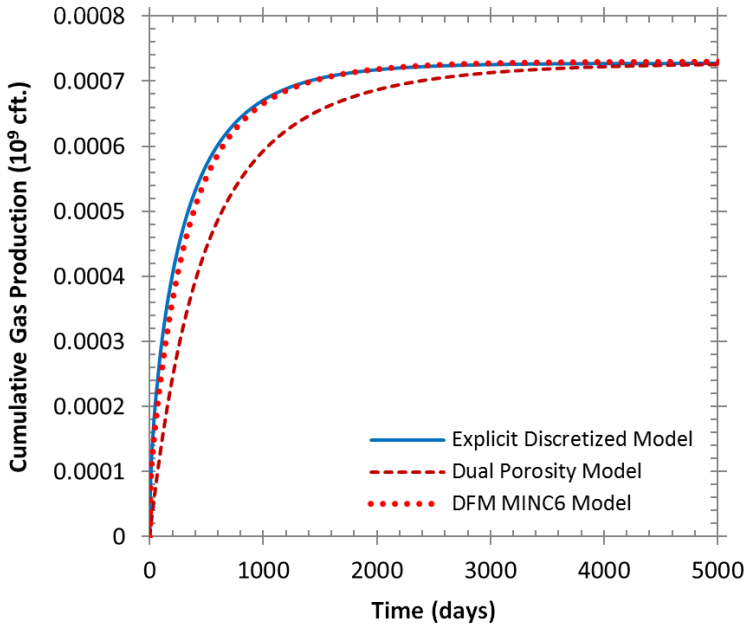

Figure 4.21: Cumulative gas production vs. time for example 3.

4.2.4 Example 4 – Diagonal Fracture

In this part, we test a diagonal fracture case for a single phase flow in order to quantify our approach. The following example consists in a grid block of 91.92388 ft (65√2 ft) in x and y direction with the presence of two hydraulic diagonal fractures, with a fracture aperture fixed at 0.004 ft, as shown in the Figure 4.22(a). The net thickness of the block is 330 ft. The permeability and porosity are the same as in the previous case.

First, a reference solution is simulated. To get the reference solution, the domain is discretized with very small matrix grid cells, because the fracture are not aligned with the grid axes. The reference solution consists in 40000 grid cells (Figure 4.22(b))) after discretizing the domain into 200 grid cells in each x and y directions. This model uses a very small grid for the exchange between the fractures and the matrix cells, where the transmissibility is calculated using the similar technique as explained in part 4.1.1 for the exchange between a discrete hydraulic fracture and a homogenized fracture cell (see, also Sarda *et al.* (2002)). This simulation is considered as a reference solution.

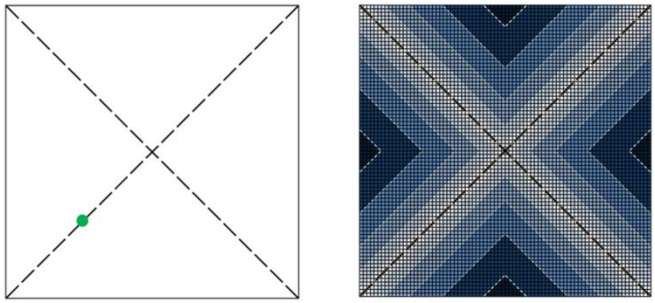

Figure 4.22: Illustration of (a) two diagonal fractures case and (b) the reference solution consisting in a small matrix grid cells.

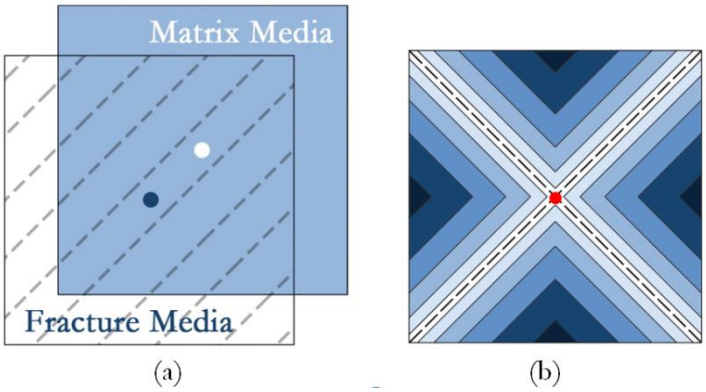

Figure 4.23: Illustration of (a) the standard dual-porosity model and (b) the application of the MINC proximity function.

Moreover, a dual-porosity model (Figure 4.23(a)) and the discrete fracture model based on the MINC proximity function using a stochastic process for a MINC6 (Figure 4.23(b)) and MINC16 are also performed.

The results of the different simulations are illustrated in Figure 4.24. The reference solution is presented with the blue solid line. The DP model (dashed line) is not accurate comparing to the reference solution. Obviously, the transient period could not be handled by DP model. Note that, our DFM based on a MINC proximity function is able to handle much better the transient flow from the matrix into the fractures during the whole production period. Moreover, both DFMs with a MINC6 and MINC16 models present an accurate result, comparing to the reference solution.

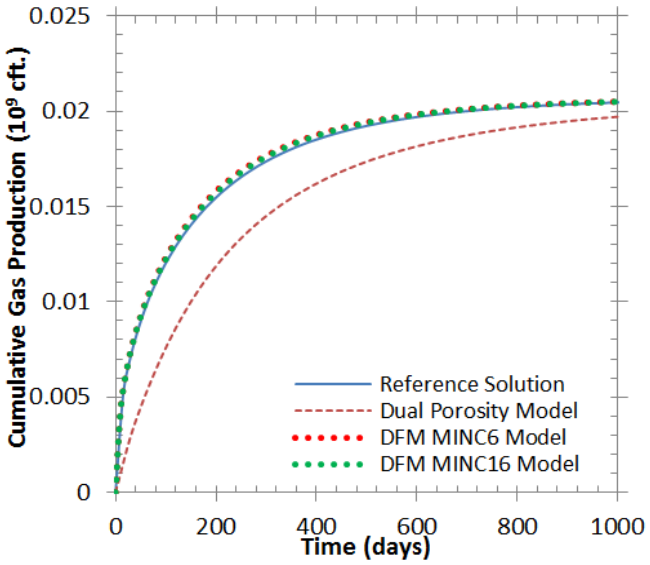

Figure 4.24: The comparison of the cumulative gas production for example 4 for different simulation models (the reference solution, the DP model, the DFM MINC6 and a MINC16) for 1000 days of production.

It has to be mentioned that our reference solution used in this part is reliable even if the fractures are not parallel to the grid axes. Let's consider a large regular fracture network as shown in Figure 4.25. Thanks to the symmetrical geometry, the simulation can be limited on a small domain described by Example 1 or Example 4 (Figure 4.25). The volume of the domain in Example 4 is two times of the volume in Example 1. So the gas production in Example 4 should be theoretically twice as that in Example 1.

Figure 4.26 presents the comparison of the cumulative gas production between the reference solution of example 4 and the explicit discretized model of example 1. In fact, example 1 produces $0.01*10^9$ cft while example 4 produces the double $0.02*10^9$ cft. Thus, multiplying the cumulative gas production of example 1 by a factor of 2, the cumulative gas production of example 4 is found perfectly as shown in Figure 4.26 (dotted red line).

Finally, as the fractures in Example 1 are parallel to the grid axes, and fine grid cells associated with local grid refinement around the fractures are used, the reference solution in Example 1 is reliable. Here, as our reference solution used in this part (Example 4) is compared to that of Example 1, we can consider it is reliable. In general, we believe that using this technique (very fine matrix cells together with discrete fractures) can provide a reliable reference solution for any irregular fracture distributions, as long as the matrix cells are fine enough. This kind of technique is used to perform a reference solution later in this work.

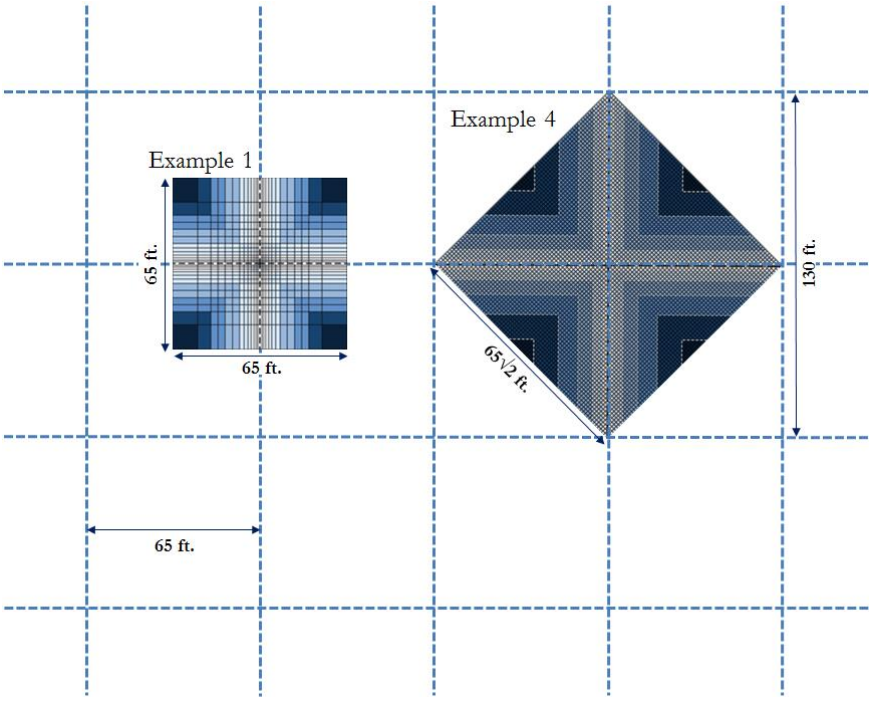

Figure 4.25: Illustration of an infinite regular fracture network describing example 1 and 4.

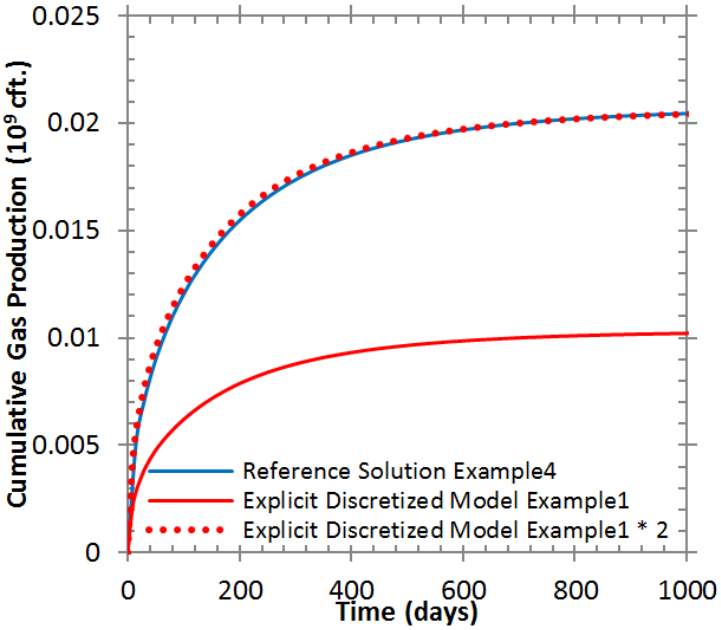

Figure 4.26: Comparison of the cumulative gas production from the reference solution of example 4 and example 1.

4.2.5 Example 5 – Irregular Fractures Distribution

In the following, we consider a block of 330 ft in x and y directions containing 5 irregular fractures distribution as shown in Figure 4.27(a). The net thickness of the reservoir in z direction is of 20 ft. In this study, the permeabilities are defined as 0.0001 mD in the matrix and 3 D in the fractures. The fracture aperture is fixed at 0.004 ft. The porosity of the matrix media is 0.05. Only a single phase (gas only) flow simulation is taken into consideration. The initial reservoir pressure is 3800 psi. A horizontal well (green dot Figure 4.27(a)) is connected to the fracture, and the bottom hole well flowing pressure is 1000 psi.

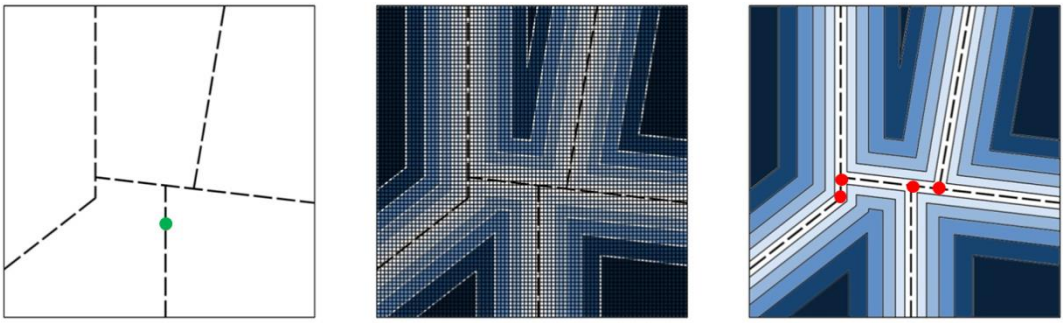

Figure 4.27: illustration of (a) an irregular fracture network, (b) the reference solution and (c) the DFM.

The same approach used in the previous part is done on this example in order to perform the reference solution as shown in Figure 4.27(b). Note that, the reference solution consists in 250000 grid cells after discretizing the domain into 500 grid cells in each x and y directions leading to a very fine matrix grid cells for the discretization of matrix media. On the other hand, a dual-porosity model is performed and our DFM based on a MINC proximity function is also performed (see, Figure 4.27(c)).

The cumulative gas production for different simulation models are shown in Figure 4.28 for 800 days of production. Based on the simulation results, clearly the DFM presents very satisfactory result comparing to the reference model. However, the standard dual-porosity model underestimates the gas production and it is not accurate comparing to the reference solution. Moreover, the DFM approach decreases greatly the CPU time from 30 minutes for the reference

solution to only 2 seconds with our DFM approach. In fact, decreasing the number of grid cell will result in decreasing significantly the CPU time.

The difference between the reference solution and our DFM in term of CPU time could be explained by the number of grid cells used to describe the problem. The reference model consists in 250000 grid cells while our DFM uses only 11 nodes to describe the same case. In fact, the discrete fracture network is represented by fracture and matrix nodes using the DFM model. This model consists in assigning a fracture node for each fracture/well and fractures/fractures intersections. For example, the case presented in Figure 4.27 will be described using 11 nodes (1 for the well intersection (green node in Figure 4.27(a)), 4 for the fracture intersections (red nodes in Figure 4.27(c)) and 6 nodes for the matrix media. In fact, here a MINC6 model was performed so 6 matrix nodes representing 6 matrix subdivisions are assigned to the matrix media (Figure 4.27(c)).

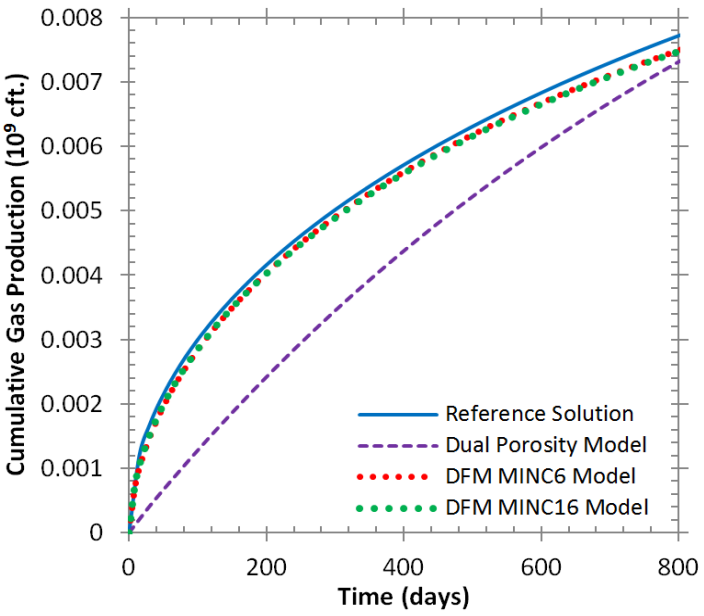

Figure 4.28: Cumulative gas production vs. time for example 5 for different simulation model.

4.3 Validation Test on a Large SRV Cases

In this section, in order to validate the discrete fracture model, a large SRV case, where simulations are first performed for a single-phase (reservoir water is not mobile) to compare

different simulation models, is studied. Once our DFM is validated for single-phase flow, a multiphase flow case consist in a 2D synthetic tight-oil reservoir will be studied in Chapter 5.

4.3.1 Regular Fractures Distribution

In this part a regular fracture distribution is tested in order to validate our DFM. Table 4.3 summarizes the reservoir properties. A horizontal well (green line in Figure 4.29) in the x-direction is placed in the middle of the reservoir intersecting with the hydraulic fracture (red solid line in Figure 4.29). It is assumed that the well production comes only directly through the hydraulic fracture. Inside the SRV, 41 natural fractures exist (blue dotted lines in Figure 4.29), where 21 natural fractures perpendicular to the well along the y-direction and 20 in the x-direction are created.

Table 4.3: Reservoir properties for the shale-gas reservoir example.

Property / Parameter	Value	Unit
Matrix Permeability	0.0001	mD
Hydraulic Fracture Permeability	50	D
Induced-fracture Permeability	200	mD
Fracture Width	0.01	ft
Induced-fracture Width	0.001	ft
Reservoir Net Thickness	300	ft
Top of the Reservoir	5800	ft
Initial Reservoir Pressure	3800	psi
Bottom Hole Well Pressure	1000	psi

A volume of 1050×1000×300 cft corresponds to the stimulated reservoir volume. Apart from the high conductive hydraulic fracture, all other fractures are homogenized in the SRV and the MINC method is applied and the matrix media is subdivided based on the distance from the fractures. The hydraulic fracture half-length is 150 ft (total length of 300 ft in y-direction), and the total length of natural fractures is 1050 ft in x-direction and 1000 ft in y-direction. Note that, the fracture spacing is 50 ft in x and y-directions. Furthermore, our reservoir model presents different scales of fractures, where the grids which are donated to the hydraulic fractures presented in y-direction have a width of 0.01 ft and a permeability of 50 D, while the stimulated natural fractures are presented in x and y-directions with a width of 0.001 ft and a permeability of 200 mD. The top of the reservoir is at a depth of 5800 ft.

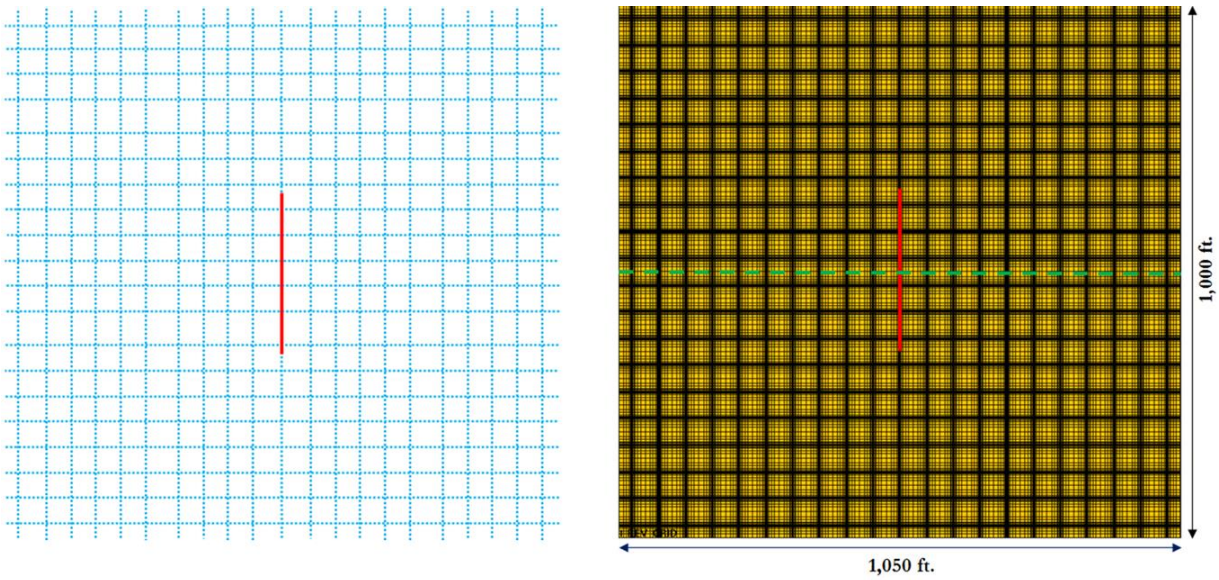

Figure 4.29: Illustration of (a) a regular fracture distribution Warren and Root type and (b) the explicit discretization of the fracture network set as a reference solution.

On one hand, a base model named "Explicit Discretized Model", which explicitly discretized all sort of fractures (hydraulic and natural fractures) using a LGR logarithmically spaced around each fracture, is considered as the reference solution. On the other hand, a standard dual-porosity model and our DFM are performed. Note that, the DP model consists in grid block size of 50 ft in x and y directions.

The three simulation models (Explicit Discretized Model, Dual-Porosity Model and the Discrete Fracture Model) are compared. Figure 4.30 presents the cumulative gas production for this regular discrete fracture network during 16000 days of production performed with these three simulation models. Obviously, our DFM based on a MINC proximity function provides a much better result than the dual-porosity model and can almost match the explicit discretized model (reference solution). Clearly, the dual-porosity model underestimates the gas production. Our DFM shows the ability of predicting gas production from unconventional fractured gas reservoirs, while a dual-porosity model is inaccurate for such problems.

We also noticed that using our DFM in this example underestimates lightly the gas production comparing to the reference solution. This could be explained by the low natural fracture or the homogenized fracture permeability (k_{nf}=200 mD). In order to improve the flow prediction using our DFM, we suggest to modified (or correct) the transmissibility connection

between the homogenized media around the hydraulic fracture. In fact, we propose to adjust the transmissibility calculation between homogenized grid cells (red nodes in Figure 4.31) using the transmissibility formulas Equations (4.4) and (4.10) which takes into account a more realistic pressure distributions around the hydraulic fractures with integral methods.

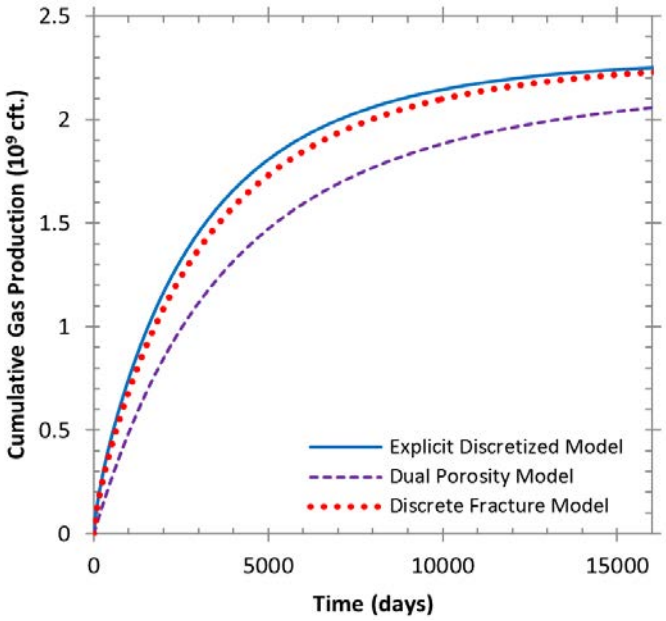

Figure 4.30: Cumulative gas production vs. time.

Once the presence of the hydraulic fracture is taken into account and the transmissibility between homogenized grid cells around the hydraulic are fixed, the flow modelling from the homogenized fractures to the hydraulic one is better simulated. Figure 4.32 presents the comparison of the cumulative gas production for 16000 days of production for our DFM without and with correction using the integral approach to the reference solution. Obviously, the gas prediction is ameliorated using our corrected DFM with the integral approach, comparing to the reference solution.

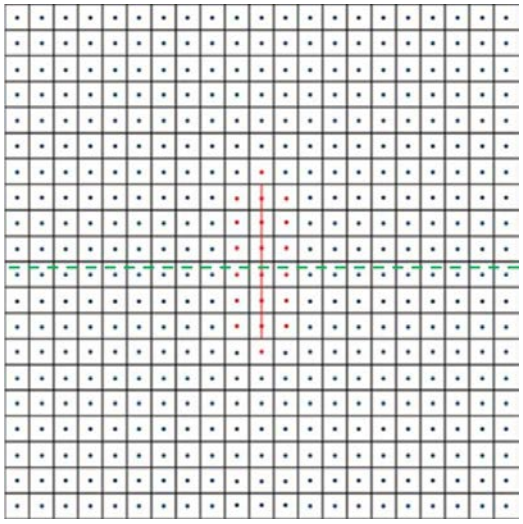

Figure 4.31: Illustration of the grid cells affected by the improvement transmissibility calculation process.

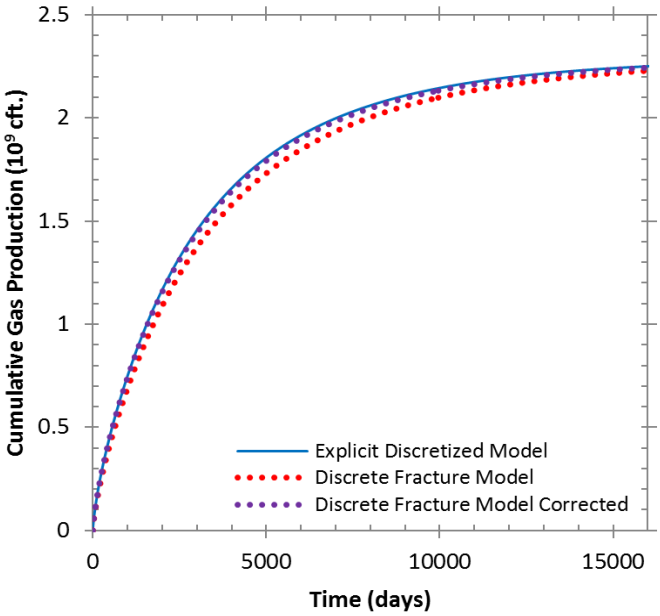

Figure 4.32: Comparison of the cumulative gas production for the hybrid approach with and without transmissibility improvement with the reference solution.

However, working with high natural fracture permeability in low matrix permeability reservoirs, no transmissibility correction is needed. In fact, if the natural fracture permeability (k_{nf}) is high enough, then the gas will flow quickly to the hydraulic fracture and the well through the natural fractures. The pressures in natural fractures are as low as that in the hydraulic fracture, and the accuracy of transmissibility calculation in the homogenized fracture media is not a key issue as long as the natural fracture permeability is high enough. Otherwise, the accuracy of transmissibility values for flow exchange between hydraulic fracture and homogenized natural fractures is important.

This claim is supported by Figure 4.33 where the natural fracture permeability k_{nf} is set as 2 D instead of 200 mD. Figure 4.33 presents the comparison of the cumulative gas production between the DFM and the reference solution.

Clearly, our DFM is able to predict the cumulative gas for 5000 days of production without any transmissibility correction as the induced fracture permeability is high enough. On the other hand, the gas production increases by increasing the natural fractures permeability. Our DFM reacts perfectly and it is able to predict gas production for different fracture permeability comparing to the reference solution.

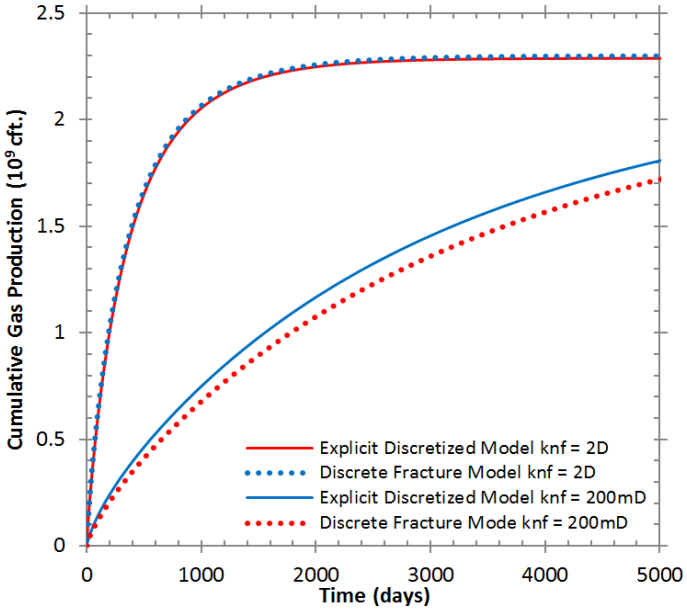

Figure 4.33: Cumulative gas production vs. time.

Finally, our DFM based on MINC proximity function proves its accuracy for the application on shale-gas reservoirs, at least for single-phase flow problems. In fact, discretizing the matrix blocks into a sequence of volume elements can handle much better the transient flow from the matrix into the fractures during the whole production period.

4.3.2 Regular Fracture Distribution with a Non-Uniform SRV

The purpose of this second example is to investigate if our MINC proximity function based model is able to modelling the fluid flow between SRV and non-SRV region. A synthetic 2D model reservoir shown in Figure 4.34 is evaluated. The reservoir dimensions remain the same as before, where the reservoir consist in 1050×1000×300 cft. The model contains 49 natural fractures (blue dotted line in Figure 4.34) with one hydraulic fracture of 300 ft placed in the middle of the reservoir. Note that, fracture spacing is set at 50 ft in x and y direction. The hydraulic fracture intercepts a horizontal well (green dashed line in Figure 4.35).

The water saturation in the rock matrix is at the irreducible water saturation of 0.35. The initial reservoir pressure is 3800 psi and the horizontal well produces at a constant bottom hole pressure of 1000 psi. It must be mentioned that, we consider that all fractures in our model are propped and open. Furthermore, we don't simulate the hydraulic fracturing operation. The

aperture of stimulated natural fractures and the hydraulic fracture are set as 0.001 ft and 0.01 ft, respectively.

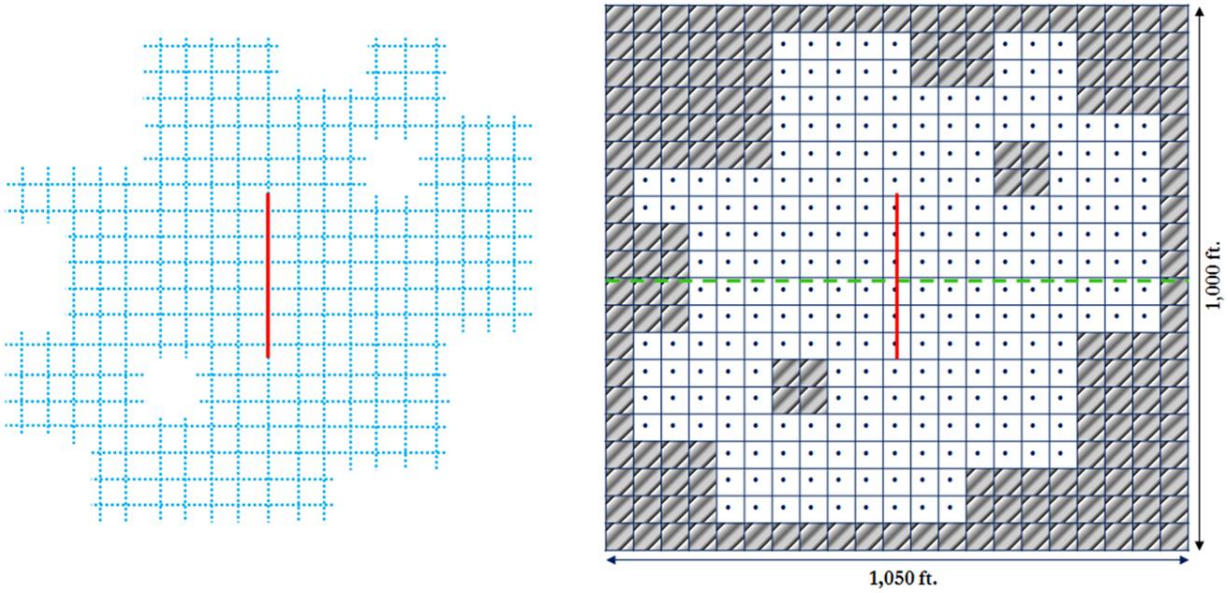

Figure 4.34: A DFN with a regular fracture distribution presenting an non regular SRV shape.

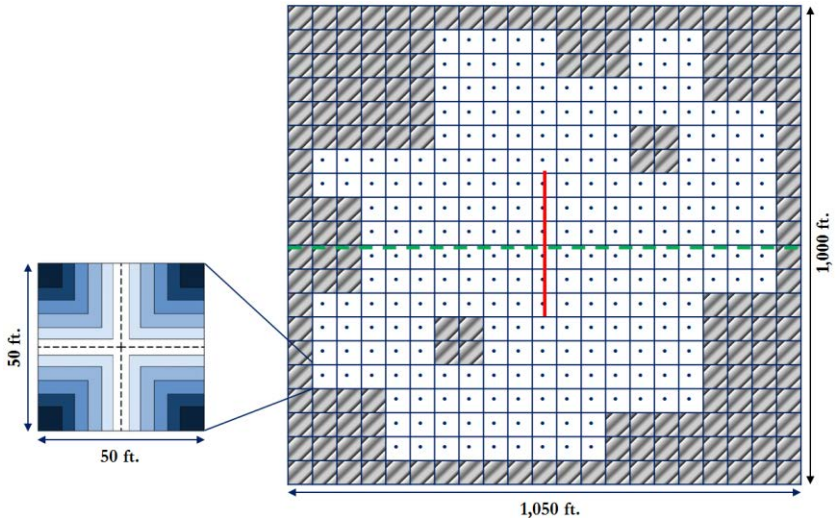

Figure 4.35: Illustration of the hybrid approach technique using the MINC method inside the SRV region while the hydraulic fracture is explicitly discretized.

The reference solution consists in 567×540×1 grid cells in x, y, and z directions, respectively in order to discretize the 50 fractures contained in the model. In this part, we investigate if our model could be able to take into account the presence of a non-SRV region (as explained in part 4.1.5 earlier in this chapter). Also, the hydraulic fracture is directly connected to

the wellbore while the rest of the fractures are connected between themselves and the hydraulic fracture.

For this example, the well has been put into production for 16000 days. Figure 4.36 presents the pressure profiles over the simulation for 1000 days, 2500 days and at 5000 days of production. Also, Figure 4.37 compares the cumulative gas production for 16000 days of production for three simulations models, the reference solution (explicit discretize model) and the discrete fracture model with and without correction discussed earlier in this chapter.

The cumulative gas volume predicted at the end of production, for 16000 days, by our DFM is very similar to one using the reference solution. Note that, our DFM is able to predict gas production with presence of a SRV and non-SRV zone and especially for treating a non-uniform SRV zone. On the other hand, the computational time for the reference solution is 6.7 hours, while using our DFM we were able to predict the gas production in only 24 seconds. Once again, our DFM proves its ability to predict gas production and to perform such simulations in much less time than the reference solution.

Our discrete fracture model proves its ability in modelling fluid flow from shale-gas reservoirs with simple cases from isolated fractures to a large regular fracture distribution case with a non-uniform stimulated reservoir volume. So, this DFM represents an accurate method for studying flow through fractured formations and could be attractive to be applied to field problems. In the next chapter an application to a field scale problem will be investigated using the DFM based on a MINC proximity function for multiphase flow problems with phase change for both shale-gas and tight-oil reservoirs.

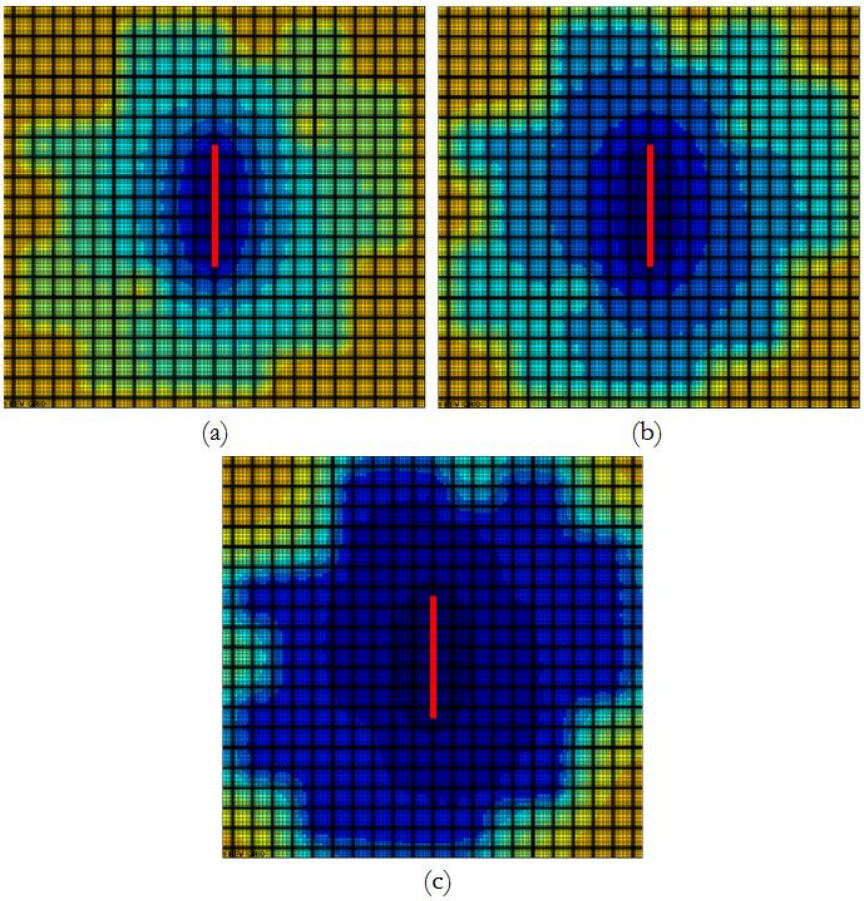

Figure 4.36: Pressure profile of the reference solution at (a) t = 1000 days, (b) t = 2500 days and (c) t = 5000 days.

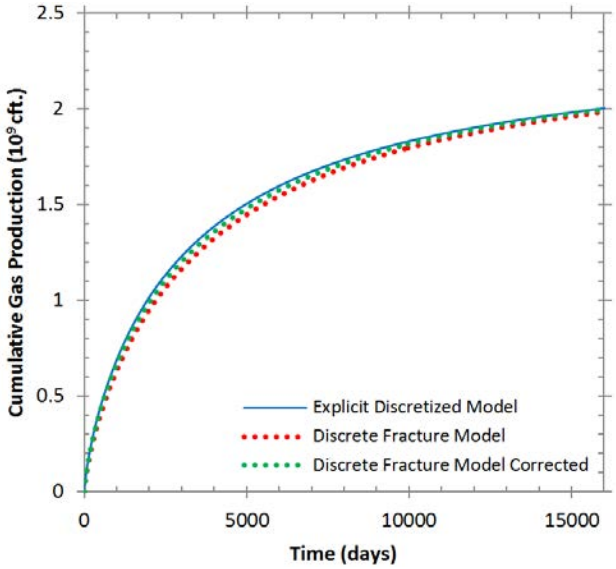

Figure 4.37: The comparison of the cumulative gas production for the hybrid approach with and without correction with the reference solution.

Chapter 5 - APPLICATION OF THE DISCRETE FRACTURE MODEL TO A FIELD SCALE PROBLEM

A complex Discrete Fracture Network is a common occurrence for unconventional reservoirs. Since we use the DFM approach for modelling shale reservoirs, we should be able to treat simple fracture geometries as well as complex ones.

In this chapter, a more realistic case observed in unconventional reservoirs is presented and studied. The DFM based on a MINC proximity function is applied to a synthetic 2D field scale problem. This study takes into account the presence of a hydraulic fracture and two sets of stimulated natural fractures leading to a complex DFN.

The ability of our DFM in treating the complex fracture network within an irregular fracture distribution is tested. First, the efficiency of our developed DFM is tested on shale-gas reservoirs for a single-phase flow case. Then, both shale-gas condensate and tight-oil reservoir cases are presented in order to express the robustness of our DFM based on a MINC proximity function to model multiphase flow problem. These multiphase problems associate with phase change, which makes the simulation quite challenge. For example, for the tight-oil reservoir case, when the fracture pressure drops below the bubble point, gas starts to appear in the matrix formation near the fracture faces. Standard DFMs cannot correctly handle this kind of problems. However, our approach based on the MINC method is suitable to simulate this kind of phenomena by quantifying the occurrence of the liberated gas.

5.1 A Synthetic 2D Discrete Fracture Network

In order to validate our DFM on a more realistic reservoir, a synthetic case is constructed in this part. A single-phase shale-gas example (gas with immobile water), a retrograde gas reservoir and a multi-phase (oil, gas and water) tight-oil reservoir examples are studied in this chapter. First, a single-phase gas case is studied in order to perform a reliable reference solution.

Table 5.1 summarizes the reservoir properties of the 2D synthetic reservoir example. A horizontal well (dashed blue line in Figure 5.1) is placed in the x-direction and in the middle of the reservoir, where one stage hydraulic fracture perpendicular to the well along the y-direction is created. Note that, our reservoir consists in 3 sets of fractures defined as following: two sets of natural fractures with different orientation and one set of hydraulic fracture. The two sets of natural fractures consist in 275 stimulated and induced secondary fractures with irregular non-uniform distribution in the SRV region (Figure 5.1). On the other hand, the third set consists in one hydraulic fracture (solid blue line in Figure 5.1) set in the middle of the reservoir. In this example, we assume that natural fractures are not propped, even if they are stimulated. So, apart from the high conductive hydraulic fracture, all other fractures, including stimulated and un-stimulated natural fractures are homogenized in the SRV.

Table 5.1: Reservoir properties of the 2D synthetic reservoir.

Property / Parameter	Value	Unit
Hydraulic Fracture Permeability	20	D
Induced-fracture Permeability	300 – 400	mD
Hydraulic Fracture Width	0.012	ft
Induced-fracture Width	0.004 – 0.005	ft
Reservoir Net Thickness	20	ft
Top of the Reservoir	3950	ft

For all the performed cases, the hydraulic fracture is considered as a rectangular in a vertical plane with the half-length of 738 ft (total length of 1476 ft) in y-direction. A base model named Explicit Discretized Model (using single porosity approach), which explicitly discretized hydraulic and natural fractures with 2.2 million matrix grid cells, is computed and considered as the reference solution. The hydraulic fracture oriented in y-direction has a width of 0.012 ft and a

permeability of 20 Darcy, while the two sets of natural fractures are stimulated with a thickness varying from 0.004 ft – 0.005 ft and the permeability from 300 mD – 400 mD. One set of natural fractures is oriented with an average angle of 15° to the north and has a mean of 200 ft in length. The second set of fractures has an average orientation of 115° to the north and a mean length of 400 ft.

Concerning the DFM approach, the hydraulic fracture is discretized explicitly while the stimulated natural fractures in the SRV are homogenized where a calculation of the effective fracture permeability and porosity is done. However, isolated fractures are not taken into consideration neither in computing the reference solution nor in our DFM. In fact, only a connect discrete fracture network is considered and studied.

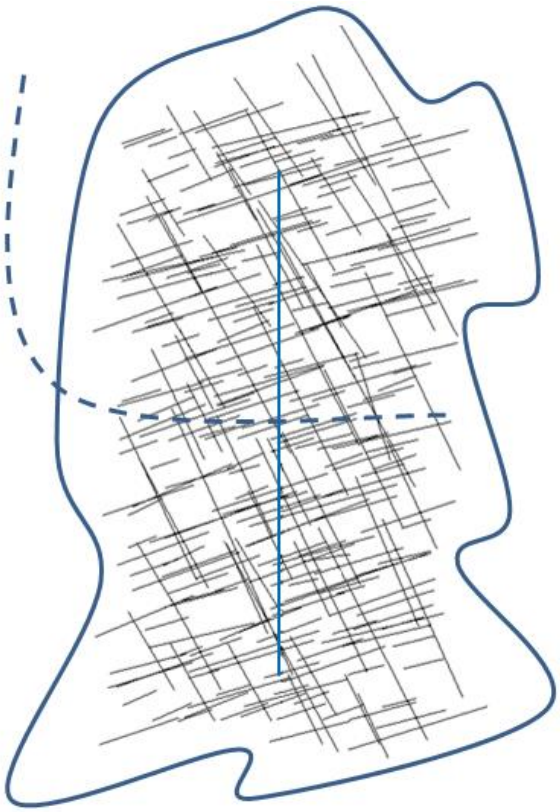

Figure 5.1: A synthetic 2D reservoir consisting in a discrete fracture network with the presence of 275 natural fractures and 1 hydraulic fracture (blue solid line in y-direction).

5.1.1 Generation of the Reference Solution

In order to provide a reference solution, the discrete fracture network is explicitly discretized taking into account all sort of fractures. This approach consists in using our DFM approach without the implementation of the MINC proximity function. In order to have a reliable solution a reference solution is generated using very fine grid cells discretizing the matrix media. Note that, all 275 fractures existing in the reservoirs are modeled explicitly and the matrix cells exchange with fracture nodes as described in Sarda *et al.* (2002).

We limit our simulation in a bounding box size (or Stimulated Reservoir Volume) containing the three sets of fractures. The bounding box volume is fixed at 820×1804×20 cft as shown in Figure 5.2. An illustration of the Cartesian grid used to perform the reference solution is presented in Figure 5.2(b).

In order to provide a reliable reference solution, three simulations consisting in three different mesh refinements, called Solution #1, #2 and #3, are performed. The first consists in 550000 grid cells. The second and the third consist in 2.2 and 8.8 million grid cells respectively. In fact, the bounding box has been discretized in x, y and z direction as following; 500×1100×1; 1000×2200×1 and 2000×4400×1 matrix grid cells, respectively for simulations #1, #2 and #3. It must be mentioned that, all simulation models consist in a Cartesian uniform grid in x and y directions (see, Figure 5.2(b)). The grid size of the first simulation (Solution #1) is 1.64 ft in x and y direction. The grid size of Solution #2 is 0.82 ft in x and y direction. Finally, the third (Solution #3) consists in a grid cell of 0.41 ft in x and y direction.

The three simulations have been performed for a single-phase flow case taking a matrix permeability of km=10^{-4} mD. The results are illustrated in Figure 5.3. Clearly, all solutions are very close comparing to each other. In particular, Solutions #2 and #3, with 2.2 and 8.8 million grid cells respectively, provide almost the same results concerning the cumulative gas production after 5000 days of production. So, a simulation with 2.2 million grid cells can be reasonably considered as a reference solution, which will be used for the rest of this work (for single and multiphase flow simulations). Note that, the CPU time of the reference solution #1, #2 and #3 are 2, 7 and 34 hours respectively.

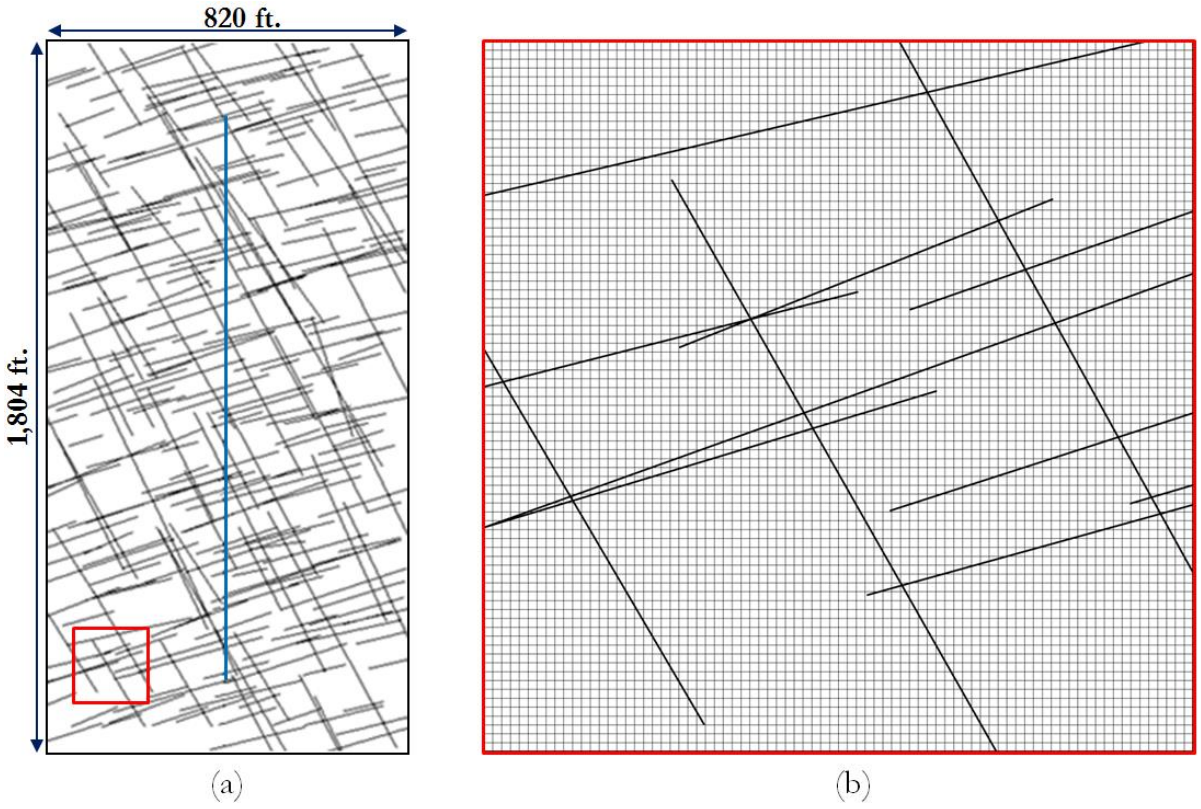

Figure 5.2: Illustration of (a) the reservoir bounding box taking into account the DFN and (b) the grid discretization in order to perform the reference solution.

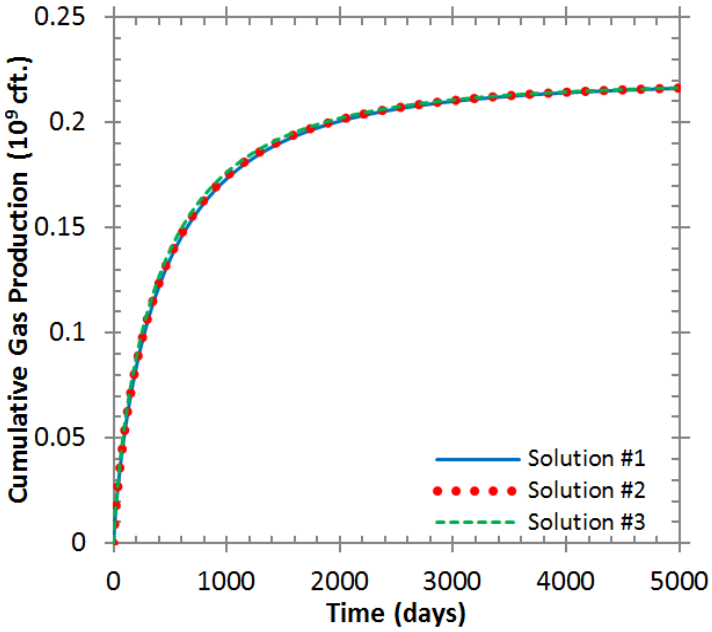

Figure 5.3: Comparison of three simulation models with different grid cells discretization.

5.1.2 Homogenization of the Discrete Fracture Network

The main purpose of homogenization methods is to be efficient in terms of computational time while conserving the physics of flow transfer at fracture scale (see, for example, De Dreuzy *et al.,* 2012). In this part, two upscaling methods are considered. The first one is an analytical method and the second one is the numerical method. Hereafter, the two homogenization methods are briefly described and tested in order to estimate the equivalent permeability of our discrete fracture network. The purpose of this study is to select an upscaling method which is able to provide us an accurate result for this example.

Figure 5.4 presents the grid mesh definition of the stimulated reservoir volume (bounding box) with 55 grid cells. In fact, the bounding box is discretized into 5 and 11 in x and y direction respectively. Note that there is only one cell in the z direction, no flow is simulated in the z direction and the upscaling in this direction is not needed. This reservoir discretization is used for the dual-porosity model and for our discrete fracture model.

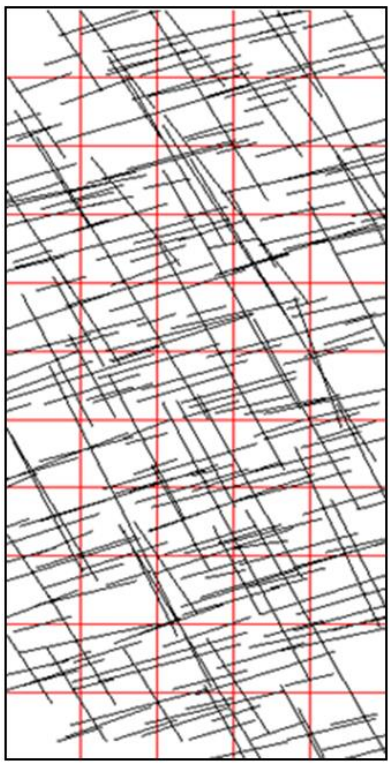

Figure 5.4: Illustration of the discretization of the bounding box into 55 grid cells.

5.1.2.1 Analytical Method

The analytical method is inspired by Oda's model (1986) and it consists in a numerical integration without any DFN generation. Also, the analytical method is efficient and valid only for well-connected discrete fracture network and high fractures density.

The equivalent permeability tensor $\mathbf{K_f}$ for one reservoir cell is expressed in Equation (5.1):

$$K_f = \frac{1}{V_{cell}} * \sum_{s=1}^{NbSets} \sum_{if=1}^{NbFracs} V_{f,s} * \frac{C_{f,s}}{12 e_{f,s}} * \overline{N_{f,s}} \tag{5.1}$$

where, V_{cell} is the volume cell, $NbSets$ is the number of fractures sets, $NbFracs$ is the number of fractures in the set s. $V_{f,s}$ is the fracture volume, $C_{f,s}$ and $e_{f,s}$ correspond to the fracture conductivity and aperture. $\overline{N_{f,s}}$ is the unitary projection matrix of the cell-scale pressure gradient on the fracture plane.

The analytical method is applied to homogenized fracture cells presented in Figure 5.4. It must be mentioned that, the analytical method delivers a lower CPU time comparing to the numerical approach as there is no need to generate the DFN mesh.

5.1.2.2 Numerical Method

The numerical upscaling method (see, for example, Bourbiaux *et al.*, 1997) consists in simulating the Darcy flow on the DFN taking into consideration an equivalent volume while respecting the fractures density. Note that, this method uses a finite volume scheme and it could be applicable for any kind of DFN.

In order to perform the numerical upscaling on a reservoir, the discrete fracture network should be used. The definition of a mesh for modelling the Darcy flow and finally the inversion of the linear system to get the pressure solution must be done. Note that, the CPU time of the numerical method depends enormously from the fractures nodes number (see, Khvoenkova N. and Delorme M. (2009)).

Figure 5.5 illustrates the application of the numerical method to our discrete fracture model using different mesh definition for modelling the Darcy flow. For example, in Figure 5.5(a) each grid cell is taken as a representative volume for modelling the Darcy flow using the numerical upscaling approach. This approach is called local numerical homogenization method. On the other hand, the global numerical homogenization method (Figure 5.5(b)) sets the bounding box as a representative volume. It must be mentioned that, the numerical method is well known to be efficient for a low fractures density, but too CPU time consuming due to the numerical flow simulations.

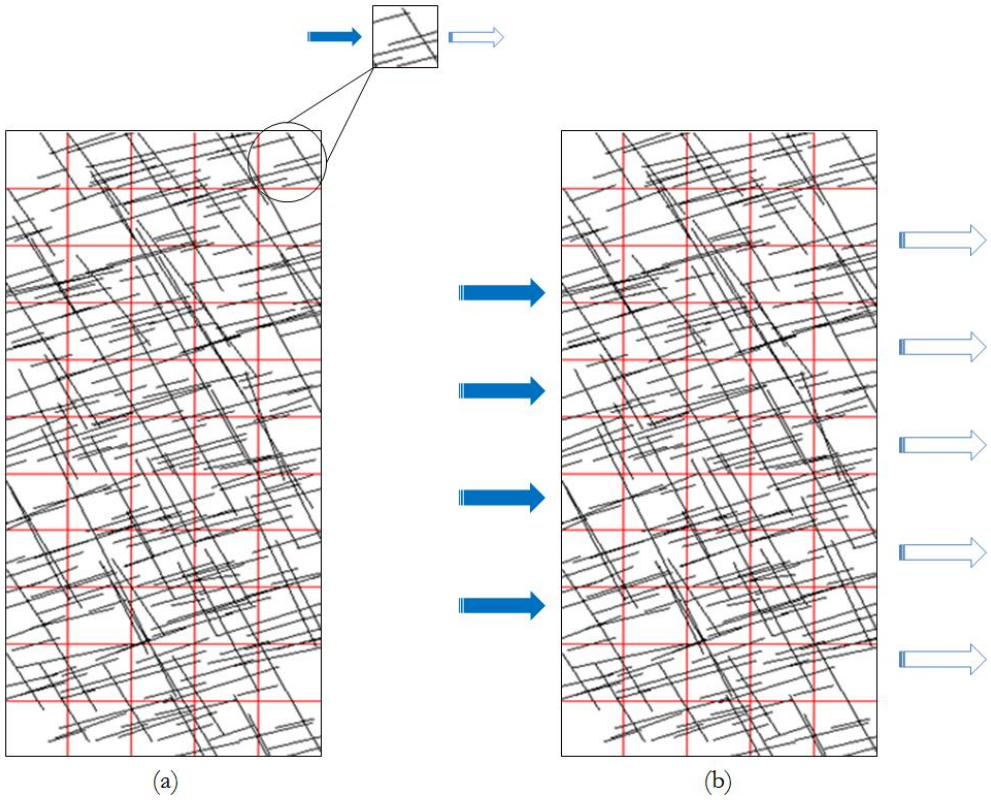

Figure 5.5: Illustration of the numerical homogenization method for modelling the Darcy flow for (a) local and (b) global approach.

5.1.2.3 Application of the Homogenization Methods

In this part a study concerning the homogenization of our DFM approach is considered. Several DFM based on a MINC proximity function taking into account different homogenization (analytical and numerical) approaches are tested. These different DFM approaches are compared to the reference solution in order to quantify the effect of the homogenization method on our DFM and to select the most accurate homogenization method.

To do so, three simulations models based on our DFM will be performed. First, the homogenization of the natural fractures network consists in the analytical homogenization method is considered. This model is called DFM Analytical. The second called DFM Numerical local consists in a local numerical homogenization method where the grid cell is taken as a representative volume as defined in Figure 5.5(a). The third called DFM Numerical Global consists in a global numerical homogenization method to homogenize the natural fractures network. However, the bounding box is set as a representative volume as shown in Figure 5.5(b).

Hereafter, Figure 5.6(a) presents the discrete fracture model and the concept of the equivalent optimization with our DFM concept after the homogenization process. Note that, after applying a conductivity criterion on the discrete fracture network only the hydraulic fractures with high conductivity are explicitly discretized where the others set of fractures are homogenized. In our case only one hydraulic fracture is explicitly discretized. Furthermore, due to the homogenization process the equivalent parameters such as porosity and permeability in each of the 55 grid cells will be assigned to the blue node in Figure 5.6(b).

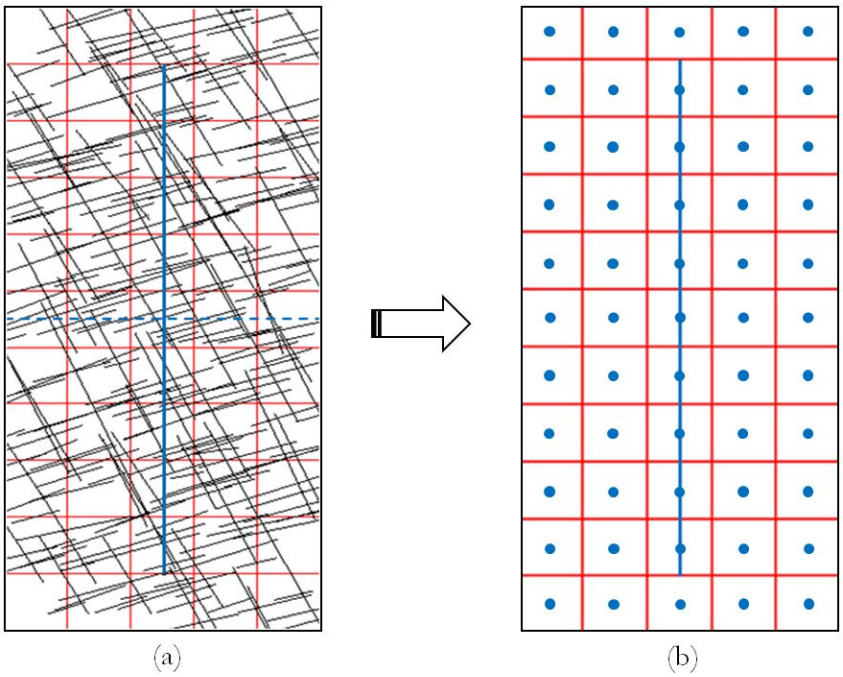

Figure 5.6: Illustration of (a) the DFN and (b) our DFM after the homogenization process.

Table 5.2 presents the average homogenized permeability values using different homogenization approaches. Obviously, the homogenized permeability value depend greatly on the

homogenization method. An average value of 0.02 mD and 0.06 mD was found performing the analytical and the local numerical method respectively. However, a value of 0.011 mD is found computing the global numerical homogenization method.

Figure 5.7 shows the comparison of the cumulative gas production for different homogenization methods during 5000 days of production. Clearly, our DFM is sensitive to the homogenization method implemented in the model. The DFM which used the analytical method overestimates the gas production comparing to reference solution. Also, the DFM which used a local numerical method overestimates the gas production. This difference is related to the representative elementary volume for modelling the Darcy flow. However, the DFM using the global numerical approach presents a quite accurate result, where it is able to predict the gas production for 5000 days of production comparing to the reference solution.

Table 5.2: Homogenized permeability value using different homogenization methods.

Homogenization Method	Permeability Value	Unit
Analytical	0.02	mD
Numerical Local	0.06	mD
Numerical Global	0.011	mD

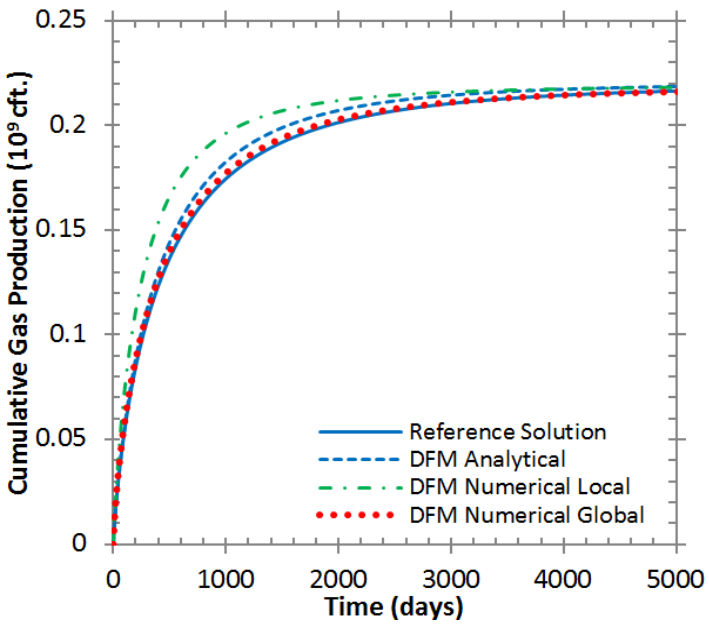

Figure 5.7: The comparison of the cumulative gas production from the DFM using different homogenization methods to the reference solution.

5.2 Shale-Gas Reservoir

In this part the example presented previously is studied (see, Figure 5.2) for shale-gas simulations. In the following, as mentioned in section 5.1.1, the reference solution is obtained with 2.2 million grid cells. It must be mentioned that the equivalent permeabilities are computed with the global numerical upscaling method on the homogenized fracture cells.

5.2.1 Single-Phase Flow

In this section only a single phase flow (gas only) is taken into account. Moreover, three simulation models, an explicit discretized model, a dual-porosity model and the DFM based on a MINC proximity function, are compared. A comparison between the reference solution technique (Figure 5.8(a)) and our DFM approach (Figure 5.8(b)) is illustrated in Figure 5.8. Moreover, Figure 5.9 presents the comparison of the dual-porosity model and the DFM to the reference solution for 5000 days of production. Clearly, the DFM presents a better result than the dual-porosity model where obviously the DP model cannot handle the flow modelling during the transient period. In fact, our DFM can handle much better the transient flow from the matrix into the fractures during the whole production period due to the discretization of the matrix grid cells into a sequence of nested volume.

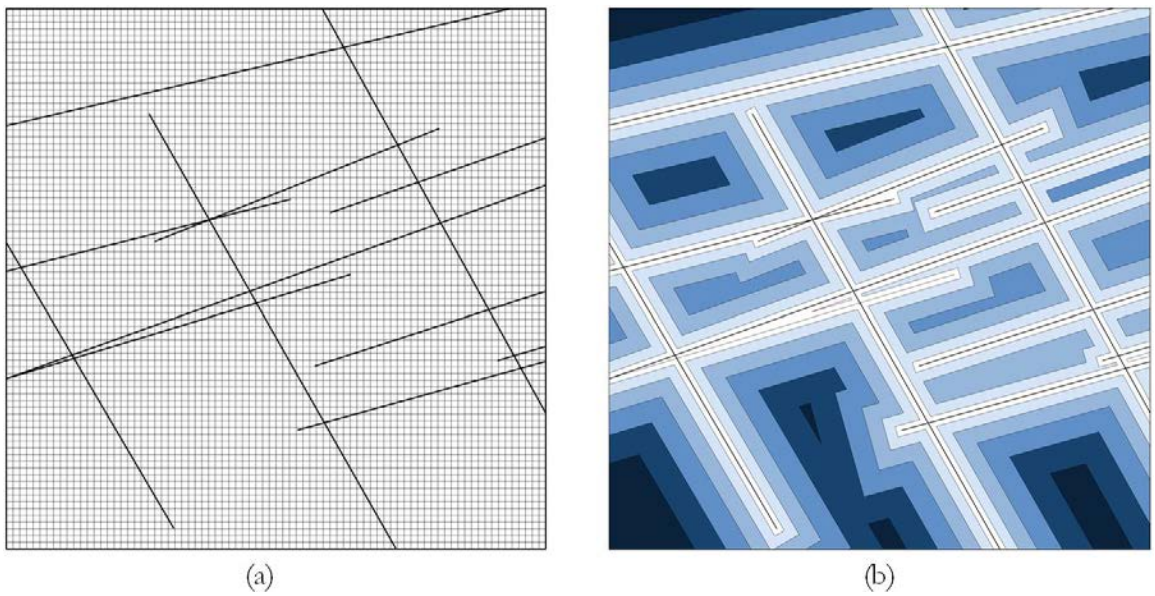

Figure 5.8: A comparison between (a) the reference solution and (b) the DFM based on a MINC proximity function computed on the case selected in Figure 5.2.

The implementation of the MINC proximity function into our DFM improves significantly the capability to predict inter-porosity flow exchange. Based on these results, the proposed DFM based on a MINC proximity function is able to predict gas production from unconventional fractured shale-gas reservoirs and provides an accurate result. Besides matching the reference solution, the DFM decreases greatly the CPU time. In fact, the DFM took only 20 secs. to perform the 2D synthetic shale-gas reservoirs case, while the reference solution took around 6 hours to be accomplished using the same computer. The proposed DFM proves its efficiency delivering an accurate result for the application on shale-gas reservoirs, at least for single-phase flow problems.

Table 5.3: Reservoir properties for the shale-gas reservoir.

Property / Parameter	Value	Unit
Matrix Permeability	0.0001	mD
Hydraulic Fracture Permeability	20	D
Induced-fracture Permeability	300 – 400	mD
Fracture Width	0.012	ft
Induced-fracture Width	0.004 – 0.005	ft
Reservoir Net Thickness	20	ft
Top of the Reservoir	3950	ft
Initial Reservoir Pressure	3800	psi
Bottom Hole Well Pressure	1000	psi

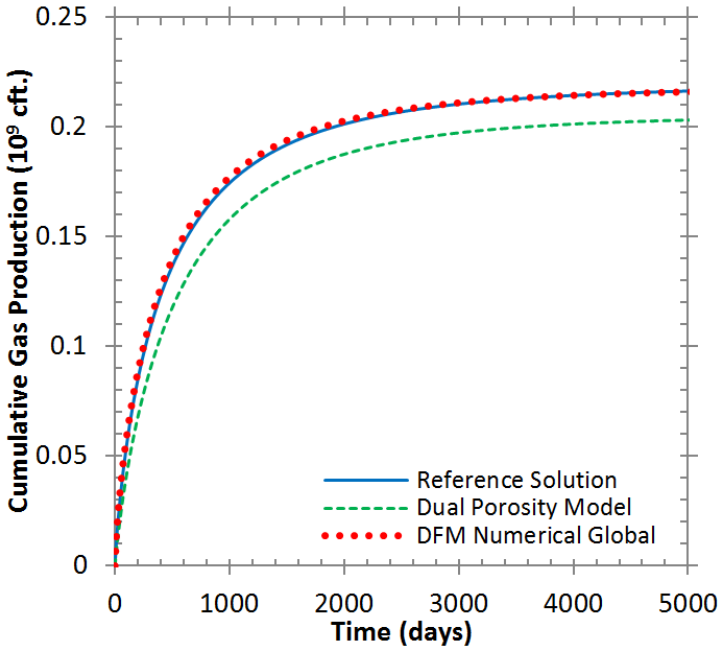

Figure 5.9: Cumulative gas production vs. time of the 2D synthetic shale-gas reservoir example.

5.2.2 Retrograde Gas Reservoir

Gas condensate arises some difficulties in numerical simulations with a dual-porosity model with phase change. In fact, during production from shale reservoirs, as pressure is reduced, the gas will pass through the dew point where a liquid starts to condense. As the reservoir further depletes and the pressure drops, liquid condenses from the gas to form a free liquid inside the reservoir. This is particularly true near the fracture faces, where the matrix pressure is very low and close to the fracture pressure. Thus, the presence of free liquid near fracture faces could decrease highly the gas relative permeability and impedes gas recovery. Moreover, using large matrix grid cells (DP model) near the fractures might provide significantly different results as noticed with shale-gas reservoir in the previous part. In this section, a retrograded condensate reservoir is studied. Furthermore, a compositional model is used for the retrograde gas simulation. The reservoir properties are summarized in Table 5.4.

Table 5.4: Reservoir properties for the retrograde gas reservoir.

Property / Parameter	Value	Unit
Matrix Permeability	0.00001	mD
Reservoir Net Thickness	20	ft
Top of the Reservoir	3950	ft
Initial Reservoir Pressure	4800	psi
Dew Point Pressure	3000	psi
Bottom Hole Well Pressure	2000	psi

The simulations results are presented in Figure 5.10. Our DFM, based on different MINC subdivisions (MINC2, MINC4 and MINC8), is compared to the reference solution. Figures 5.10(a) and (b) illustrate the daily gas and oil rate for 1000 days of production for the three simulations models. Besides, if we are interested in long-term production, Figure 5.10(c) and (d) presents the cumulative gas and oil production for 1000 days of production. Clearly, our DFM based on a MINC8 model (dotted red line) is accurate comparing to the reference solution. The reference solution and our DFM predict the same amount of cumulative gas production (around $100*10^6$ cft) after 1000 days. Moreover, our DFM and the reference solution predict around 2500 bbl concerning the cumulative oil production at the end of production. Also, Figure 5.10(f) illustrates the CGR for 1000 days. Our DFM based on a MINC8 model presents an accurate result comparing to the reference solution, where both models have the same trends. Finally, our

DFM based on a MINC proximity function treats the fracture/matrix interaction entirely by a fully transient way and it is able to predict flow production from retrograde condensate reservoirs.

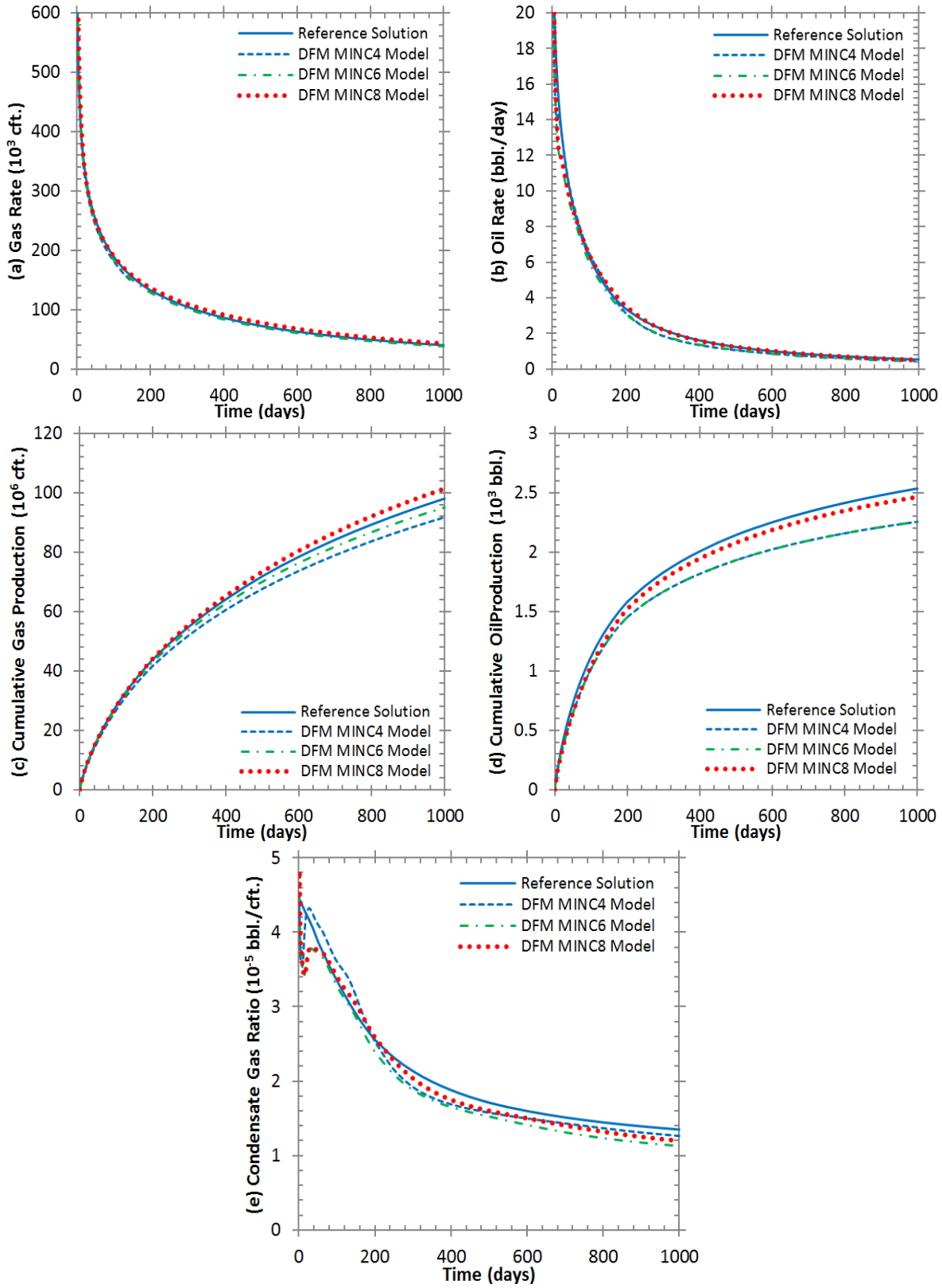

Figure 5.10: Simulation results of the gas condensate reservoir with km=10^{-5} mD (a) gas rate, (b) oil rate, (c) the cumulative gas production, (d) the cumulative oil production and (e) the CGR

5.3 Tight-oil Reservoir

The next simulation scenario retains the same fracture network as presented earlier in this chapter (see, Figure 5.2). In this section, we evaluate the accuracy and the ability of our DFM coupled with the MINC proximity function treating a multiphase flow case. Initially, both oil and water exist in the reservoir. We consider the initial water saturation in this shale oil reservoir at 0.4 where the irreducible water saturation is set at 0.1. Also, the formation porosity is 0.05.

5.3.1 Matrix Permeability km=10^{-3} mD

In this section, a tight-oil reservoir is studied. The matrix permeability is set as 0.001 mD. The initial reservoir pressure is 2740 psi and the horizontal well produces at a constant bottom hole pressure of 1450 psi, which is below the bubble point pressure set as 2030 psi. of this section. The top of the reservoir is set at 3940 ft and the reservoir thickness is 20 ft.

Figures 5.11(a) and (b) illustrate the relative permeabilities in the matrix media for the oil-water system and the gas-oil system, respectively. Also, Figures 5.12(a) and (b) present the water-oil capillary pressure and gas-oil capillary pressure curves, respectively.

Once the well is put into production, the reservoir pressure begins to decrease. Furthermore, when the reservoir pressure decreases below the bubble point pressure, gas will start to appear inside the reservoir. It is quite difficult to simulate such phenomena with a commonly-used model such as a dual-porosity model due to the large block and low matrix permeability. Also, during the transient period, a non-linear variation of the pressure in the matrix media emphasizes the duration of the transient period. Thus, the implementation of the MINC method could present a solution of this problem due to the fine sub-grid continuum near the fractures faces.

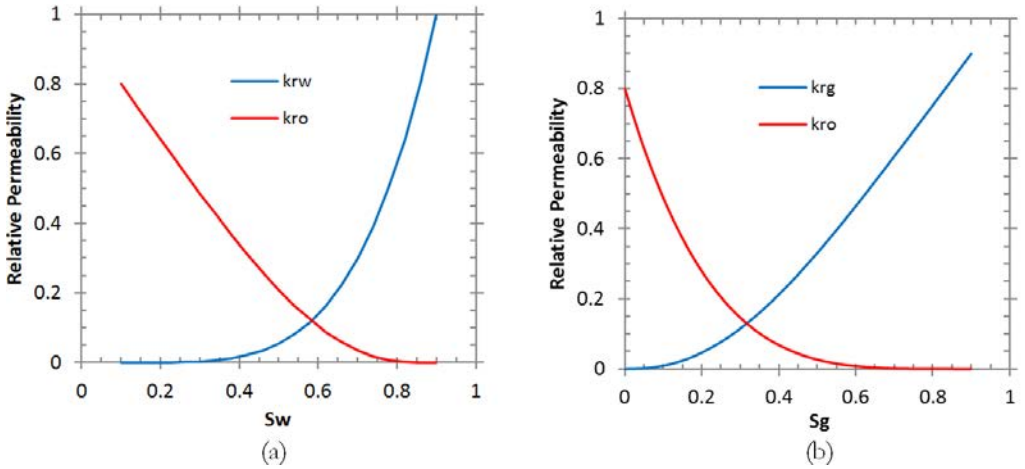

Figure 5.11: (a)Water/oil and (b) gas/oil relative permeability curves.

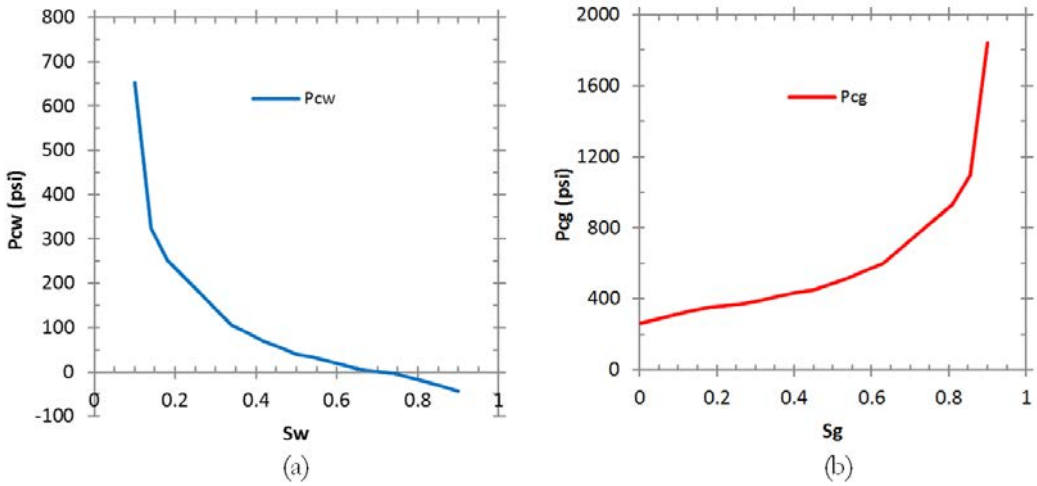

Figure 5.12: (a) Water/oil and (b) gas/oil capillary pressures.

The results of three simulation models are presented in Figure 5.13. The DFM based on the MINC8 model and the dual-porosity model are compared to the reference solution. Figures 5.13(a), (b), (c), (d), (e) and (f) represent respectively the results of daily gas rate, daily oil rate, the cumulative gas production, the cumulative oil production, the water cut and the gas oil ratio (GOR).

Figures 5.13(a) and (b) illustrate the daily gas and oil rate for 2000 days of production for the three simulations models. Besides, if we are interested in long-term production, Figures 5.13(c) and (d) presents the cumulative gas and oil production for 5000 days of production. Clearly, our DFM based on a MINC proximity function (dotted red line) presents a better result than the dual-porosity model (dashed green line) comparing to the reference solution. Note that,

the reference solution and the DFM predict the same amount of cumulative gas production (around $13*10^6$ cft) after 5000 days. Also, concerning the cumulative oil production, our DFM is accurate comparing to the reference solution, where both models predict around 10000 bbl at the end of production. However, the dual-porosity model highly overestimates the cumulative gas production (around $23*10^6$ cft) and underestimates the cumulative oil production (around 6500 bbl) comparing to the reference solution $13*10^6$ cft and 10000 bbl respectively for the cumulative gas and oil production.

Figure 5.13(e) presents the water cut for early time of production for 30 days. The reference solution and the DFM based on the MINC proximity function produce around the same amount of water during the first 20 days of production. The DFM gives approximately a similar water production as the reference solution while the dual-porosity model is not accurate at all.

Finally, Figure 5.13(f) illustrates the gas oil ratio for the three simulations models. Our DFM presents an accurate result concerning the GOR for 5000 days comparing to the reference solution. However, the dual-porosity model is not accurate.

Dealing with three-phase (oil/gas/water) flow simulation, our DFM presents good results comparing to the reference solution. The DFM based on the MINC proximity function method gives quite accurate results. Besides, the CPU time was greatly reduced using our proposed DFM. The numerical results are summarized in Table 5.5. Clearly, the CPU time was reduced from 7 hours concerning the reference solution (2200624 grid cells) to only 30 seconds using our DFM approach consisting in 387 grid cells to describe the same reservoir problem using a MINC6 model.

Table 5.5: Numerical results comparing the DFM based on a MINC proximity function to the reference solution.

Model / Case	Explicit Discretized Model		Discrete Fracture Model	
	Number of grid cells	CPU Time	Number of grid Cells	CPU Time
Single-phase Flow	2200624	6 hrs.	387	20 secs.
Multiphase Flow		7 hrs.		30 secs.

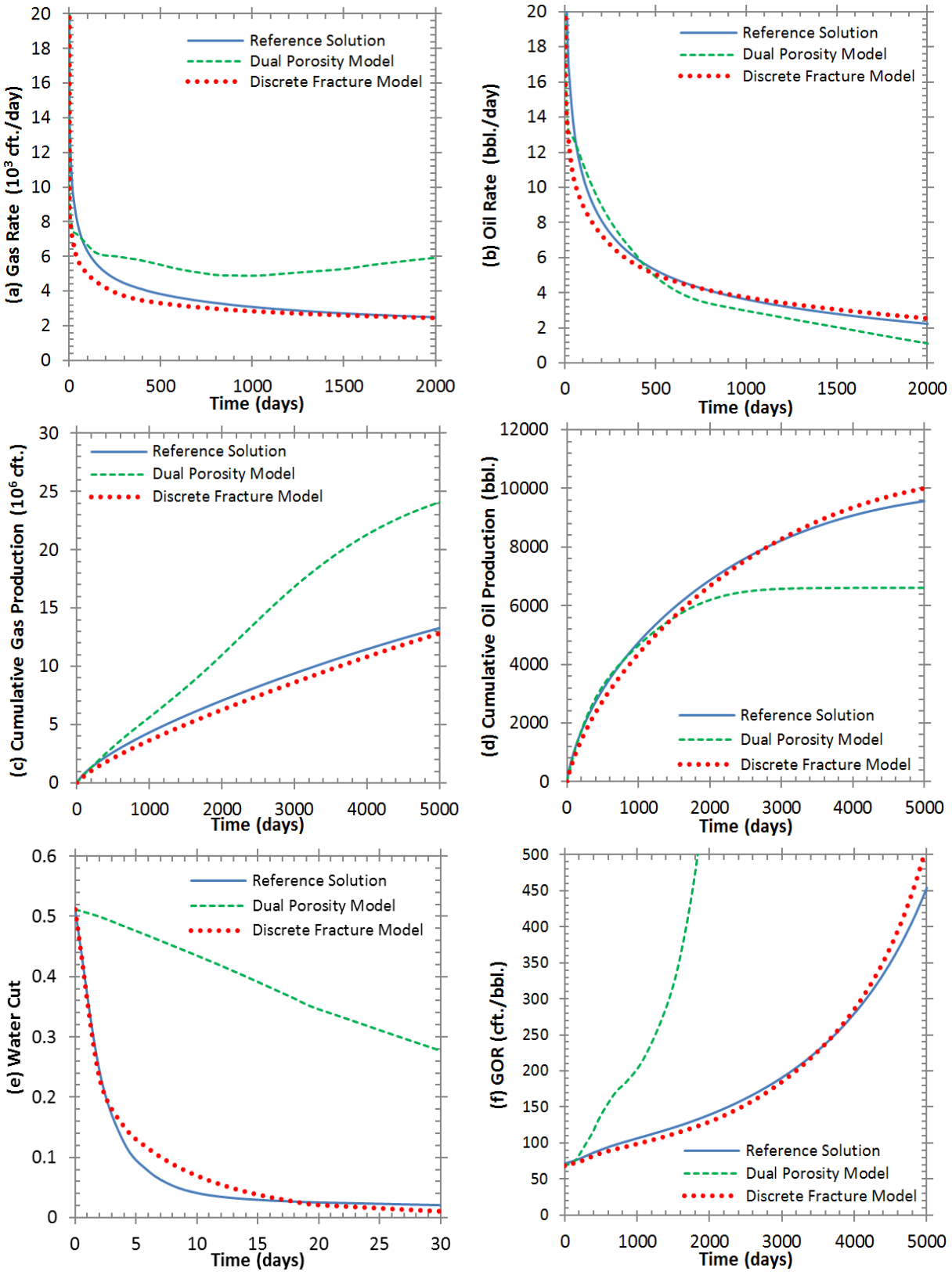

Figure 5.13: Simulation results of the tight-oil reservoir with km=10^{-3} mD (a) gas rate, (b) oil rate, (c) the cumulative gas production, (d) the cumulative oil production, (e) water cut and (f) the GOR.

5.3.2 Matrix Permeability km=10^{-4} mD

In this section, a tight-oil reservoir is studied. Table 5.6 summarizes the reservoir properties used in this part. The matrix permeability is set as 0.0001 mD. The initial reservoir pressure is 3800 psi and the horizontal well produces at a constant bottom hole pressure of 1160 psi, which is below the bubble point pressure set as 2710 psi. The top of the reservoir is 3950 ft.

Table 5.6: Reservoir properties for the tight-oil reservoir.

Property / Parameter	Value	Unit
Matrix Permeability	0.0001	mD
Reservoir Net Thickness	20	ft
Top of the Reservoir	3950	ft
Initial Reservoir Pressure	3800	psi
Bubble Point Pressure	2710	psi
Bottom Hole Well Pressure	1160	psi

The simulations results are presented in Figure 5.14. Our DFM, based on different MINC model (MINC2, MINC4 and MINC8), is compared to the reference solution. Figures 5.14(a), (b), (c), (d), (e) and (f) represent respectively the results of daily gas rate, daily oil rate, the cumulative gas production, the cumulative oil production, the water cut and the gas oil ratio (GOR).

Figures 5.14(a) and (b) illustrate the daily gas and oil rate for 2000 days of production for the three simulation models. Besides, if we are interested in long-term production, Figures 5.14(c) and (d) presents the cumulative gas and oil production for 5000 days of production. Clearly, our DFM based on a MINC8 model (dotted red line) is accurate comparing to the reference solution. The reference solution and our DFM predict the same amount of cumulative gas production (around $30*10^6$ cft) after 5000 days. Also, concerning the cumulative oil production, our DFM predicts around 14000 bbl where the reference solution predict around 13500 bbl at the end of production. Figure 5.14(e) presents the water cut for 5000 days. Our DFM is not very accurate at early time. However, if we are interested in long-term production our DFM presents a satisfactory result comparing to the reference solution. Also, Figure 5.14(f) illustrates the GOR for 5000 days. Our DFM based on a MINC8 model presents an accurate result comparing to the reference solution, where both models have the same trends.

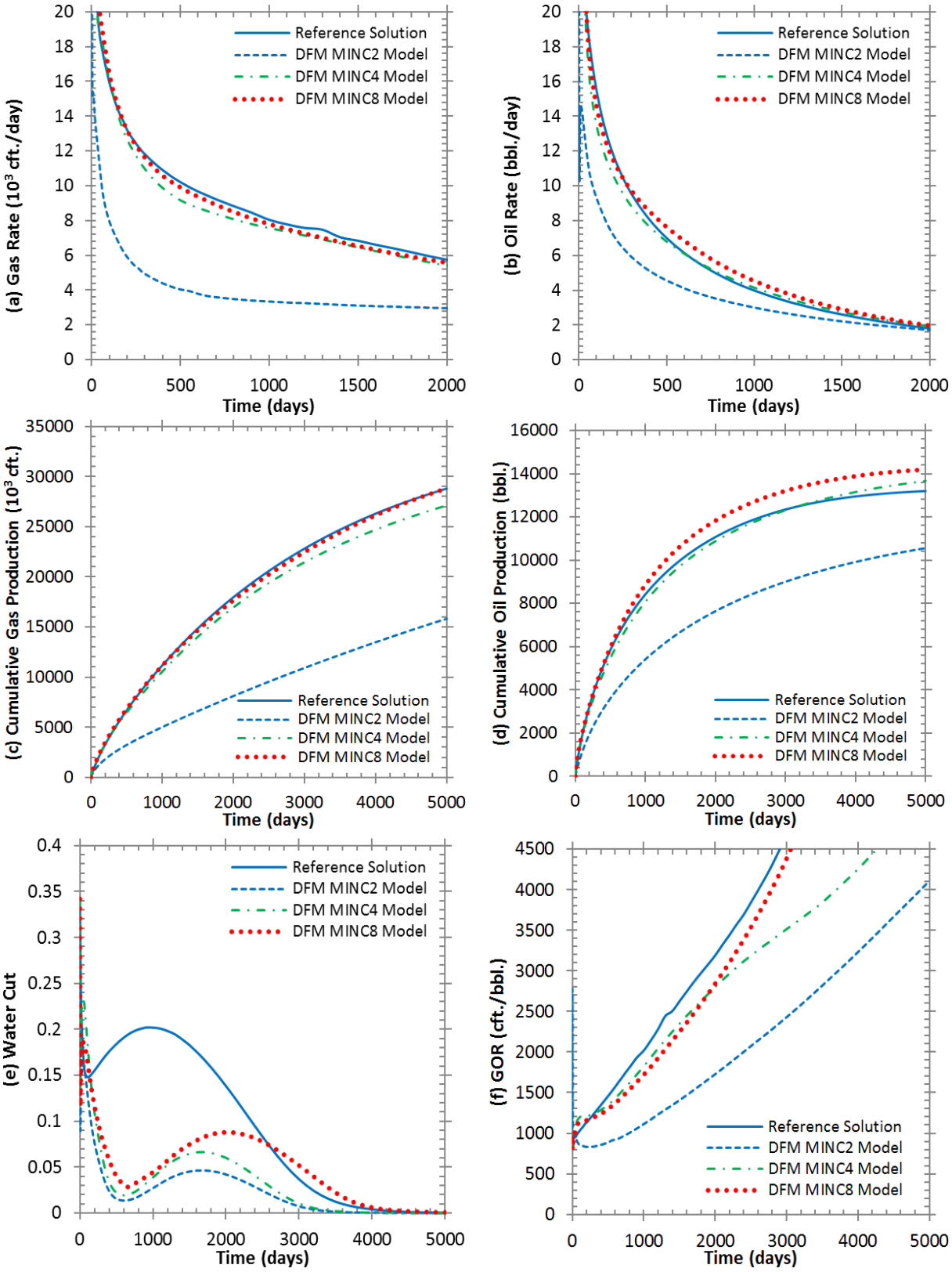

Figure 5.14: Simulation results of the tight-oil reservoir with km=10^{-4} mD (a) gas rate, (b) oil rate, (c) the cumulative gas production, (d) the cumulative oil production (e) water cut and (f) the GOR.

5.3.3 Matrix Permeability km=10^{-5} mD

In this section, a tight-oil reservoir is studied and a comparison between this case (km=10^{-5} mD) and the previous one (km=10^{-4} mD) is done in order to see how our DFM reacts to the different matrix permeability. The same reservoir properties presented in Table 5.6 are used in this part. However, the matrix permeability is set as 0.00001 mD. The simulations results are presented in Figure 5.15. Our DFM, based on different MINC model (MINC2, MINC4 and MINC8), is compared to the reference solution. Figures 5.15(a), (b), (c), (d), (e) and (f) represent respectively the results of daily gas rate, daily oil rate, the cumulative gas production, the cumulative oil production, the water cut and the gas oil ratio (GOR).

Figures 5.15(a) and (b) illustrate the daily gas and oil rate for 2000 days of production for the three simulations models. Besides, if we are interested in long-term production, Figures 5.15(c) and (d) presents the cumulative gas and oil production for 5000 days of production. Clearly, our DFM based on a MINC8 model (dotted red line) is accurate comparing to the reference solution. The reference solution and our DFM predict the same amount of cumulative gas production (around 14*10^{6} cft) after 5000 days. Moreover, our DFM and the reference solution predict around 8000 bbl concerning the cumulative oil production at the end of production. Figure 5.15 (e) presents the water cut for 5000 days. Our DFM gives quite satisfactory results comparing to the reference solution. Also, Figure 5.15 (f) illustrates the GOR for 5000 days. Our DFM based on a MINC8 model presents a satisfactory result comparing to the reference solution, where both models have the same trends. Moreover, a comparison of tight-oil reservoir simulations for different matrix permeability km=10^{-4} mD and km=10^{-5} mD is presented in Figure 5.16. The purpose from this comparison is to show how our Discrete Fracture Model is reacting to different matrix permeability.

Finally, neither a standard dual-porosity model nor an explicit discretized model are suitable flow modelling from shale-gas/tight-oil reservoirs. The dual-porosity model is not accurate due to the pseudo-steady-state regime concerning the matrix-fracture flow exchange. On the other hand, due to the large number of grid cells, an explicit discretized model required a lot of CPU time. Nevertheless, our DFM based on the MINC method treats the inter-porosity flow entirely in a fully transient way for the matrix-fracture flow exchange. Based on the results from Figure 5.9, Figure 5.10, Figure 5.13, Figure 5.14 and Figure 5.15 our DFM is able to predict well productions for both single and multi-phase flows in shale-gas or tight-oil reservoirs.

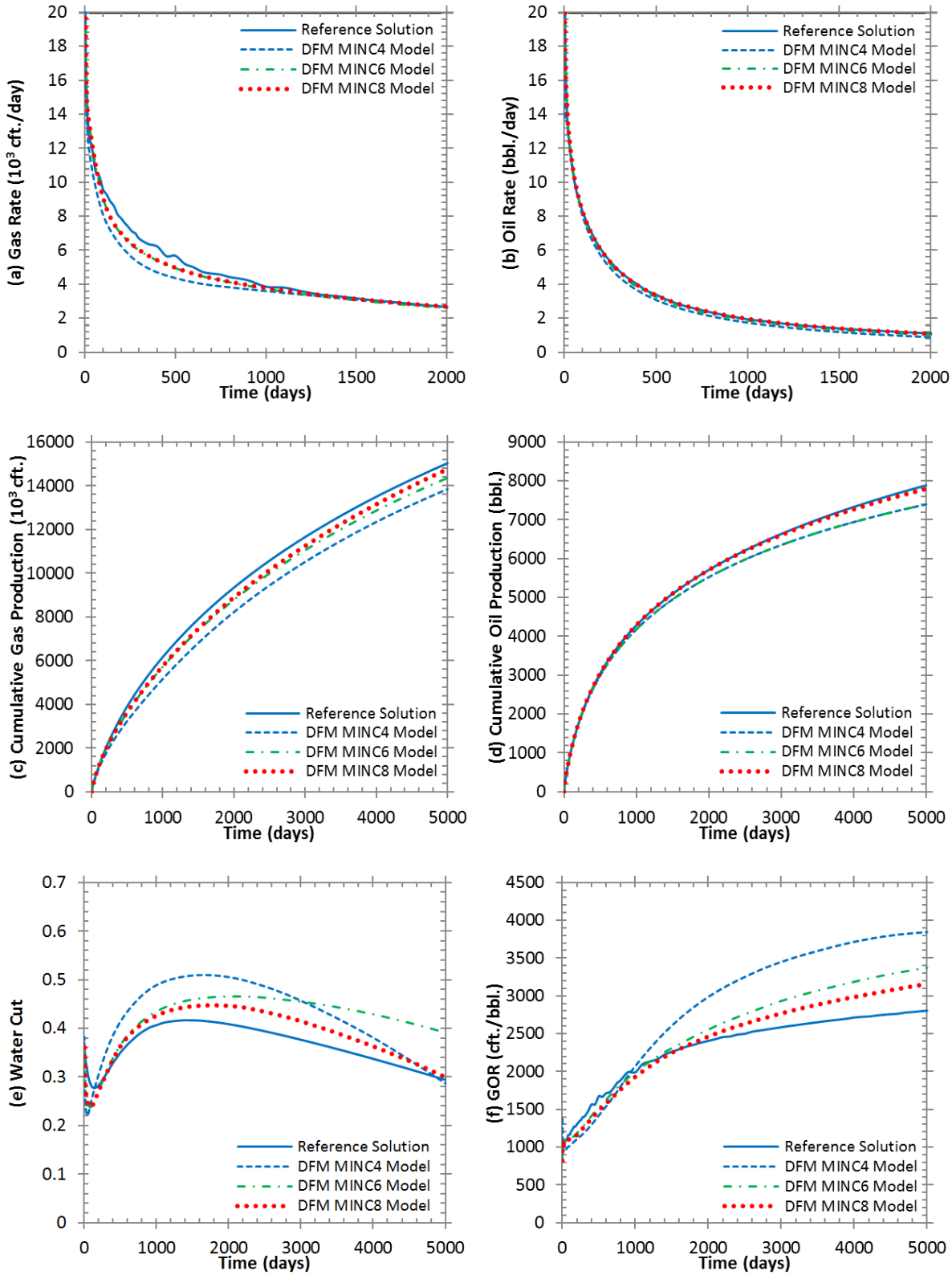

Figure 5.15: Simulation results of the tight-oil reservoir with km=10^{-5} mD (a) gas rate, (b) oil rate, (c) the cumulative gas production, (d) the cumulative oil production, (e) water cut and (f) the GOR.

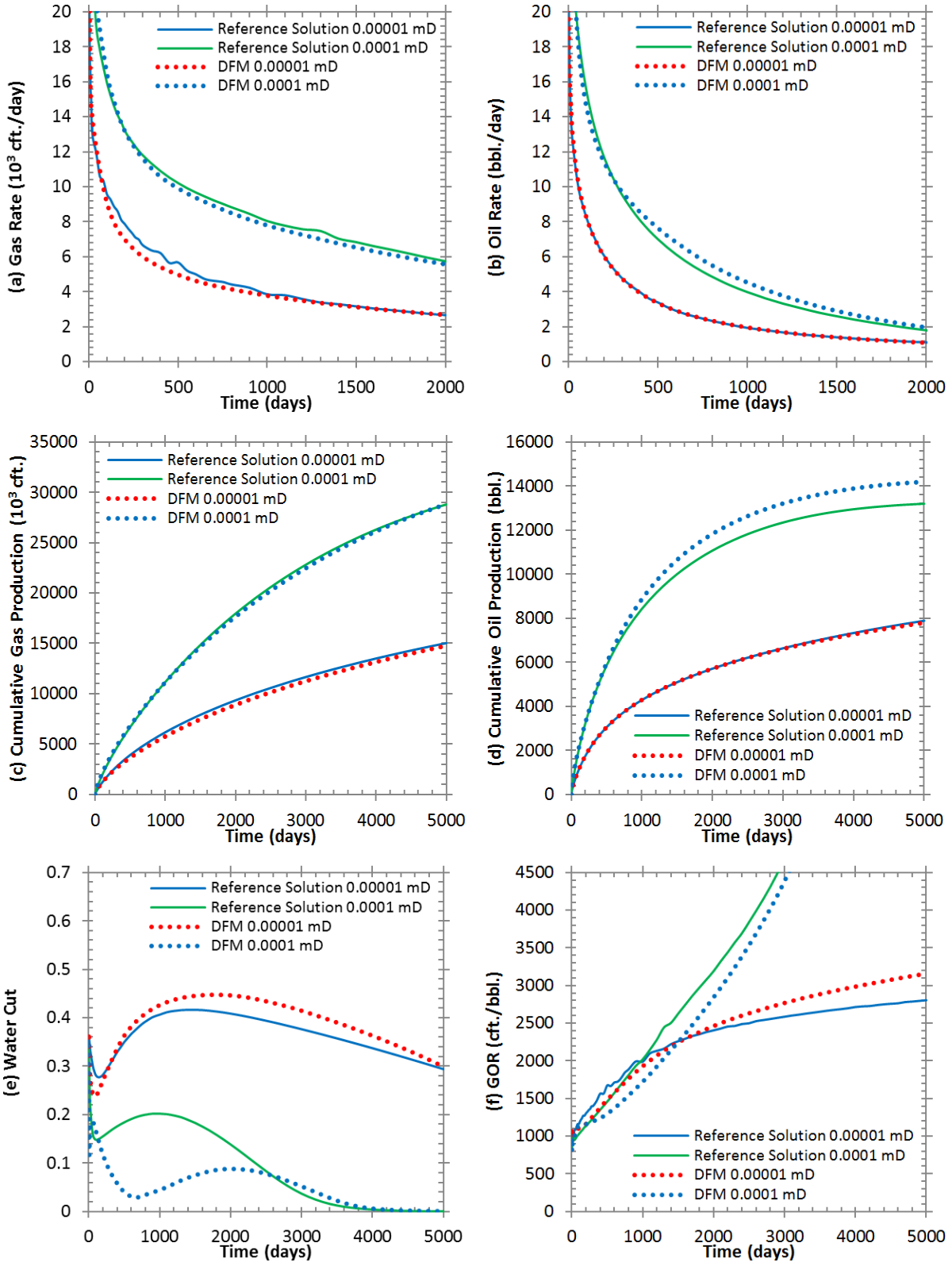

Figure 5.16: Comparison of the simulation results between the reference solution and our DFM of the tight-oil reservoir for km=10-5 mD and km=10-4 mD (a) gas rate, (b) oil rate, (c) the cumulative gas production, (d) the cumulative oil production and (e) water cut and (f) the gas oil ratio (GOR).

Chapter 6 - DISCUSSIONS AND PROSPECTS

Computing the MINC method using the proximity function stochastic process is an efficient method to simulate flow for fractured reservoirs, especially for low-permeability unconventional reservoirs. Basically, this DFM was introduced to simulate shale-gas reservoirs. However, as shown in the previous part, our DFM is able to model properly the flow from a tight-oil reservoir.

In fact, the application of the present method of the MINC proximity function is able to simulate properly fluid flow from unconventional reservoirs. In this section, we will discuss the two potential problems of our approach. The explication of the two problems and solution propositions are detailed and described hereafter.

6.1 The Presence of Different Block Size Inside a Grid Cell

In this part, we will discuss the first problem of our approach consisting in the presence of different block size in a grid cell. This problem in our discrete fracture model might overestimate the prediction of the flow production. Examples concerning a regular and an irregular fracture distribution are presented. The purpose from these examples is to study a matrix grid cell containing different block size for a better comprehension of the MINC proximity function.

6.1.1 Regular Fracture Distribution

First, an example of two regular non-symmetric orthogonal fractures is presented. The following example in Figure 6.1 consists in a matrix block of 164 ft in x and y direction with the presence of two hydraulic fractures as shown in the Figure 6.1(a). The fracture aperture and permeability are set at 0.004 ft and 2500 mD respectively. The matrix permeability is 0.0001 mD. This domain contains four matrix blocks with different sizes. The thickness of the block is 20 ft in z direction. A horizontal well is placed into the formation. The intersection of the well with the hydraulic fracture is illustrated by the green node in Figure 6.1(a).

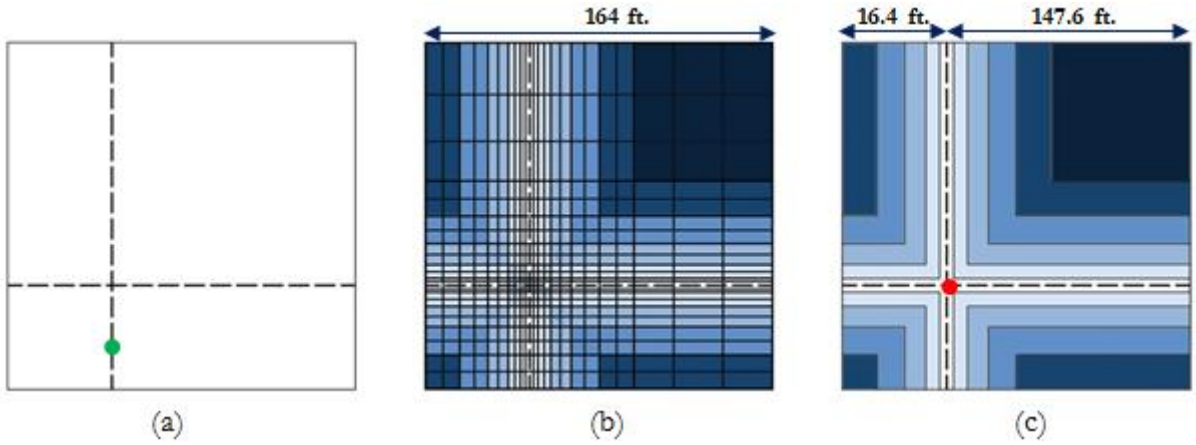

Figure 6.1: Illustration of (a) a non-symmetric two orthogonal fractures case, (b) the explicit discretized model and (c) the MINC proximity function model.

The reference solution consists in a LGR technique (Figure 6.1(b)) where the fractures has been explicitly discretized. On the other hand, the discrete fracture model is performed

(Figure 6.1(c)) on the whole domain using the MINC method. Note that, a MINC6 model (#1, 2, 3, 4, 5 and 6 represents the matrix media) was performed to compute the DFM.

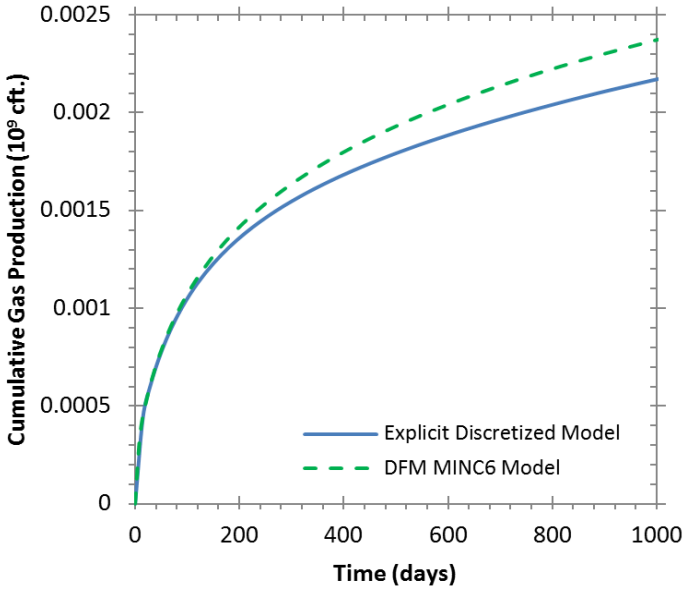

Figure 6.2: The comparison of the cumulative gas production for the explicit discretized model and the DFM MINC6 model for 1000 days of production.

Obviously, based on the results of the cumulative gas production from Figure 6.2 our DFM overestimates the gas production comparing to the reference solution. Clearly, as the fracture distribution is not symmetric in the matrix grid cell, the repartition of the matrix subdivision is not the same around the fractures in each sub-volume (V_1, V_2, V_3 and V_4). An illustration of the DFM MINC6 model is presented in Figure 6.3 for a better description of the problem.

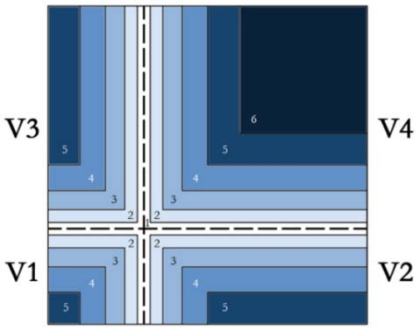

Figure 6.3: Illustration of the application of the MINC proximity function where a MINC6 model is taken into consideration in this example.

Also, Figure 6.4 presents the cumulative matrix volume of the distribution function for the total matrix grid cell and per sub-volume function of the distance from fractures. Clearly, the maximum distance found in volume V_1 is the same as V_2 and V_3. However, a larger distance is found from sub-volume V_4 due to the fracture distribution and to a bigger volume presented by V_4.

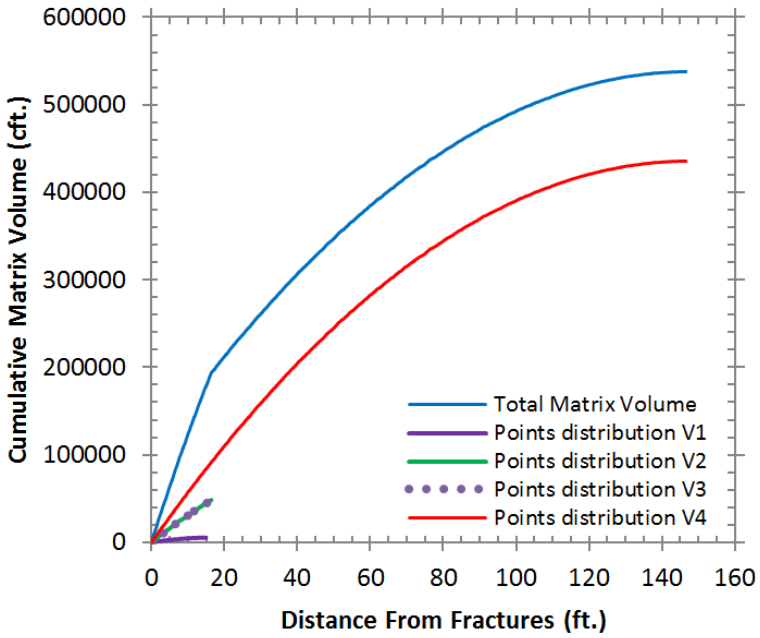

Figure 6.4: The cumulative matrix volume per sub-volume for the case presented in Figure 6.3.

As mentioned above, a MINC6 model was performed. However, based on the distribution function (Figure 6.4) generated for this case, only a sixth matrix subdivision (continuum) could exist in sub-volume (V_4) as shown in Figure 6.3 due to the different block size inside the grid cell. Note that, the subdivision of the matrix media based on the distance from the fractures is done using a volume fraction defined by the user. Due to different size block inside the grid cell, two solutions could be done in order to solve this problem. The first one consists in subdividing each sub-volume into 6 subdivisions (see, Figure 6.5). In fact, as we have the cumulative matrix volume distribution function per sub-volume (V_1, V_2, V_3 and V_4) as shown in Figure 6.4 this proposition could be done. However, the numbers of matrix unknown nodes will increase from 6 to 24. As explained before, each matrix subdivision is assigned with a matrix node. Based on this solution, as a MINC6 model is performed per sub-volume, a node must be assigned per subdivision per sub-volume which makes 24 matrix nodes as shown in Figure 6.5.

Note that, this kind of proposition solution might increase the CPU time of a simulation and this solution will not be taken into consideration. This approach is not consistent with our MINC model proposed in this work.

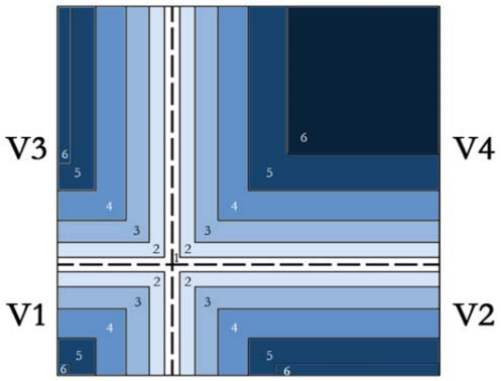

Figure 6.5: A possible solution by computing a MINC6 model in each sub-volume based on the distance from the fractures dependently for each sub-volume.

On the other hand, as our aim consists in maintaining the number of unknowns matrix nodes without increasing the CPU time, a correction of the transmissibility value could be done concerning the connection of subdivisions #5 and 6 for this example. In other words, the surface exchange between subdivisions #5 and #6 must be corrected in order to model properly the fluid flow between subdivision #5 and 6. Note that, only a connection between subdivision #5 and 6 exist in sub-volume V_4.

The corrected transmissibility must be calculated taking into account subdivision #5 and 6 only from sub-volume V_4 in order to modelling properly the flow exchange between these two continuum. Unfortunately, in the present DFM the subdivision #6 from sub-volume V_4 exchange flow with all subdivisions #5 from different sub-volume (V_1, V_2, V_3 and V_4) which is not correct and obviously will increase and overestimate the gas production as shown previously in Figure 6.2. So, a correction on the transmissibility calculation must be done taking into consideration the right surface exchange between the two continuums (#5 and 6 only from sub-volume V_4). Hereafter, a description of the methodology will be proposed and detailed.

Let's consider that a MINC6 model (see, Figure 6.1) is performed. So, the total transmissibility through the subdivisions could be written as following:

$$\frac{1}{T} = \sum_{i=1}^{N-1} \frac{1}{T_{i,i+1}} \tag{6.1}$$

where, N represents the number of subdivisions.

Moreover, the number of sub-volumes existing in the matrix grid cell is known. These sub-volumes are resulting from fracture network. Here, 4 sub-volumes (V_1, V_2, V_3 and V_4) exist in this example. It must be mentioned that there is a difference between the sub-volumes and sub grids. Taking the example above, the number of sub-volume is 4 (V=4), where the number of sub grids could reach 6 (N=6) related to the MINC proximity function.

Table 6.1: Description of the transmissibility calculation for the case presented in Figure 6.3.

		Sub-volumes			
	Transmissibility	V_1	V_2	V_3	V_4
Connection between the subgrid i and i+1	$T_{1,2}$	$T_{1/1,2}$	$T_{2/1,2}$	$T_{3/1,2}$	$T_{4/1,2}$
	$T_{2,3}$	$T_{1/2,3}$	$T_{2/2,3}$	$T_{3/2,3}$	$T_{4/2,3}$
	$T_{3,4}$	$T_{1/3,4}$	$T_{2/3,4}$	$T_{3/3,4}$	$T_{4/3,4}$
	$T_{4,5}$	$T_{1/4,5}$	$T_{2/4,5}$	$T_{3/4,5}$	$T_{4/4,5}$
	$T_{5,6}$	$T_{1/5,6} = 0$	$T_{2/5,6} = 0$	$T_{3/5,6} = 0$	$T_{4/5,6}$

Also, considering that the total flow between two continuums is equal to the sum of the flow from these continuums taking into account all existing sub-volumes. So, the transmissibility value between continuum $\#i$ and $\#i+1$ taking into account all the sub-volumes is described by the following equation:

$$T_{i,i+1(i=1,N-1)} = \sum_{j=1}^{V} T_{j/i,i+1} \tag{6.2}$$

where, N and V represent the number of subdivisions and sub-volumes of the studied grid cell respectively.

Let's consider that, N =6 and V =4 then:

$$\begin{aligned} T_{1,2} &= T_{1/1,2} + T_{2/1,2} + T_{3/1,2} + T_{4/1,2} \\ T_{2,3} &= T_{1/2,3} + T_{2/2,3} + T_{3/2,3} + T_{4/2,3} \\ T_{3,4} &= T_{1/3,4} + T_{2/3,4} + T_{3/3,4} + T_{4/3,4} \\ T_{4,5} &= T_{1/4,5} + T_{2/4,5} + T_{3/4,5} + T_{4/4,5} \\ T_{5,6} &= T_{4/5,6}, \quad Need\ Correction \end{aligned} \tag{6.3}$$

In fact, the fluid flow with the connection $T_{4/5,6}$ will flow to the fracture only within the sub-volume V_4, while the fluid with the connection $T_{5,6}$ will flow to the fracture through also other sub-volumes. So, based on Equation (6.3) the transmissibility $T_{5,6}$ should overestimate the fluid exchange from the subdivision #6 to the fracture. A correction must be done. To do so, let $T'_{i,i+1}$ be the transmissibility between continuums only in sub-Volume V_4, that is:

$$\begin{aligned} T'_{1,2} &= T_{4/1,2} \\ T'_{2,3} &= T_{4/2,3} \\ T'_{3,4} &= T_{4/3,4} \\ T'_{4,5} &= T_{4/4,5} \\ T'_{5,6} &= T_{4/5,6} \end{aligned} \tag{6.4}$$

To find $T_{5,6}$, we apply Equation (6.1):

$$\frac{1}{T_{1,2}}+\frac{1}{T_{2,3}}+\frac{1}{T_{3,4}}+\frac{1}{T_{4,5}}+\frac{1}{T_{5,6}}=\frac{1}{T'_{1,2}}+\frac{1}{T'_{2,3}}+\frac{1}{T'_{3,4}}+\frac{1}{T'_{4,5}}+\frac{1}{T'_{5,6}} \tag{6.5}$$

In the above equation, all parameters are known except $T_{5,6}$. So, the transmissibility correction can be easily obtained from Equation (6.5). Figure 6.6 presents a comparison of cumulative gas production for the case presented in Figure 6.1. Clearly, by correcting the transmissibility between #5 and #6, our DFM is able to predict the gas production comparing to the explicit discretized model set as a reference solution. Based on the results from cumulative gas production, our DFM gives us a very accurate result comparing to the reference solution.

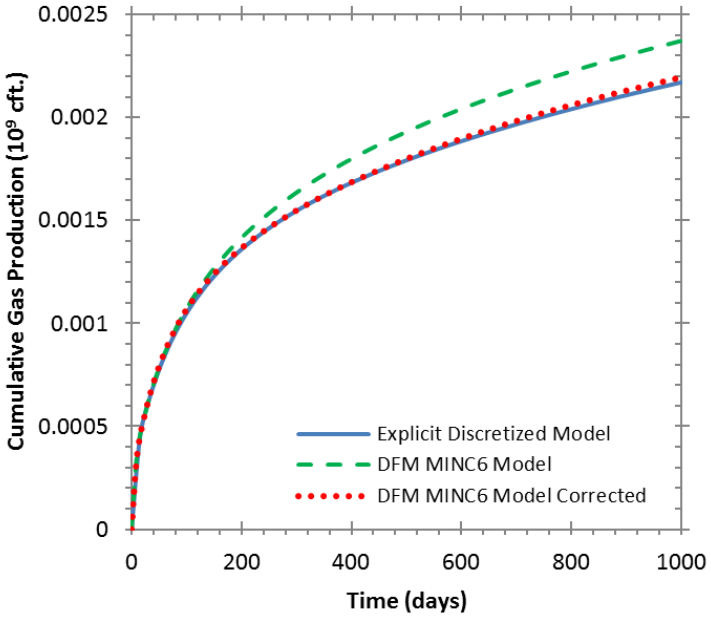

Figure 6.6: The comparison of the cumulative gas production for the explicit discretized model, the DFM MINC6 model and the corrected DFM MINC6 model for 1000 days of production.

6.1.2 Irregular Fracture Distribution

In the following, we consider a block of 164 ft in x and y directions containing 3 fractures as shown in Figure 6.7(a). The net thickness of the reservoir in z direction is of 20 ft. In this study, the permeabilities are defined as 0.0001 mD in the matrix and 3 D in the fractures. The fracture aperture is fixed at 0.004 ft. The porosity of the matrix media is 0.05. Only a single phase (gas only) flow simulation is taken into consideration. The initial reservoir pressure is 3800 psi. A

horizontal well (green node Figure 6.7(a)) is connected to the fracture, and the bottom hole well flowing pressure is 1000 psi.

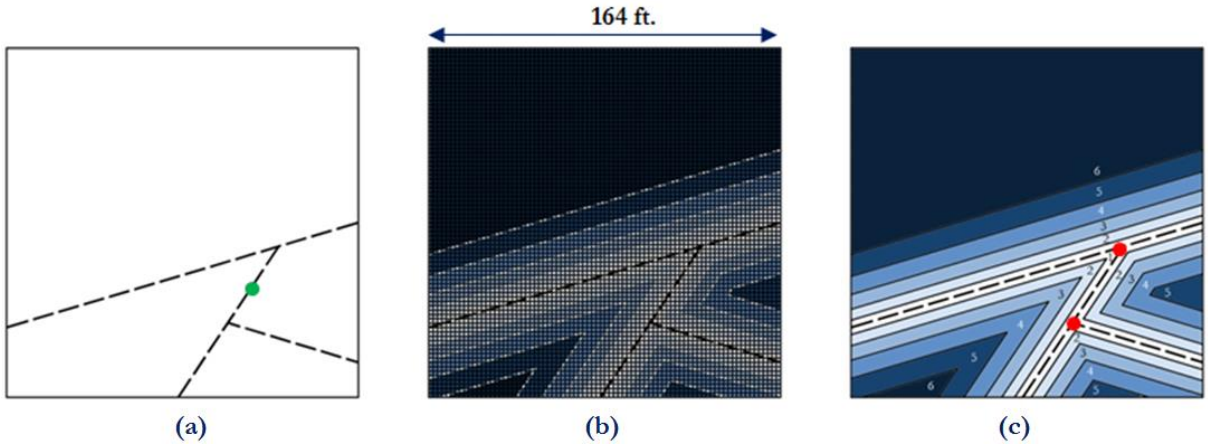

Figure 6.7: Illustration of (a) an irregular fracture distribution, (b) the reference solution and (c) the DFM MINC proximity function.

According to the reference solution, the same approach used in the previous part (see, section 4.2.4 and 4.2.5 in the previous chapter) is done on this example in order to perform the reference solution with a very fine matrix grid cells for the discretization of matrix media. On the other hand, our DFM MINC proximity method is also performed.

The reference model consists in 1000000 grid cells (see, Figure 6.7(b)) after discretizing the domain into 1000 grid cells in each x and y directions while our DFM uses only 9 nodes (1 for the well intersection (green node in Figure 6.7(a), 3 fractures nodes (red nodes in Figure 6.7(c) and 6 nodes corresponds to the matrix refinement) to describe the same problem.

The cumulative gas production for different simulation models are shown in Figure 6.8 for 5000 days of production. Based on the simulation results, clearly the DFM presents very satisfactory result comparing to the reference solution (explicit discretized model). Moreover, our DFM for a MINC6 and a MINC8 model overestimates the gas production and it is not accurate comparing to the reference solution. However, after the correction done on the MINC6 and MINC8 models (explained in the previous section), clearly the DFM approach is able to predict gas production comparing to the reference solution. Our DFM decreases greatly the CPU time from 5 hours for the reference solution to only 2 seconds with our DFM approach. In fact, decreasing the number of grid cell will result in decreasing the CPU time.

So, the MINC method can model the matrix-fracture exchange taking into account a grid cell containing various block sizes. Note that, this kind of problem cannot be handled using a standard dual-porosity approach.

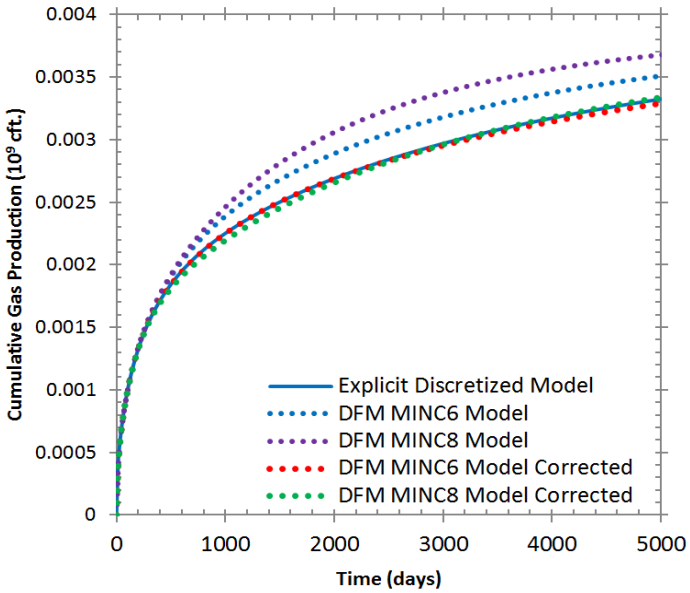

Figure 6.8: The cumulative gas production comparing the DFM MINC6 and MINC8 models with and without correction to the reference solution.

6.2 Matrix-Fracture Flow Exchange Between Different Grid Cells

In this section, a discussion concerning the second potential problem of our approach which could also be ameliorated. Hereafter, the explication of the problem and the proposed solution are described only for a regular fracture network and for a single-phase flow (gas only). The objective of this study is to simulate the matrix-fracture flow exchange by considering the presence of fractures outside the considered grid cell. So, the MINC proximity function is computed by taking into account the presence of fractures nearby the studied grid cell (including fractures inside and outside the studied grid cell).

To illustrate the problem, the example presented in Figure 6.9 consisting in a regular fracture network is simulatedn. Note that, the fractures are represented by dashed blue lines and the mesh definition in solid black lines in Figure 6.9(a) and (b). This example consists in a fracture spacing of 164 ft in x and y direction and the depth is 20 ft in z direction. The fracture aperture and permeability are set at 0.004 ft and 2500 mD respectively. The matrix porosity and

permeability are 0.05 and 0.0001 mD respectively. This repeated (infinite) fracture network can be simulated with either the mesh definition presented in Figure 6.9(a) or Figure 6.9(b). However, the fractures are centered in Figure 6.9(a) while they are shifted in Figure 6.9(b) based on the mesh definition. Note that, using an explicit discretized model (where the fracture network is explicitly discretized), the gas prediction from Figure 6.9(a) or Figure 6.9(b) should be the same from both models as we have the same fracture volumes. Two simulation models, an explicit discretized model and our DFM, are performed per case. Figure 6.10 compares the cumulative gas production for the explicit model for case (a) and (b) and our DFM for case (a) and (b).

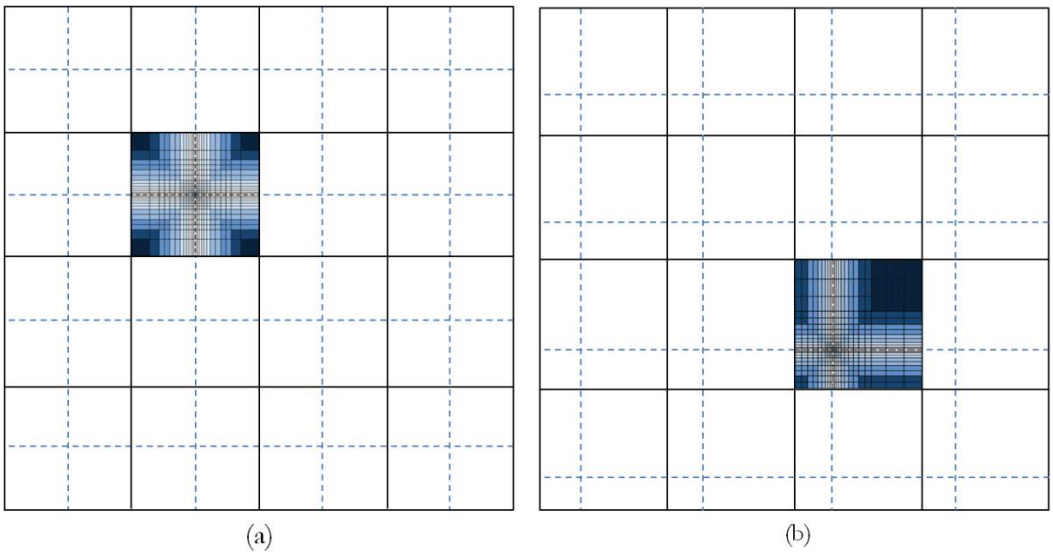

Figure 6.9: A part of the fracture network consisting in a regular distribution with a 164 ft of fractures spacing's where (a) fractures are centered and (b) fractures are shifted compared to the mesh definition.

As expected, based on Figure 6.10, the cumulative gas production of the explicit model (a) and (b) is the same. Explicit discretized models (a) and (b) are set as the reference solution. On the other hand, our DFM based on a MINC6 model modelling case (a) is able to match the reference solution as the fractures aren't shifted, while computing our DFM on case (b) underestimates the gas production for 5000 days. However, it should not be the case if our DFM takes into account the presence of nearby fractures around the studied cell (see, Figure 6.11). Our actual DFM takes into account only the presence of the fractures inside the studied grid cell for matrix-fracture exchange. In fact, our DFM treats each grid cell on it is own without taking into account the presence of nearby fractures around the studied grid cell. In other words, our DFM treats each grid cell as if a zero flux on the boundary exist and there is no exchange between

matrix from different grid cells. So, there is no flow exchange with nearby fractures, even if they are very close to the matrix cell. This may rise inaccuracy in flow simulations. So, a solution is proposed hereafter in order to solve this problem.

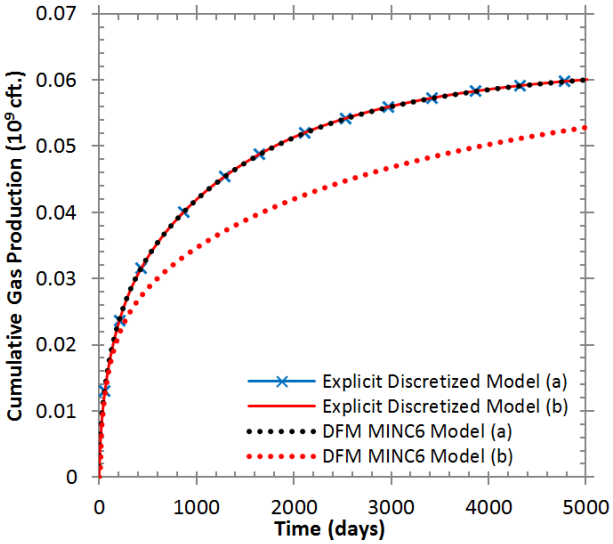

Figure 6.10: Comparison of the cumulative gas production from case (a) and (b).

As shown in Figure 6.11, the MINC proximity function is computed in the studied cell, where 100 random points (green dots in Figure 6.11) are launched in order to plot the distribution function. The actual DFM is taking into account the presence of red fractures inside the grid cell only. However, it should also consider the green fractures nearby. In fact, nearby fractures should be taken into consideration if the distance from sample points (the green dots) to nearby fractures (d pt-NF) is smallest then the distance to the fractures inside the studied grid cell (d pt-frac Cell) as shown in Figure 6.11).

Our DFM performed on the case presented in Figure 6.9(b) underestimates the gas production due to the non-consideration of the presence of nearby fractures. Figure 6.12 presents the cumulative distribution function for the grid cell presented in Figure 6.11. The curves of case (b) do not take into account the presence pf nearby fractures and the curves of case "(b) – NF" considers the presence of nearby fractures. As mentioned before, the grid block size is 164 ft.

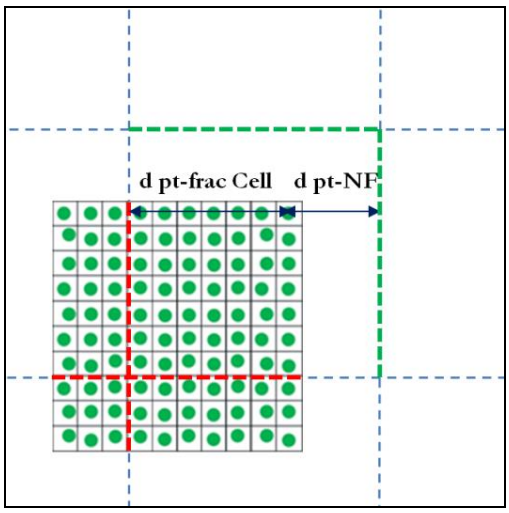

Figure 6.11: Illustration of the MINC proximity function computed into the studied grid cell.

Clearly, based on Figure 6.12, the point distribution of the sub-volume V_4 is affected by the presence of fractures nearby and obviously the total distribution is affected. In fact, the sum of the four point distribution curves resulting from V_1, V_2, V_3 and V_4 is the total matrix volume distribution function. Figure 6.12 indicates that the maximum distance from a random sample point (green dot in Figure 6.11) from fractures is 145 ft and 82 ft without and with considering nearby fractures.

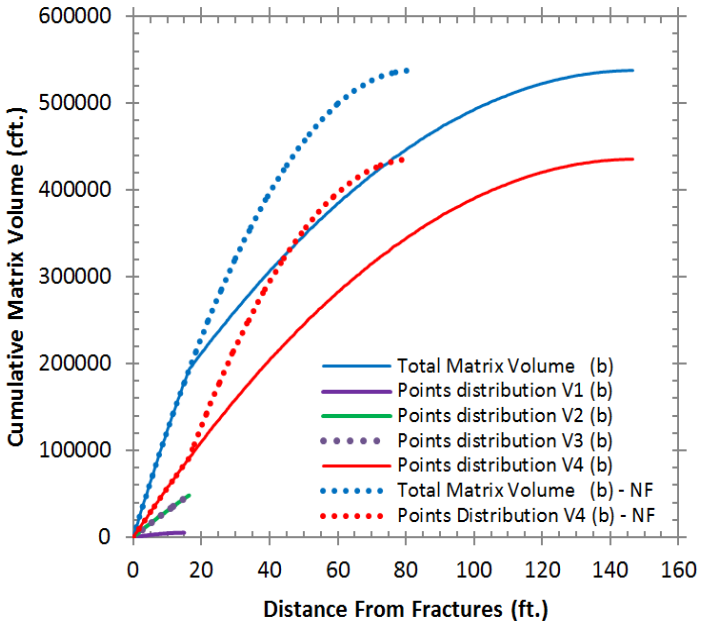

Figure 6.12: The cumulative matrix volume per sub-volume for case (b) and (b) – NF.

Figure 6.13 presents the comparison of the cumulative gas production for the explicit discretized model (a), (b), our DFM MINC6 model (b) and "(b) – Nearby Fractures". Clearly, based on results from Figure 6.12 and Figure 6.13, taking into account the presence of nearby fractures conserves the matrix block size (the distance distribution from the studied cell to the fractures) and improves the gas production. This claim is clearly supported by comparing our DFM MINC6 model "(b) – Nearby Fractures" to the reference solution (Explicit Discretized Model (b)). Considering the presence of nearby fractures around a grid cell improves the simulation for matrix-fracture exchange.

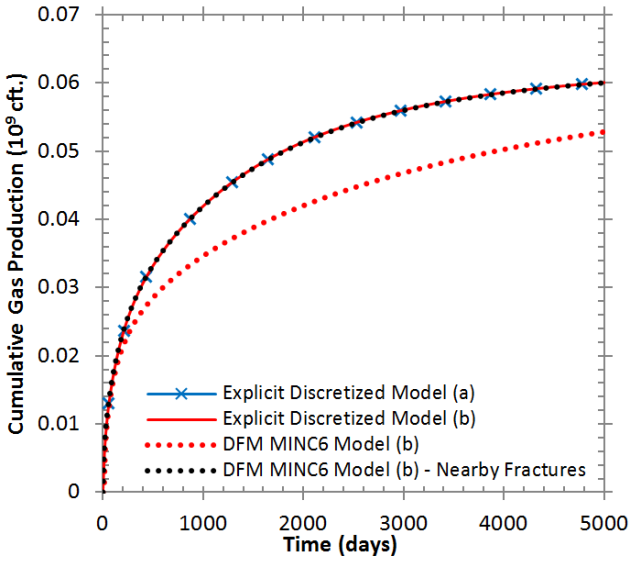

Figure 6.13: Comparison of the cumulative gas production for case (a), (b) and (b) – NF.

Chapter 7 - CONCLUSIONS

Modelling of shale formations presents several challenges such as the presence of a complex multi-scale discrete fracture network, high heterogeneity through the matrix media, very low reservoir permeability and complex physics including adsorption/desorption, Klikinberg effect, geomechanics aspect, etc. to take into account. This work presents an Discrete Fracture Model for flow modelling in unconventional shale reservoirs. The proposed DFM is based on a MINC proximity function in order to improve flow exchange between matrix and fracture media. Through this report we have shown the applicability and the efficiency of our DFM based on the MINC proximity function.

As known and proved in this report, neither an explicit discretized model with a single-porosity approach nor a dual-porosity model are suitable for flow simulations from unconventional shale reservoirs. A single-porosity model by explicitly discretizing all sort of fractures could be a solution for reservoirs simulation, but it takes too much CPU time and almost unfeasible for field applications. On the other, the standard dual-porosity model cannot accurately model the matrix-fracture interaction due to the extremely low matrix permeability and the presence of a non-linear pressure variation into the matrix block during the transient period.

In this work, we developed first a hybrid approach based on the concept of the classic MINC method. Note that, the MINC method can treat matrix-fracture flow exchange (inter-porosity flow) in a fully transient way. On one hand this approach allowed us to model properly matrix-fracture flow exchange especially during the transient period. On the other hand, this technique decreases significantly the number of grid cells leading to a decreasing in the CPU time comparing to an explicit discretized model. This approach is validated in Chapter 3 on regular fracture networks. We proved its applicability and ability to model flow behavior from shale-gas

reservoirs formation and it can provide accurate simulations for both single and two-phase flow problems. The impact of fracturing fluid induced formation damage was particularly investigated. The simulation of fracturing fluid invasion and its backflow needs very fine grid cells near the fractures faces for a better flow modelling into and from the fractures. Our hybrid approach can handle this kind of formation damage issue due to implementation of the MINC method which subdivides the matrix block based on the distance from the fractures into nested sub-cells. The impact of fracturing fluid formation damage on gas recovery may be great, depending on fracturing fluid invasion depth into the matrix formation.

Once our hybrid approach was validated for a regular fracture network, we aimed to generalize it in order to treat an irregular fracture distribution networks.

Unconventional reservoirs present multi-scale fractures of various sizes embedded in extremely low permeability formation, which increase the complexity of the reservoir simulation. To overcome this challenge, the fractures are classified using a hierarchical method based on fractures conductivity criterion. The hydraulic and propped (or high conductive) fractures are explicitly discretized and the other fractures (low conductive fractures) are homogenized. This is a triple-porosity approach. The MINC proximity function is computed by taking into account all discrete fractures. In other words, the proposed DFM uses a MINC proximity function by considering the effect of both high conductivity explicitly discretized fractures and low conductive homogenized fractures.

Our DFM was tested on various cases with discrete fracture networks, including an isolated fracture, three orthogonal fractures, two diagonal fractures and an irregular fractures distribution in Chapter 4. Large cases taking into consideration a regular fracture distribution with a uniform and a non-uniform SRV zone were studied. Once more, our DFM based on the MINC proximity model proves its efficiency by modelling properly flow from shale reservoirs.

The robustness of the proposed DFM was put on the line when a 2D synthetic irregular fracture network was studied. Note that, the irregular fracture distribution case studied in Chapter 5 presents the complexity of a typical fractured shale reservoir. A single-phase flow was tested first. Based on the simulation results, our DFM is able to predict well productions from such fractured reservoirs with a good accuracy and with a CPU time in order of seconds in our case.

The proposed DFM is particularly useful for multi-phase flow simulations. For example, in a tight-oil reservoir, when the fracture pressure drops below the bubble point, gas starts to

appear in the matrix formation near the fracture faces. This kind of phenomena cannot be handled with a standard approach due to the large grid cells. However, using our DFM based on a MINC proximity function could easily treat such phenomena due to the very small nested matrix sub-cells near the fractures faces. An application to shale-gas condensate reservoir, a tight-oil three-phase flow case (water, oil and gas) were presented and simulated with our DFM. The results from the shale-gas and the tight-oil applications are good enough comparing to an explicit model set as the reference solution, while a standard DP model is not accurate at all.

As shown from our numerical results, our DFM allows us to obtain similar results as the explicit discretized fracture model with a gain of an order of magnitude of 3 - 4 in CPU time. So, the approach offers a computationally efficient method for simulating fluid flow from low permeability shale-gas and tight-oil reservoirs. It could easily be implemented in an existing reservoir simulator through an option of non-neighbor connections.

Initially, our study was based on flow modelling for shale-gas reservoirs. However, the proposed DFM is also suitable for other unconventional low permeability reservoirs, such as tight-oil reservoir. Finally, our model proved its ability to predict flow behavior, for both single-phase and multiphase flow problems for regular and irregular fracture distributions, from different kinds of shale reservoirs. Moreover, due to the very low CPU time (several seconds) resulting from our hybrid approach, sensitivity tests (fracture apertures, fracture permeability, matrix permeability, etc.) and advanced physical processes (adsorption/desorption, geomechanics aspect, Klinkenberg effect, etc., together with the formation damage issue for a large SRV case), could be efficiently performed.

Finally, the problems discussed in Chapter 6 could be taken into account in the future work. The proposed solutions could be further developed to improve the ability and the efficiency of the DFM approach for unconventional reservoir simulations.

APPENDIX A - PUBLICATIONS

Farah, N., Ding, D.Y., "Discrete Fracture Model based on Multiple Interacting Continua Proximity Function for Unconventional Low Permeability Reservoir Simulations", EAGE 30105, European Conference of Mathematics for Oil Recovery (ECMOR), Amsterdam, The Netherlands, August 29 – September 1, Oral, 2016.

Farah, N., Ding, D.Y. & Delorme, M., "Extension of the Multiple Interacting Continua Method to Discrete Fracture Models for Unconventional Low Permeability Reservoir Simulations", URTeC 2443586, Unconventional Resources Technology Conference (URTeC), San Antonio, Texas, USA, August 1 - 3, Oral, 2016.

Farah, N., Ding, D.Y., and Wu, Y.S., "Simulation of the Impact of Fracturing Fluid Induced Formation Damage in Shale-Gas Reservoirs", SPE-173264-PA, Symposium Reservoir Simulation, Houston, Texas, 23-25 February, Oral, 2015, Accepted for Society of Petroleum Engineers - Reservoir Evaluation and Engineering Journal.

Farah, N., Ding, D.Y., Khrouf, A.M., and Wu, Y.S., "Simulation of Fracturing Water Invasion and Its Impact on Gas Production in Shale-Gas Reservoirs", EAGE 21676, ECMOR XIV, Catania, Sicily, 8-11 September, Oral, 2014.

Ding, D.Y., Wu, Y.S., Farah, N., Wang, C. and Bourbiaux, B., "Numerical Simulation of Low Permeability Unconventional Gas Reservoirs", SPE-167711-MS, Unconventional conference held in Vienna, Austria, 25-27 February, Oral, 2014.

APPENDIX B - MINC PROXIMITY FUNCTION

To construct the N subdivisions of MINC, we divide the considered grid cell G according to the distance to the fractures inside this grid cell. Let $G(x,y,z)$ be the distance of a point (x, y, z) to the fractures. The domain with the distance to the fractures smaller than a given r is defined by:

$$D(r) = \{(x,y,z) \epsilon\, G;\ r(x,y,z) \leq r\} \tag{B.1}$$

and it corresponding volume can be calculated by:

$$V(r) = \int_{D(r)} dxdydz \tag{B.2}$$

The N subdivisions of MINC can therefore be defined as follows:

$$D_1 = \{(x,y,z) \epsilon\, G;\ r(x,y,z) \leq r_1\}$$

$$D_2 = \{(x,y,z) \epsilon\, G;\ r_1 \leq r(x,y,z) \leq r_2\} \tag{B.3}$$

.

$$D_N = \{(x,y,z)\epsilon\ G;\ r_{N-1} \leq r(x,y,z) \leq r_N\}$$

where $r_1 \leq r_2 \leq \cdots \leq r_N$.

The corresponding volumes are given by:

$$vol(D_i) = \int_{D_i} dxdydz; (i = 1, 2, \ldots, N) \tag{B.4}$$

Usually, the subdivisions are constrained by a given percentage of the total volume, defined by the user. So, we can consider the volumes are known. Instead, we need to determine the distances which separate two subdivisions. This is not a difficult task. The biggest challenge in this work is to calculate the area of an interface between two subdivisions.

We notice that the volume of a subdivision can also be calculated in another way. Let $S(r)$ be the area of the surface (inside the grid cell G) with a distance r to the fractures. The volume of the domain $\mathbf{D}$ with a distance smaller than r to the fractures can be computed by:

$$V(r) = \int_0^r S(l)dl \tag{B.5}$$

So, if the volume of the subdivision at a distance r to the fractures is known, the area of its surface is just the derivative of the volume with respect to the distance:

$$S(r) = \frac{dV(r)}{dr} \tag{B.6}$$

In some particular cases, the volume of a subdivision $V(r)$ can be expressed analytically, and so the interface areas are obtained by an analytical expression. However, in most cases, analytical expressions cannot be found, and numerical methods should be used to compute the subdivision volumes and their interface areas.

Numerical Method

In most cases, we cannot find an analytical expression for the volume computation, and we can determine neither the distance r to separate two subdivisions of a MINC. A numerical solution is required. The grid cell G is first discretized in p sub-domains of equal volumes ($\mathbf{vol}(G_i) = \frac{\mathbf{vol}(G)}{p}$) with $G = \bigcup_{i=1}^{p} G_i$ and $G_i \cap G_j = \emptyset$ for $\mathbf{i} \neq$j. Any integral over a domain inside G can be computed as the sum of the integral over the domain G_i. Therefore, the volume of a MINC subdivisions D_k $(k = 1, 2, \dots, \mathrm{N})$ can be calculated by:

$$vol(D_k) = \int_{D_k} dxdydz = \sum_{i=1}^{p} \int_{G_i \cap D_k} dxdydz = \sum_{i=1}^{p} vol(G_i \bigcap D_k) \tag{B.7}$$

On the other hand, we have:

$$vol\left(G_i \bigcap D_k\right) = \begin{cases} \frac{1}{p} vol(G); if \;\; G_i c D_k \\ 0; \; if \; G_i \bigcap D_k = \emptyset \end{cases} \tag{B.8}$$

For a very small domain G_i, we assume that it is either inside or outside the domain D_k by choosing a point pt_i (the center of gravity or and randomly selected point) of G_i and checking if it belongs to D_k. This assumption is reasonable if the discretization is fine enough, that is, for $p \to \infty$ and $\mathbf{vol}(G_i) \to 0$. So, the volume of D_k is approximated by:

$$vol(D_k) \approx \frac{p_k}{p} \; vol(G) \tag{B.9}$$

where p_k is the number of discretized sub-domain G_i inside the MINC subdivision D_k.

In Equation (B.9), approximation errors are committed around the boundary of D_k, where a discretized sub-domain G_i is neither inside nor outside D_k. But this kind of errors can be neglected due to small sub-domain size of G_i and the compensation of positive and negative errors in the summation in Equation (B.7).

It is easy to check if a point pt_i is inside a MINC subdivision, as the MINC subdivisions are constructed according to the distance to the fractures. A subdivision D_k is delimited by two bounds r_{k-1} and r_k. If the distance of P to the fractures is inside the interval $[r_{k-1}; r_k]$, the point p belongs to the domain D_k. Otherwise, it is outside. Discretizing the grid cell G provides also a way to construct the MINC subdivisions. In fact, a point is selected in each discretized domain G_i, and its distance to the fractures is calculated and can be ranked by $r_1 \leq r_2 \leq \cdots \leq r_N$. The MINC volume defined with r_1 is approximately $\mathbf{vol(G)}/p$, and the MINC volume defined with r_2 is approximately $2 * \mathbf{vol(G)}/p$, etc. So we have a direct relation between the distance to the fractures and its corresponding volume. For a given volume partition $V_1, V_2, \ldots V_N$ it is not difficult to find the corresponding distances to delimit the MINC subdivisions.

In the above approach, G is first discretized into n sub-domains G_i, and a point is (randomly) selected in each sub-domain and its distance to the fractures is calculated and ranked. If the selection of the points is not constrained by the sub-domains G_i, this method is close to the stochastic approach proposed by Khvoenkova and Delorme (2011)).

So, we can obtain the probability density function of the distance to the fractures. The frequency of a distance r in the distribution function is the surface of the iso-distance r to the

fracture, normalized by the volume. The area under the distribution function between r_1 and r_2 corresponds to the volume proportion of the subdivision delimited by r_1 and r_2.

So, we can also use the probability density function and/or its cumulative distribution function to construct the MINC sub-divisions and compute their volumes and the interface areas. Given a partition of volume percentages for the MINC, we can easily determine the distances $r_1, r_2, \ldots, r_N$, which separate MINC subdivisions, by partitioning the cumulative distribution function. The volume in each subdivision is known by the construction. The area of the interface between two subdivisions is calculated by the derivative of the cumulative function. To construct the probability density function, a large number of samples is required.

In practice, if the integral of Equation (B.4) can be expressed analytically, we use the analytical expression to calculate the interface areas and so the connection factors between two MINC subdivisions. If analytical expressions cannot be found, the numerical method will be used. Usually, we are limited by the number of sampling points in the numerical approach due to CPU time constraint. In numerical modelling, we suggest to discretizing first the domain G into p equal volume (cubic or rectangular) sub-domains and then select randomly a point pt_i in each discretized sub-domain. If n is not very large, the selected points are more uniformly distributed over the grid cell G than a random selection inside G (Khvoenkova and Delorme (2011).

REFERENCES

Agrawal, S., Sharma, M., "Liquid Loading Within Hydraulic Fractures and its Impact on Unconventional Reservoir Productivity", SPE 168781 /URTeC 1580636, Unconventional Resources Technology Conference held in Denver, Colorado, USA, August 12-14, 2013.

Barenblatt, G.I., Zheltov, Iu.P., kochina, I.N., "Basic concepts in the theory of seepage of homogeneous liquids in fissured rocks", Journal of applied mathematics and mechanics, vol. 24, PP. 1286-1303, 1960.

Bertoncello, A., Wallace, J.; Blyton, C., Honarpour, M., and kabir, C.S., "Imbibition and Water Blockage in Unconventional Reservoirs: Well Management Implications During Flowback and Early Production", SPE 167698, Austria, February 25-27, 2014.

Bicheng, Y., Yuhe, W., and John E.K., "Beyond Dual-Porosity Modelling for the Simulation of Complex Flow Mechanisms in Shale Reservoirs", SPE 163651, February 18-20, 2013.

Bourbiaux, B., Cascas, M.C., Sarda, S., and Sabathier, J.C., "A Fast and Efficient Methodology to Convert Fractured reservoir Images Into a Dual-porosity Model", Paper SPE 38907 presented at the SPE Annual Technical Conference and Exhibition, San Antonio, TX, October 5-8, 1997.

Bourbiaux, B., Granet, S., Landereau, P., Noetinger, B., Sarda, S., Sabathier, J.C., "Scaling Up Matrix-Fracture Transfers in Dual-Porosity Models: Theory and Application", Paper SPE 56557 presented at the SPE Annual Technical Conference and Exhibition, Houston, TX, October 3-6, 1999.

Bustin, R.M., Bustin, A.M.M., Cui, X., Rose, D.J.K. and Murthy Pathi, V.S., "Impact of Shale Properties on Pore Structure and Storage Characteristics", SPE 119892 presented at the SPE Gas Production Conference, Fort Worth, TX, November 16-18, 2008.

Chang, M., "Deriving the Shape Factor of a Fractured Rock Matrix", Technical Report NIPER-696 (DE93000170), Niper, Bartlesville, Oklahoma, 1993.

Cheng, Y., "Impact of Water Dynamics in Fractures on the Performance of Hydraulically Fractured Wells in Gas-Shale Reservoirs", Journal of Canadian Pet. Tech., pp143-151, March, 2013.

Chong, K.K., Grieser, B., Jaripatke O., Passman, A., "A Completions Roadmap to Shale-Play Development: A Review of Successful Approaches toward Shale-Play Stimulation in the Last Two Decades", SPE 13369, 2010.

Civan, F., Rai, C. S., Sondergeld, C.H., "Effective Correlation of Apparent Gas Permeability in Tight Porous Media", Transport in Porous Media, Vol. 82:375-384, 2010.

Cipolla, C.L., Warpinski, N.R., Mayerhofefr, M.J., and Lolon, E.P., and Vincent, M.C., "The Relationship Between Fracture Complexity, Reservoir Properties, and Fracture Treatment design", paper SPE 115769, Conference and Exhibition held in Denver, Colorado, USA, September 21-24, 2008.

Cipolla, C.L., Carbo Ceramics, Lolon, E.P., and Mayerhofer, M.J., "Reservoirs Modelling and Production Evaluation in Shale-Gas Reservoirs", paper IPTC 13185, International Petroleum Technology Conference held in Doha, Qatar, December 7-9, 2009a.

Cipolla, C.P., Carbo; Lolon, E.P., J.C., and Tathed, V., "Modelling Well Performance in Shale-Gas Reservoirs", paper SPE 125532, prepared for presentation at the 2009 SPE/EAGE Reservoir Characterization and Simulation Conference held in Abu Dhabi, UAE, October 19-21, 2009b.

Cipolla, C.L., and Lolon, E.P., Erdle, J.C., and Rubin, B., "Reservoir Modelling in Shale-Gas Reservoirs", SPE Eastern Regional meeting, Charleston West Virginia, 1 March, 2010.

Clarkson, C. R., Ertekin, T., "A New Model for Shale-Gas Matrix Flow Using the Dynamic-Slippage Concept", AAPG Hedberg Conference, Austin TX, December 5-10, 2010.

Clarkson, C.R. and Bustin, R.M., "Coalbed Methane: Current Evaluation Methods, Future Technical Chanllenges" SPE 131791 presented at the SPE Unconventional Gas Conf., Pittsburgh, Pennsylvania, USA, February 23-25, 2010.

De Dreuzy, J.R., Meheust, Y., and Pichot, G., "Influence of Fracture Scale Heterogeneity on the Flow Properties of Three-Dimensional Discrete Fracture Networks", Journal of Geophysical Research, Solid Earth (1978–2012), 117(B11), 2012.

De Dreuzy, J.R., Pichot, G., Poirriez, B., and Erhel, J., "Synthetic Benchmark for Modelling Flow in 3D Fractured Media", Computers and Geosciences 50, 59–71, 2013.

Delorme, M., Atfeh, B., Allken, V., and Bourbiaux, B., "Upscaling Improvement for Heterogeneous Fractured Reservoirs Using a Geostatical Connectivity Index", VIII International Geostatistics Congress, Santiago, Chile, December, 2008.

Delorme, M., and Khvoenkova, N., "Maillage 3D de Réseaux de Fractures pour la Modélisation de Réservoirs, Méthode Multi-Échelle.", February, 2011.

Delorme, M., Daniel, J.M., Kada-Kloucha, C., Khvoenkova, N., Schueller, S., and Souque, C. "An Efficient Model to Simulate Reservoir Stimulation and Induced Microseismic Events on 3D Discrete Fracture Network for Unconventional Reservoirs", paper SPE 168726, presented at URTeC, Denver, CO, USA, August, 2013.

Devegowda, D., Sapmanee, K., Civan, F. and Sigal, R.F., "Phase Behavior of Gas Condensates in Shales Due to Pore Proximity Effects: Implications for Transport, Reserves and Well Productivity". Presented at Annual Technical Conference and Exhibition, San Antonio, Texas, 8–10 October. SPE-160099-MS, 2012.

Ding, D.Y., "Well Modelling in Reservoir Simulation" Proceeding of the 5th ECMOR, Leoben, Austria, Sept. 3-6, 1996.

Ding, D.Y., Langouet, H., and Jeannin, L., "Simulation of Fracturing Induced Formation Damage and Gas Production from Fractured Wells in Tight Gas Reservoirs", SPE Production & Operations, vol.28, issue 3, pp246-258, 2013.

Ding, D.Y., Longeron, D., Renard, G., and Audibert, A., "Modelling of Both Near-Wellbore Damage and Natural Cleanup of Horizontal Wells Drilled With a Water Based Mud" Proceeding of the 5th ECMOR, Leoben, Austria, Sept. 3-6, 2002.

Ding, D.Y., Wu, Y.S., Farah, N., Wang, C. and Bourbiaux, B., "Numerical Simulation of Low Permeability Unconventional Gas Reservoirs", SPE 167711-MS, Unconventional confenrence held in Vienna, Austria, February 25-27, 2014a.

Ding, D.Y., Wu, Y-S. and Jeannin, L. "Efficient Simulation of Hydraulic Fractured Wells in Unconventional Reservoirs" J. of Pet. Sci. & Eng., vol.122, pp631-642. October 2014b.

Ehrl, E., and Schueler, S.K., "Simulation of a Tight-Gas Reservoir with Horizontal Multi-fractured Wells", SPE 65108 presented at the SPE EUROPEC, Paris, France, October 24-25, 2000.

EIA (U.S. Energy Information Administration), "Annual Energy Outlook 2016 with Projections to 2040", DOE/EIA-0383, August, 2016.

EIA (U.S. Energy Information Administration), "Analysis and Projections World Shale Resource Assessments", September 24, 2015.

EIA (U.S. Energy Information Administration), "Technically Recoverable Shale Oil and Shale-Gas Resources: An Assessment of 137 Shale Formations in 41 Countries Outside the United States", U.S. Department of Energy Estimates, November 23, 2013.

Ertekin, T., King, G. R., Schwerer, F. C., "Dynamic Gas Slippage: A Unique Dual-Mechanism Approach to the Flow of Gas in Tight Formations, SPE Formation Evaluation", Paper SPE 12045-PA, 1986.

Farhadinia, M.A. and Delshad, M., "Modelling and Assessment of Wettability Alteration Processes in Fractured Carbonates Using Dual-porosity and Discrete Fracture Approaches" SPE 129749 presented at the SPE Improved Oil Recovery, Tulsa, OK, USA, April 24-28, 2010.

Fazelipour, W., "Development of Techniques to Integrate Hydraulic Fracturing Design and Reservoir Simulation Technologies - Application to Forecast Production of Stimulated Wells in Unconventional Gas Reservoirs", paper SPE 142337, Middle East Unconventional Gas Conference and Exhibition, Muscat, Oman, January 31 - February 2, 2011.

Fredd, C.N., McConnell, S.B., Boney, C.L., England, K.W., "Experimental study of fracture conductivity for water-fracturing and conventional fracturing applications", SPE Journal 6(3), 288–298, 2001.

Friedel, T., "Numerical Simulation of Production from Tight-Gas Reservoirs by Advanced Stimulation Technologies", PhD Thesis, Freiberg University, 2004.

Gdanski, R., Fulton, D., and Chen, C., "Fracture Face Skin Evolution During Cleanup", paper SPE 101083, SPE ATC&E, San Antonio, TX, September 24-27, 2006.

Holditch, S.A., "Factors Affecting Water Blocking and Gas Flow from Hydraulically Fractured Gas Wells", JPT, pp1515-1524, December, 1979.

Hudson, J., "Quad-Porosity Model for Description of Gas Transport in Shale-Gas Reservoirs", Master's thesis, Oklahoma University, Norman, 2011.

Javadpour, F., Fisher, D., "Nanopores Gas Flow in Shale Sediments", Journal of Canadian Petroleum Technology, 46(10), 55-61, 2007.

Javadpour, F., "Nanopores and Apparent Permeability of Gas Flow in Mudrocks (Shale and Siltstone)", Journal of Canadian Petroleum Technology, v. 48, pp 16-21, 2009.

Jarvie, D., "Evaluation of Hydrocarbon Generation and Storage in Barnett Shale", Fort Worth Basin, Texas; The University of Texas at Austin, Bureau of Economic Geology/PTTC, 116p, 2004.

Hajibeygi, H., Karvounis, D., and Jenny, P., "A Hierarchical Fracture Model for the Iterative Multi-Scale Finite Volume Method", Journal of Computational Physics, Vol. 230, 8729-8743, 2011.

Karimi-fard, M., Durlofsky, L.J., and Aziz, K., "An Efficient Discrete-Fracture Model Applicable for General Purpose Reservoir Simulators", SPE Journal, Vol. 9, 227-236, 2004.

Karimi-Fard, M., Gong, B., and Durlofsky, L.J., "Generation of Coarse-Scale Continuum Flow Models From Detailed Fracture Characterizations", Department of Energy Resources Engineering, Stanford University, California, USA, October, 2006.

Kazemi, H., "Pressure Transient Analysis of Naturally Fractured Reservoirs with Uniform Fracture Distribution", SPE Journal, Vol. 9, 451-462, 1969.

Kazemi, H., Merrill, J.R, Porterfield, K.L., and Zeman, P.R., "Numerical Simulation of Water-Oil Flow in Naturally Fractured Reservoirs", SPE Journal, 16 (6), pp. 317-326, December, 1976.

Khvoenkova, N., and Delorme, M., "Performance Analysis of the Hybrid Fracture Media Upscaling Approach on a realistic Case of Naturally Fractured Reservoir", paper IPTC 13935, presented at IPTC, Doha, Qatar, December, 2009.

Khvoenkova, N., and Delorme, M. "An Optimal Method to Model Transient Flows in 3D Discrete Fracture Network", In IAMG Conference, 2011.

Langmuir, I., "The Constitution and Fundamental Properties of Solids and Liquids", Journal of the American Chemical Society, 38 (11): 2221–2295, 1916.

Leahy-Dios, A., Das, M., Agarwal, A. and Kaminsky, R. D., "Modelling of Transport Phenomena and Multicomponent Sorption for Shale-Gas and Coalbed Methane in an unstructured Grid Simulator," SPE 147352, presented at the SPE Annual Technical Conference, Denver, Colorado, October 30 - November 2, 2011.

Lee, S.H., Lough, M.F., and Jensen, C.L., "Hierarchical modelling of flow in naturally fractured formations with multiple length scale", Water Resources Research, 37 (3), pp. 443-445, December, 2001.

Li, L., and Lee; S. H., Chevron Energy Technology, "Efficient Field-Scale Simulation of Black Oil in a Naturally Fractured Reservoir Through Discrete Fracture Networks and Homogenized Media", January, 2008.

Li, J., Mike Du, C., and Zhang, X., "Critical Evaluation of Shale-Gas Reservoirs Simulation Approaches: Single-Porosity and Dual-Porosity Modelling", paper SPE 141756, Middle East Unconventional Gas Conference and Exhibition held in Muscat, Oman, January 31 - February 1, 2011.

Li, J., Guo, B., Gao, D., and Ai, C., "The Effect of Fracture-Face Matrix Damage on Productivity of Fractures with Infinite and Finite Conductivities in Shale-Gas Reservoirs" SPE Drilling & Completion, pp. 347-353, September, 2012.

Lim, K.T., and Aziz, K., "Matrix-fracture transfer functions for dual-porosity simulators", J. Petroleum Sci. Eng., vol. 13, pp. 169-178, 1995.

Lolon, E.P., Shaoul, J.R., and Mayerhofer, M.J., "Application of 3-D Reservoir Simulator for Hydraulically Fractured Wells", paper SPE 110093, Asia Pacific Oil and Gas Conference and Exhibition, Jakarta, Indonesia, October 30 - November 1, 2007.

McClure, M. W. and Horne, R. N., "Discrete Fracture Network Modelling of Hydraulic Stimulation", Springer Briefs in Earth Sciences, 2012.

Mengal, S.A. and R.A. Wattenbarger, "Accounting for Adsorbed Gas in Shale-Gas Reservoirs," SPE 141085, presented at the SPE Middle East Oil and Gas Show and Conference held in Manama, Bahrain, September 25–28, 2011.

Mirzaei and Cipolla, C.L., "A Workflow for Modelling and Simulation of Hydraulic fractures in Unconventional Gas Reservoirs", paper SPE 153022, Middle East Unconventional Gas Conference and Exhibition held in Abu Dhabi, UAE, January 23-25, 2012.

Moinfar, A., Narr, W., Hui, M.H., Mallison, B., and Lee, S.H., "Comparison of Discrete-Fracture and Dual Permeability Models for Multiphase Flow in Naturally Fractured Reservoirs", paper SPE 142295, Reservoir Simulation Symposium held in The Woodlands, Texas, USA, February 21-23, 2011.

Moinfar, A., "Development of an Efficient Embedded Discrete Fracture Model for 3D Compositional Reservoir Simulation in Fractured Reservoirs", PhD Thesis presented at The University of Texas, Austin, 2013a.

Moinfar, A., Varavei, A., Sepehnoori, K., and Johns, R.T., "Development of a coupled Dual Continuum and Discrete Fracture Model for the Simulation of Unconventional Reservoirs", paper SPE 163647, Reservoir Simulation Symposium held in The Woodlands, Texas, USA, February 18-20, 2013b.

Moridis, G.J., Lawrence Berkeley national laboratory, "Analysis of Mechanisms of Flow in Fractured Tight-Gas and Shale-Gas Reservoirs", paper SPE 139250, Latin American & Caribbean Petroleum Engineering Conference held in Lima, Peru, December 1-3, 2010.

Morishige, K., Fujii, H., Uga, M. and Kinukawa, D., "Capillary Critical Point of Argon, Nitrogen, Oxygen, Ethylene, and Carbon Dioxide in MCM-41", Langmuir 13 (13): 3494–3498, 1997.

Nanba, T., "Numerical Simulation of Pressure Transient in Naturally Fractured Reservoirs with Unsteady-State Matrix-to-Fracture Flow", SPE 22719 presented at the 66th ATC&E, Dallas, USA, Oct. 6-9, 1991.

Nassir, M., Settari, A., and Wan, R., "Prediction and optimization of fracturing in tight gas and shale using a coupled geomechanical model of combined tensile and shear fracturing", presented at the SPE Hydraulic Fracturing Technology Conference, February, 2012.

Nederlof, M. H. "The Scope for Natural Gas Supplies from Unconventional Sources", Ann. Rev. Energy.13:95-117, 1988.

Nojabaei, B., Johns, R. and Chu, L., "Effect of Capillary Pressure on Phase Behavior in Tight Rocks and Shales" SPEREE, August, pp281-289, 2013.

Norbeck, J., Huang, H., Podgorney, R., and Horne, R., "An Integrate Discrete Fracture Model for Description of Dynamic Behavior in Fractured Reservoirs", Department of Energy Resources Engineering, Stanford University, California, USA, February 24-26, 2014.

Oda, M., "Permeability Tensor for Discontinuous Rock Masses", Geotechnique Volume 35, 483-495, 8-10, 1986.

Passey, Q.R., Bohacs, K.M., Esch, W.L., Klimentidis, R. and Sinha, S., "From Oil-Prone Source Rock to Gas-Producing Shale Reservoir – Geological and Petrophysical Characterization of Unconventional Shale-Gas Reservoirs", SPE 131350 presented at the CPS/SPE International Oil and Gas Conference and Exhibition, Beijing, China, June 8-10, 2010.

Pruess, K., "Brief Guide to the MINC-Method for Modelling Flow and Transport in Fractured Media", Lawrence Berkeley Laboratory, University of California, May, 1992.

Pruess, K., Karasaki, K., Earth Sciences Division, Lawrence Berkeley Laboratory, University of California, Berkeley, California 94720, "Proximity Functions for Modelling Fluid and Heat Flow in Reservoirs with Stochastic Fracture Distributions", Submitted to the Stanford Geothermal Reservoir Engineering Workshop, December 14-16, 1982.

Pruess, K., Narasimhan, T.N., "A Practical Method for Modelling Fluid and Heat Flow in Fractured Porous Media", Society of Petroleum Engineers Journal, paper SPE 10509, Reservoir Simulation Symposium held in New Orleans, January 31 - February 3, 1985.

Quintard, M., Whitaker, S., "Transport in Chemically and Mechanically Heterogeneous Porous Media I: Theoretical Development of Region-Averaged Equations for Slightly Compressible Single-Phase Flow", Advance Water Resources 19, 1, 29-47, 1996.

Shabro, V., Torres-Verdin, C., and Javadpour, F. "Numerical Simulation of Shale-Gas Production: From Pore-Scale Modelling of Slip-Flow, Knudsen Diffusion and Langmuir Desorption to Reservoir Modelling of Compressible Fluid", SPE 144355, 2011.

Shabro, V., Torres-Verdin, C., and Javadpour, F., "Forecasting gas production in organic shale with the combined numerical simulation of gas diffusion in kerogen, Langmuir desorption from kerogen surfaces, and advection in nanopores", SPE 159259, 2012.

Shapiro, A.A. and Stenby, E.H., "Kelvin Equation for a Non-Ideal Multicomponent Mixture. Fluid Phase Equilibria", 134 (1): 87–101, 1997.

Singh, S.K., Sinha, A., Deo, G. and Singh, J.K., "Vapor-Liquid Phase Coexistence, Critical Properties, and Surface Tension of Confined Alkanes", J. Phys. Chem. 113 (17): 7170–7180, 2009.

Rahman, M., Aghighi, M., Rahman, S., & Ravoof, S., "Interaction Between Induced Hydraulic Fracture and Pre-Existing Natural Fracture in a Poro-Elastic Environment: Effect of Pore Pressure Change and the Orientation of Natural Fractures". In Asia Pacific Oil and Gas Conference & Exhibition, August, 2009.

Rubin, B., "Accurate Simulation of Non-Darcy Flow in Stimulated Fractured Shale Reservoirs", paper SPE 132093, prepared for presentation at the SPE Western Regional Meeting held in Anaheim, California, USA, 27-29 May, 2010.

Travallonia, L., Castierb, M., Tavaresa, F.W. and Sandley, S.I., "Critical Behavior of Pure Confined Fluids from an Extension of the Van Der Waals Equation of State", Journal Supercrit. Fluids 55 (2): 455–461, 2010.

Teklu, T. W., Alharthy, N., Kazemi, H., Yin, X., SPE; and Graves, R., SPE, Colorado School of Mines and AlSumaiti, A.M., SPE, The Petroleum Institute, Abu Dhabi, "Phase Behavior and Minimum Miscibility Pressure in Nanopores", SPE 168865, 2014.

Van Heel, A.P.G. and Boerrigter, P.M., Shell Intl. E&P, "Shape Factor in Fractured Reservoir Simulation", paper SPE 102471, Annual Technical Conference and Exhibition held in San Antonio, Texas, USA, September 24-27, 2006.

Wang, L., Yin, X., Neeves, K.B., and Ozkan, E., "Modelling of the Effect of Pore Size Distribution on Hydrocarbon Phase Behavior in Nanopores, paper SPE 170894, 2014.

Wang, J.Y., Holditch, S.A. and McVay, D.A., "Modelling Fracture Fluid Cleanup in Tight-gas Wells", paper SPE 119624, Hydraulic Fracturing Technology Conference, the Woodlands, TX, January 19-21, 2009.

Warpinski, N. R., Mayerhofer, M.J., Vincent, M.C., Cipolla, C.L. and Lolon, E.P., "Stimulating Unconventional Reservoirs: Maximizing Network Growth While Optimizing Fracture Conductivity", Shale-Gas Production Conference, Fort Worth, Texas, November 16-18, 2008.

Warren, J. E. & Root, P. J., "The Behavior of Naturally Fractured Reservoirs", SPE Journal, Volume 3, pp. 245-255, 1963.

Wei Yu and Kamy Sepehrnoori, "Simulation of Gas Desorption and Geomechanics Effects for Unconventional Gas Reservoirs", SPE 165377, 2013.

Wu, Y.S., "A Generalized Framework Model for Simulation of Gas Production in Unconventional Gas Reservoirs", paper SPE 163609, Reservoir Simulation Symposium held in the Woodlands, Texas, USA, February 18-20, 2014.

Wu, Y.S., Li, J., Ding, D.Y., Wang, C., and Di, Y., "Resources, Technologies and Modelling Approaches of Development of Unconventional Shale-Gas Reservoirs", IFPEN Report, Reference 62658, September, 2012.

Wu, Y.S., Liu, H.H. and Bodvarsson, G.S., "A triple-continuum approach for modelling flow and transport processes in fractured rock", Journal of Contaminant Hydrology, 73, 145-179, 2004.

Wu, Y.S. and Pruess, K., "A Multiple-Porosity Method for Simulation of Naturally Fractured Petroleum Reservoirs", SPE Reservoir Engineering, 3, 327-336, 1988.

Wu, Y.S., Pruess, K. and Persoff, P., "Gas Flow in Porous Media with Klinkenberg Effects", Transport in Porous Media, vol. 32. pp117-137, 1998.

Zanganeh, B., Ahmadi, M., Awoleke, O., "Proper Inclusion of Hydraulic Fracture and Unpropped Zone Conductivity and fracturing FlowBack in Single Shale Oil Well Simulation", SPE-169511-MS, USA, April 16-18, 2014.

Zhang, X., Du, C., Deimbacher, F., Crick, M., and Harikesavanallur, A., "Sensitivity Studies of Horizontal Wells with Hydraulic Fractures in Shale-Gas reservoirs", paper IPTC 13338, International Petroleum Conference held in Doha, December 7-9, 2009.

Zarragoicoechea, G.J. and Kuz, V.A., "Critical Shift of a Confined Fluid in a Nanopore. Fluid Phase Equilibria", 220 (1): 7–9, 2004.